(2)

CRREL REPORT 89-19

US Army Corps of Engineers
Cold Regions Research & Engineering Laboratory

Development of an airborne sea ice thickness measurement system and field test results

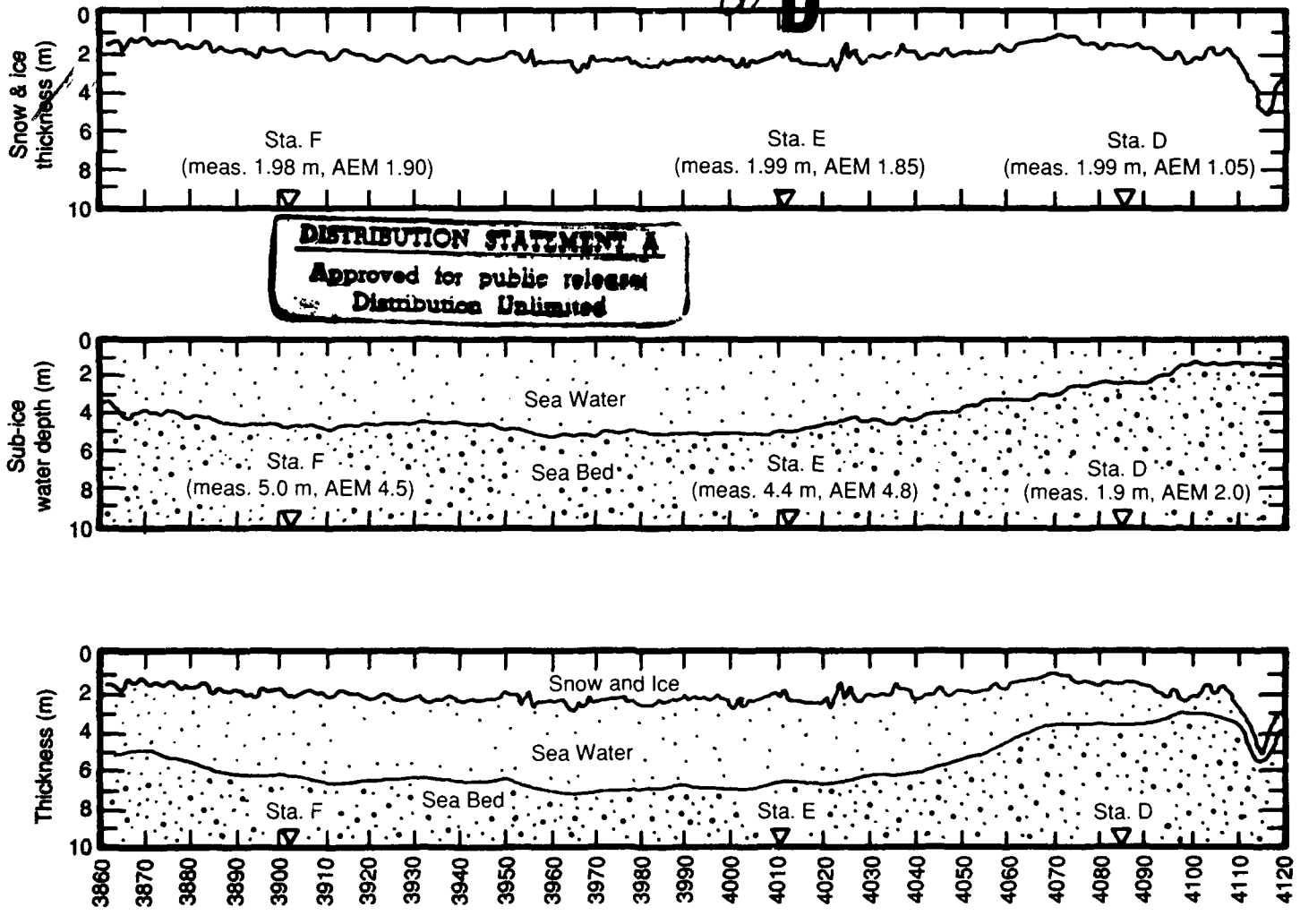

For conversion of SI metric units to U.S./British customary units of measurement consult ASTM Standard E380, Metric Practice Guide, *published by the American Society for Testing and Materials, 1916 Race St., Philadelphia, Pa. 19103.*

Cover: Airborne electromagnetically determined snow plus ice thickness and sub-ice water depth, and a composite cross section of these measurements (see Fig. 34).

CRREL Report 89-19

December 1989

Development of an airborne sea ice thickness measurement system and field test results

Austin Kovacs and J. Scott Holladay

Prepared for
U.S. DEPARTMENT OF NAVY
NAVAL OCEANOGRAPHIC AND ATMOSPHERIC RESEARCH LABORATORY

UNCLASSIFIED

SECURITY CLASSIFICATION OF THIS PAGE

REPORT DOCUMENTATION PAGE

Form Approved
OMB NO. 0704-0188
Exp. Date: Jun 30, 1986

1a. REPORT SECURITY CLASSIFICATION
Unclassified

1B. RESTRICTIVE MARKINGS

2a. SECURITY CLASSIFICATION AUTHORITY

2b. DECLASSIFICATION/DOWNGRADING SCHEDULE

3. DISTRIBUTION/AVAILABILITY OF REPORT
Approved for public release; distribution is unlimited.

4. PERFORMING ORGANIZATION REPORT NUMBER(S)
CRREL Report 89-19

5. MONITORING ORGANIZATION REPORT NUMBER(S)

6a. NAME OF PERFORMING ORGANIZATION
U.S. Army Cold Regions Research and Engineering Laboratory

6b. OFFICE SYMBOL (if applicable)
CECRL

7a. NAME OF MONITORING ORGANIZATION
U.S. Department of Navy
Naval Oceanographic and Atmospheric Research Laboratory

6c. ADDRESS (City, State, and ZIP Code)
72 Lyme Road
Hanover, N.H. 03755-1290

7b. ADDRESS (City, State, and ZIP Code)
NSTL Station, Mississippi

8a. NAME OF FUNDING/SPONSORING ORGANIZATION

8b. OFFICE SYMBOL (if applicable)

9. PROCUREMENT INSTRUMENT IDENTIFICATION NUMBER
Contract N6845286-MP60003

8c. ADDRESS (City, State, and ZIP Code)

10. SOURCE OF FUNDING NUMBERS

PROGRAM ELEMENT NO.	PROJECT NO.	TASK NO.	WORK UNIT ACCESSION NO.

11. TITLE (Include Security Classification)
Development of an Airborne Sea Ice Thickness Measurement System and Field Test Results

12. PERSONAL AUTHOR(S)
Kovacs, Austin and Holladay, J. Scott

13a. TYPE OF REPORT	13b. TIME COVERED FROM _____ TO _____	14. DATE OF REPORT (Year, Month, Day)	15. PAGE COUNT
		December 1989	54

16. SUPPLEMENTARY NOTATION

17. COSATI CODES			18. SUBJECT TERMS (Continue on reverse if necessary and identify by block number)
FIELD	GROUP	SUB-GROUP	Airborne profiling; Sea ice thickness; Electromagnetic induction–measurement tec hnology

19. ABSTRACT (Continue on reverse if necessary and identify by block number)

Recent efforts to improve airborne electromagnetic induction-measurement technology and to downsize the related helicopter-towed antenna assembly from about 7.5 m long to about 3.5 m long for use in airborne measurement of sea ice thickness are discussed, as are the results from arctic field testing. Also outlined are the system noise and drift problems encountered during arctic field evaluation, problems that adversely affected the quality of the sounding data.The sea ice sounding results indicate that it should be possible to determine thickness to within 5% for ice floes with moderate relief but that, because of sounding footprint size and current model algorithm constraints, steep-sided pressure ridge keels cannot be well defined. The findings also indicate that routine sea ice thickness profiling from an airborne platform is close at hand with further system improvement, as is the apparent capability to determine the conductivity of the sea ice, from which an assessment of sea ice strength can be made.

20. DISTRIBUTION/AVAILABILITY OF ABSTRACT
☒ UNCLASSIFIED/UNLIMITED ☐ SAME AS RPT. ☐ DTIC USERS

21. ABSTRACT SECURITY CLASSIFICATION
Unclassified

22a. NAME OF RESPONSIBLE INDIVIDUAL	22b. TELEPHONE (Include Area Code)	22c. OFFICE SYMBOL
Austin Kovacs	603-646-4100	CECRL-EA

DD FORM 1473, 84 MAR

83 APR edition may be used until exhausted.
All other editions are obsolete.

SECURITY CLASSIFICATION OF THIS PAGE

UNCLASSIFIED

PREFACE

This report was prepared by Austin Kovacs, Research Civil Engineer, of the Applied Research Branch, Experimental Engineering Division, U.S. Army Cold Regions Research and Engineering Laboratory, and by J. Scott Holladay, a consultant to CRREL.

The authors wish to acknowledge the field assistance of Walter B. Tucker III who helped organize the field ice drilling team of John W. Govoni, Dr. Anthony J. Gow, Dr. Debra A. Meese and Richard J. Roberts of CRREL. They also wish to acknowledge the AEM equipment fabrication work and data processing assistance of Walter Y.L. Chan, James L.C. Lee and Greg C.E. Luus, formerly of Geotech Ltd., the data processing performed by Gregor E. Fellers and John B. Bement of CRREL and Anthony E. Valentine of Aerodat Limited and the review comments provided by Dr. Jerome Johnson of CRREL and Rexford M. Morey, Consultant.

Funding for this study was provided by the U.S. Department of Navy, Naval Oceanographic and Atmospheric Research Laboratory, under contract N6845286-MP60003.

CONTENTS

ILLUSTRATIONS

Figure

TABLES

Development of an Airborne Sea Ice Thickness Measurement System and Field Test Results

AUSTIN KOVACS AND J. SCOTT HOLLADAY

INTRODUCTION

Airborne electromagnetic sounding technology uses multiple sets of transmitter and receiver coils that function as dipole antennas. One coil of the antenna pair is mounted forward and one aft on a stiff platform securely fixed inside a rigid cigar-shaped shell (bird). Each transmitter-receiver coil pair operates at a single frequency. The transmitted electromagnetic field induces eddy currents in a nearby electrically conductive mass such as seawater. As a result, a secondary magnetic field arises that produces an analog voltage proportional to the secondary magnetic field at the receiver. The received voltage amplitude and phase are functions of transmitter coil orientation, position with respect to the receiver coil and radiated electromagnetic field strength, the conductivity, distance and geometry of the conductive surface with respect to the transmitter, and the sensitivity, orientation, and distance of the receiver coil with respect to the seawater. Since the electromagnetic response measured at the receiver is strongly related to bird-seawater distance, an accurate measurement of this response can provide a very good estimate of this distance. When subtracted from the bird height above the sea ice surface, this distance, as measured with a laser altimeter mounted in the bird, gives an estimate of ice thickness.

This report gives an accounting of the effort made to implement improvements and validate the use of airborne electromagnetic induction technology for the measurement of sea ice thickness. The work discussed covers the period from June 1986 to February 1988 and follows the pilot study undertaken in 1985 (Kovacs et al. 1987a). In the 1985 study, airborne electromagnetic (AEM) sounding was found to be capable of measuring the thickness of sea ice from thin lead ice to thick multiyear ice. As a result of the 1985 study, a follow-on effort to improve the AEM ice measurement system was determined to be desirable. The goals of the 1986–87 effort were to

1. Improve the processing software in terms of speed, accuracy and ease of use.
2. Perform system optimization studies.
3. Make improvements to the calibration procedure.
4. Investigate the possibility of doing real-time data processing.
5. Design, construct and test a 3.5-m-long antenna (bird).
6. Design, test and install a 50-kHz coil in the bird for the purpose of improving ice thickness measurement and with the goal of measuring ice conductivity.
7. Assemble and demonstrate an in-field data processing system.
8. Perform a field validation study of the integrated AEM hardware and processing system.

Advances were made in most of the above areas, particularly in improved in-field processing and the development of a small AEM bird. In addition, funds were provided to the University of California at Berkeley for development of improved AEM interpretation techniques related to sea ice thickness and conductivity (Becker et al. 1987).

PRE-FIELD-DEPLOYMENT ACTIVITIES

Software development

The software developed for processing and analyzing AEM data for the determination of sea ice thickness, seawater conductivity and depth (Kovacs et al. 1987a) was improved to permit faster turnaround of the raw data into interpreted profile results. The processing software package used to analyze the 1985 data consisted of about 10 programs, whereas the current one used four: a tape-to-disk reading program, a "master calibration" program called MASCAL, an inversion routine

called PRICE87, and a plotting routine called LINPLOT. The entire process of reading the raw AEM data, correcting for drift, scaling of the data, interpreting the reduced data and plotting the results has been reduced to a few hours per flight. This compares to one or two days per flight with the software previously used to analyze similar data collected in 1985. Data processing is still the slowest single operation, with a throughput of roughly one data point per second. This time includes determination of ice thickness, ice conductivity and water depth. Determination of these parameters plus water conductivity and bottom conductivity can require perhaps 10 seconds per sounding point. When only ice thickness information is desired, interpretation could proceed using only the high frequency data. This can speed up the interpretation process by more than a factor of three.

System optimization

Computer studies for a 3.5-m-long bird indicated that, if the antenna system's noise level were on the order of 0.1 ppm of the primary magnetic field strength at the receiver (comparable to 1 ppm achievable in the larger 7.5-m-long bird used in 1985), the small bird would be able to resolve ice conductivity down to about 0.01 S/m. The 50-kHz quadrature data are the most applicable to this ice parameter determination. However, the estimation of ice conductivity is very sensitive to systematic errors such as drift, improper calibration, and laser altimeter errors, especially at frequencies of less than 100 kHz. A working frequency of 200–300 kHz is now considered necessary for good ice conductivity measurements of sea ice (Becker et al. 1987), which exhibits a wide conductivity range dependent upon the ice thickness, salinity, temperature, age, etc. (Kovacs et al. 1987b).

An optimal frequency domain ice-measurement system could utilize three coil pairs operating at roughly 10 kHz, 50 kHz and 300 kHz, with the last two coil pairs operating in the vertical coaxial mode to reduce system footprint size to about 1.3 times the bird elevation and provide very good sea ice thickness sounding data. The system footprint is defined as the area at the ice/seawater interface that contributes to the determination of the average bird height above the sea water. The effect of the footprint is to smooth out the seawater depressions related to ice draft variation and in turn to smooth out the ice relief with what amounts to a moving average filter with a width of about 1.3 times the bird height for the coaxial coils and about 2 times the bird height for the horizontal coplanar coils. The 10-kHz coil pair should give good bathymetry to perhaps 2 m below the ice, which would be sufficient to identify grounded ice and shoals. The two higher frequencies would provide good definition of ice thickness and ice conductivity respectively. An overall reduction in weight to about 100 kg, from the current small bird weight of about 150 kg, is also within reason and should make a fixed-wing aircraft deployment of the system more feasible as well.

Improvements to the calibration procedure

System calibration proceeded on three levels. On the basic level, an investigation of the accuracy of the standard Q–coil and ferrite bar calibration method, as used by mineral prospecting firms, yielded the result that the phase calibration is more accurate (even at high frequencies) than the amplitude calibration. However, the amplitude calibrations were not in agreement with the calculated ones determined at a known elevation over a surface or mass of known conductivity —or, in other words, with known ground truth. An effect of the secondary field produced by the ground during ground calibration probably contributed to the disagreement between the calculated and measured amplitude calibrations. It had been thought that the small but nonzero conductivity of the ferrite bar used for phasing was a limiting factor, but this effect did not appear at frequencies up to 50 kHz. In contrast, the standard"external Q–coil" used for ground calibration of the EM system appears to run into serious difficulty at high frequencies, mainly due to the parasitic capacitance of the coil. A small-diameter coil was constructed which possessed a much higher self-resonant frequency, and gave much better results than did the "standard" Q–coil.

The second level of investigation centered on the design and construction of an "absolute" calibration technique that could be used in-flight. This would eliminate the secondary field effects associated with on-the-ground system calibration. A novel technique based on increasing the area of the receiver coil in a precise way was devised and tested. However, it did not operate as required. Interaction between the calibration coil and the receiver coil caused severe departures of the calibration signal from correct levels, especially at high frequencies. As it stands, this technique is not a satisfactory stand-alone calibration aid.

The final level of calibration investigation involved the automation of the "ground-truth re-

calibration" process. In this process, the AEM bird altitude and laser altimeter results obtained over a site with known ice thickness, water depth, and water conductivities were compared with the computer-generated responses for the same bird position and orientation over the site. From these comparisons, corrections to the scaling factors for the AEM data were derived. These scaling factors relate the drift–corrected EM data, in bits, to the final EM results in parts per million of the primary field at the receiver. The raw data were then recalibrated with the revised scaling factors for reinterpretation to bring the AEM results in line with the measured ground truth data.

It should be emphasized that the system's calibration is a static quantity, and that once a good calibration, based on ground truth, has been established it should be stable for long periods of time (months or even years), as long as the coils and electronics of the bird and the receiver console parameters are not altered. Thus, the first effort on a survey, after adjustments have been made to the bird or console, would be to establish a good calibration from ground truth. When an absolute calibration technique has been fully developed and implemented, this step will not be required.

Real-time processing

Substantial effort went into investigation of the feasibility of real-time interpretation of AEM ice measurement data. Two factors have stymied efforts to process AEM data in real time to yield sea ice thickness or other desirable quantities. These are the effects of system drift and the difficulty of performing the complex computations required in a small reliable package suitable for airborne operations. The software, which was configured to run on a ground-based MicroVAX II computer, can handle from 1–3 samples per second. However, improvements in the efficiency of existing software, as well as mathematical developments by several research groups in the past year, offer the possibility of interpretation rates of up to 50 points per second or about one data point per meter at 180 knots. Even if these approaches prove unsatisfactory, computer technology has progressed so rapidly that, with a new digital receiver incorporating a 80386-based computer coupled with a small array processor, it should be possible to process AEM data in real time at the data acquisition rate.

The key factor limiting progress in real-time processing is thus not the interpretation system but the drift characteristics of present AEM systems. In particular the problem is the presence of so-called "nonlinear" drift: instrumental drift that departs significantly from a linear time dependence. Drift, for the purposes of this report, can be defined as the change vs time that would be observed in the AEM system's outputs at high altitude, when there is no change occurring in the actual electromagnetic secondary field because there are no conductive structures nearby to host eddy current flow. If this drift were highly linear as a function of time, it would be easily removed by making high-altitude measurements at both ends of a survey flight line and then interpolating between these "zeroing" points. A combination of good hardware design, assembly and testing should have virtually eliminated nonlinear drift. Unfortunately, these aspects were not adequately addressed by the manufacturer but will be incorporated into the next phase of our AEM sea ice measurement program.

Small bird design and implementation

A prototype AEM antenna bird, incorporating limited bathymetric capability in addition to its primary design goal of sea ice thickness measurement, was constructed by Geotech Ltd. (Fig. 1). The bird was suspended by a Kevlar–cored "strength member" from the survey helicopter. The principal bird characteristics were a coil sep-

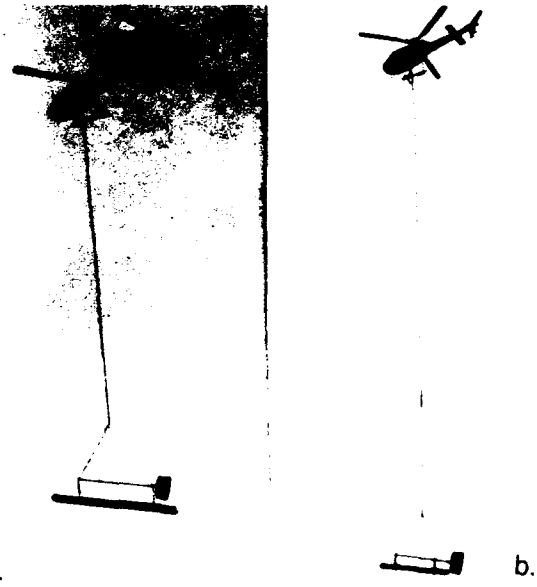

Figure 1. Standard size AEM bird (a) used in 1985 and new shorter bird (b) used in the 1987 program. The relative size difference can be observed by comparison with the length of the spreader bar with drag skirt which is the same in both photographs.

aration of 3 m and a combined bird and tow cable weight of 120 kg, or less than half the weight of a conventional 7- to 8-m-long bird and tow cable (about 255 kg). Since the smaller coil separation reduces the amplitude of the secondary-field anomaly from a given conductor at a given standoff distance, it was necessary to minimize all sources of EM noise produced within the bird. Bird EM noise arises from a variety of sources: movement of the coils with respect to one another (due to bird bending and thus internal coil platform flexure or too loose fasteners), movement of conductors (such as bird wiring) and movement of electronic housings and heat sink components within the bird. Sferic and cultural electromagnetic noise picked up in the coils or bird wiring also contributes to the overall measured noise level. To achieve a signal-to-noise ratio in a small bird with a 3-m coil separation that is comparable to that of a conventional AEM bird with a 6- to 7-m coil separation, the noise level must be about 10 times lower. This noise reduction was addressed by making the bird shell more rigid through the use of Kevlar-epoxy materials, and using substantially larger dipole moments in the transmitters than is usual. Lower noise preamplifiers were also fabricated.

A 3-m coil spacing was chosen for the approximately 3.5-m-long bird with two goals in mind: first, to minimize the difficulty of shipping the bird to remote locations (a major expense for birds 7 to 8 m long), and second, to take the first step toward making a bird that could be towed by a fixed-wing aircraft.

The coil configurations used in the small bird were horizontal coplanar for the 811-Hz (F1) and 49,927-Hz (F3) frequency coil pairs and coaxial for the 4511-Hz (F2) frequency coil pair. The coaxial coil arrangement was selected to take advantage of the inherently narrower "footprint" of this configuration and thereby obtain data for enhancing interpretability of "two-dimensional" features like pressure ridges.

The performance of the small bird on the ground and in the air was encouraging. The noise level for the quietest coil pair (4.5 Hz) using a 0.1-second detector time constant was approximately 0.1 ppm, which is comparable to the 1-ppm noise level of a conventional AEM bird with a 7-m coil separation. Drift was on the order of 5 ppm/hour for the same coil pair, which is worse than expected although quite manageable. Noise and drift levels were higher in the other channels, particularly the 50 kHz. The resulting errors affected the quality of the field data. Thorough test and evaluation of the bird and receiver electronics by the manufacturer, prior to shipment to Alaska, should have uncovered this noise problem. The major noise sources were found, but only after completion of the Prudhoe Bay field test program. Drift in all data channels was primarily a problem caused by poor stability in the analog receiver console. Again, this problem should be alleviated by use of a digital receiver or, at the very least, by use of a properly stabilized analog console. Replacement of the transmitter modules with current-regulated transmitters should further reduce drift in the bird's electronic system. With the above modifications, new equipment, etc., further shortening of the bird through reduction of the coil separation may be feasible.

Other improvements

A commercial 16-bit digital data recording system was used for acquisition of all survey data. This system was an improvement over the rather primitive 12-bit data acquisition system used during the 1985 survey. These recording systems gather analog and digital inputs from a variety of sources and store them with timing information on magnetic tape. The recording system did develop hardware problems during the field survey that caused a two-day delay and much concern. A field repair was successful.

A video flight path recovery system was used that gave good picture quality of the terrain overflown and allowed for digital annotation of the video record. This system incorporated a camera, with a wide-angle lens and image sensor, a video annotation board and a compact video tape recorder. The use of a microphone for the operator to record cockpit conversation on the audio track of the video tape cartridge made analysis of the video record easier.

A global positioning system (GPS) was used for in-flight navigation when possible; useful three-satellite "visibility windows" lasted for about 5 hours/day in 1987. Positions in latitude and longitude were recorded by the data system when available and served to guide reconstruction of flight paths. The GPS antenna was mounted on the helicopter roof above the cockpit. This position was not expected to work very well, but was in fact satisfactory; the only problem encountered was occasional blocking of the signal from satellites low on the horizon by the engine housing.

A new laser altimeter was installed in the bird to replace the less accurate unit used during the 1985 field trials. The new altimeter is much more accurate (±1 cm) than the old one (±20 cm). Difficulties

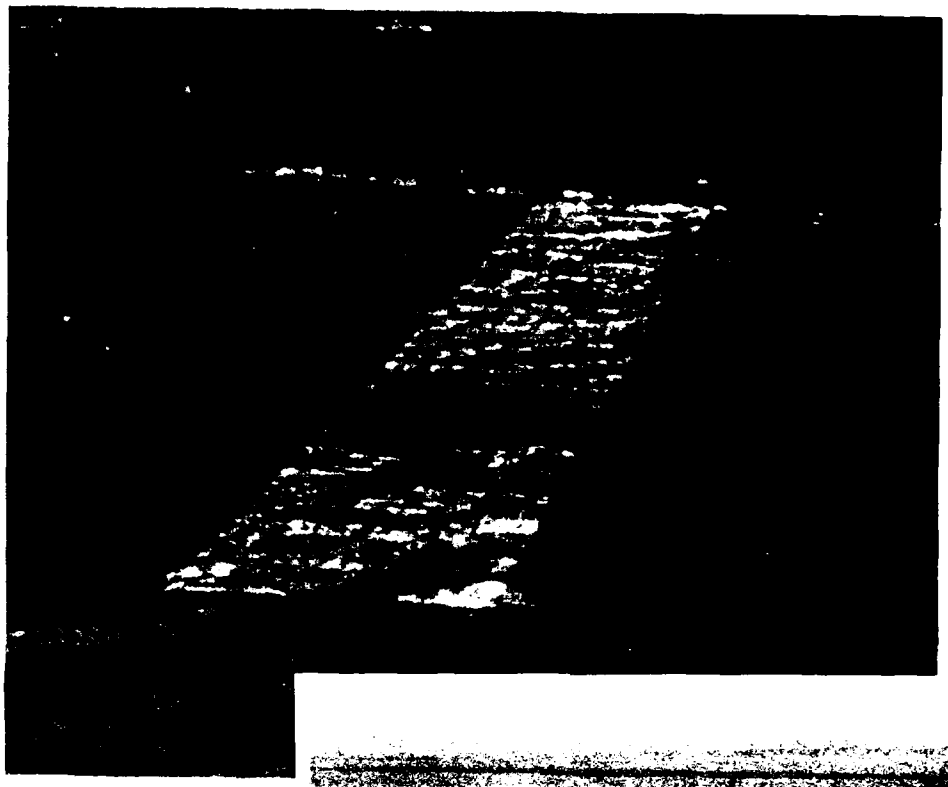

Figure 2. Outline of 50-m-wide by 450-m-long grid area on multiyear floe 1. Arrows point to grid centerline. Foot traffic during the drilling operation caused contrast seen in the snow surface.

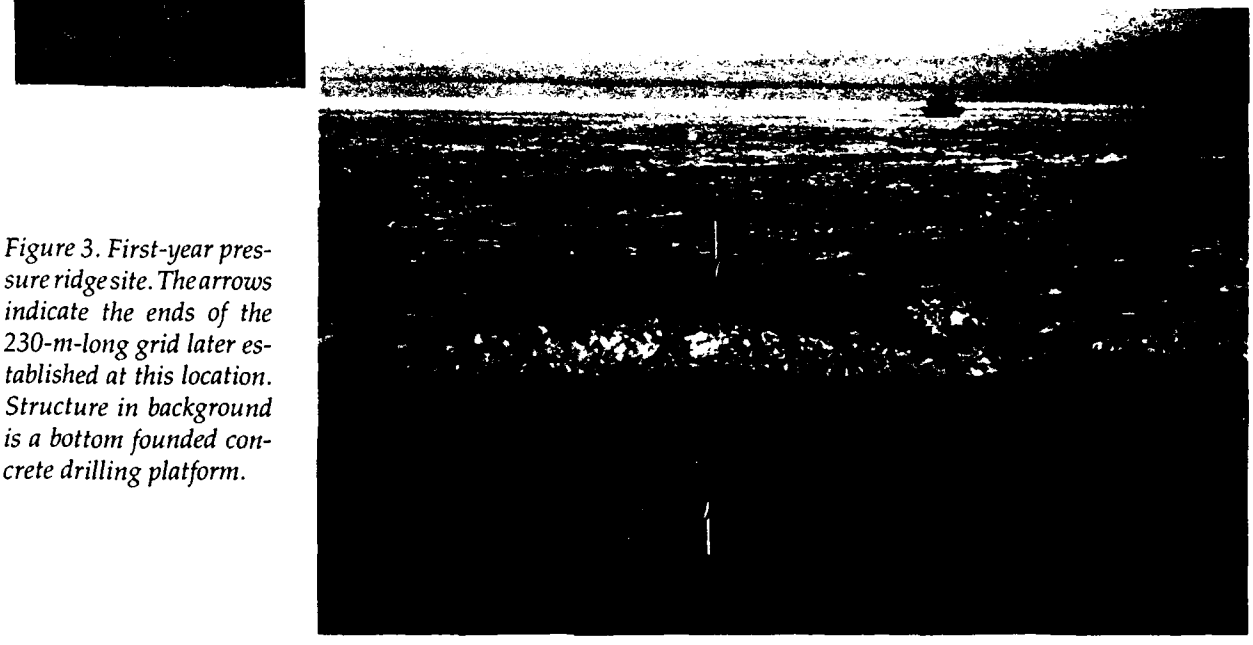

Figure 3. First-year pressure ridge site. The arrows indicate the ends of the 230-m-long grid later established at this location. Structure in background is a bottom founded concrete drilling platform.

were encountered in programming the control console for this altimeter. This appeared to be linked to problems encountered in altimeter data timing, as will be discussed later.

FIELD ACTIVITIES

Snow, ice and seawater data

Before making the AEM sounding flights, four sites were selected within the fast ice area near Prudhoe Bay, Alaska. At each site extensive "ground truth" information was collected. Three sites were on second-year ice floes, hereafter called *multiyear ice*, and one site comprised a first-year pressure ridge surrounded by first-year sea ice.

On each multiyear ice floe (Fig. 2) and at the first-year pressure ridge (Fig. 3), a grid was laid out with stations spaced 5 m apart. Grid width was 50 m. Grid lengths varied and were 450, 200, 200 and 230 m for multiyear floes 1, 2 and 3 and the first-year ridge site, respectively. At each grid station, the snow and ice thicknesses were determined, as were the ice freeboard and keel depth. Two oil-

fired hot water drilling systems were used to drill most of the holes. About 75 holes were drilled using a hand-held electrically driven 6–cm-diam continuous flight auger system. In all, about 2,500 holes were drilled.

The purpose of the grids, and related drill hole measurements, was to define the ice thickness distribution at each site. The data were used to evaluate if the snow–ice thickness determined by the AEM system agreed with the measured values. In our previous work (Kovacs et al. 1987a), we determined that the diameter of the AEM footprint, or the area over which the integrated snow–ice thickness is estimated, ranges from one to two times the bird altitude. Therefore, if the bird is flown 25 m above the sea ice, then the footprint is, as a first approximation, at least 25 m in diameter.

The object of the AEM ice thickness study was to fly down the center of each grid, sounding ice thickness and referring these measurements to the location of markers placed at 25-m intervals on the ice surface. Common fiducial numbers recorded on the AEM data and the flight path video allowed for cross correlations of the ice marker location vs the AEM data. Past experience showed that it would be extremely difficult to fly the bird down a narrow track laid out on the ice. Some bird wandering was expected due to helicopter movement. To compensate for this, the grid was made wider than the anticipated EM footprint.

An additional reason for the wide grid was to assess the track width needed to provide average snow–ice thickness information that is representative of the integrated footprint area thickness determined by AEM sounding.

In addition to the four grid sites, three long sounding lines were established across the fast ice with the use of the satellite GPS. At random distances along each line, ice stations were set up at which snow depth, ice thickness and water depth were measured. At several stations, seawater temperature and conductivity were measured and ice cores taken for ice property determinations. The above lines were later flown with the AEM system with the goal of correlating the AEM measured results and the station ground truth measurements.

Another site selected for verification purposes was a lead containing ice 0.18 to 0.22 m thick. The new ice did not have a snow cover.

The locations of flight lines containing stations A, B, and D through G are shown in Figure 4. The flight line containing stations H through O is shown in Figure 5, as is the general location of multiyear floe study sites 1, 2, and 3. The first-year pressure ridge site was located to the northwest of Reindeer Island and the refrozen lead site was northeast of this island. Flight line station positions were also determined by use of the satellite GPS. Table 1 gives station latitude and longitude as well as each site's average snow and ice thickness, and the temperatures, salinity and depth of water under the ice.

Ice thickness, over which AEM sounding flights were made, varied from a few centimeters to about 21 m in ridges. Under-ice water depths ranged from zero at grounded fast ice sites to over 30 m.

Table 1. Station GPS location and related snow, ice and water ground truth data.

			Thickness			Water	
			Snow	Ice	Depth*	salinity	Temp.
Station	Latitude	Longitude	(m)	(m)	(m)	(‰)	(°C)
A	70°20.2'N	148°20.4'W	0.28	1.70	0.55	70	3.8
B	70°22.1'	148°21.6'	0.25	1.19	Grounded ice		
D	70°24.3'	148°28.8'	0.16	1.77	1.95	31.6	1.75
E	70°24.7'	148°28.0'	0.14	1.75	4.4	31.8	1.75
F	70°26.1'	148°24.0'	0.30	1.68	5.05	30.9	1.7
G	70°27.1'	148°22.8'	0.17	1.82	5.1	31.5	1.75
H	70°30.4'	149°12.4'	0.10	1.80	0.45	40	2.5
I	70°32.4'	149°07.0'	0.15	1.76	9.1	—	—
J	70°33.0'	149°04.8'	0.15	1.73	10.0	31.0	1.7
K	70°33.4'	149°04.5'	0.10	1.74	8.85	31.3	1.74
L	70°34.4'	149°02.2'	0.15	1.78	12.1	—	
M	70°35.1'	148°59.7'	0.15	1.80	15.15	—	—
N	70°36.7'	148°55.6'	0.05	0.98	14.1	—	—
O	70°37.4'	148°53.0'	0.05	0.89	18.7	—	—

* Depth under ice.

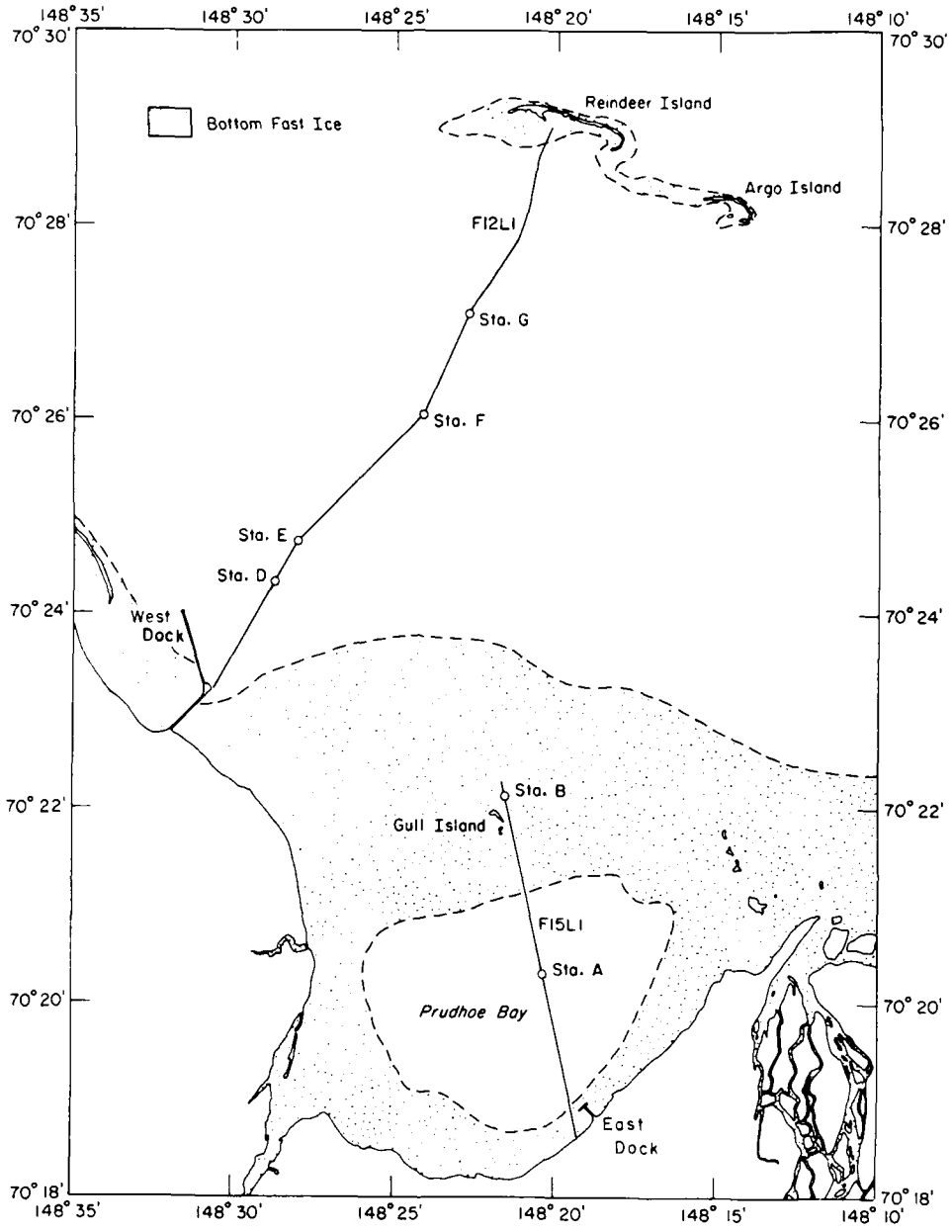

Figure 4. Location of flight lines F15L1 and F12L1 and ground truth stations A, B and D–G.

Water temperature and conductivity, as determined by instrumentation lowered below the ice sheet, were typically –1.75 C and 2.6 S/m, respectively, at locations outside of confined bays and lagoons. In Prudhoe Bay at station A (Fig. 4), higher salinity water with a conductivity of about 4.6 S/m occurred, and in Simpson Lagoon south of Cottle Island at station H (Fig. 5) the water conductivity was about 3.4 S/m. The higher conductivity of the seawater at stations A and H occurs because these bodies of water become isolated after the sea ice thickens and becomes grounded on the surrounding shallows. No longer flushed away by currents, the brine expelled into the seawater during ice growth increases the salinity and therefore the conductivity of the confined water. This enrichment also depresses the freezing point of the water, as indicated in Table 1.

AEM surveys

During the course of the field experiment, nearly 40 passes were made over the survey areas previ-

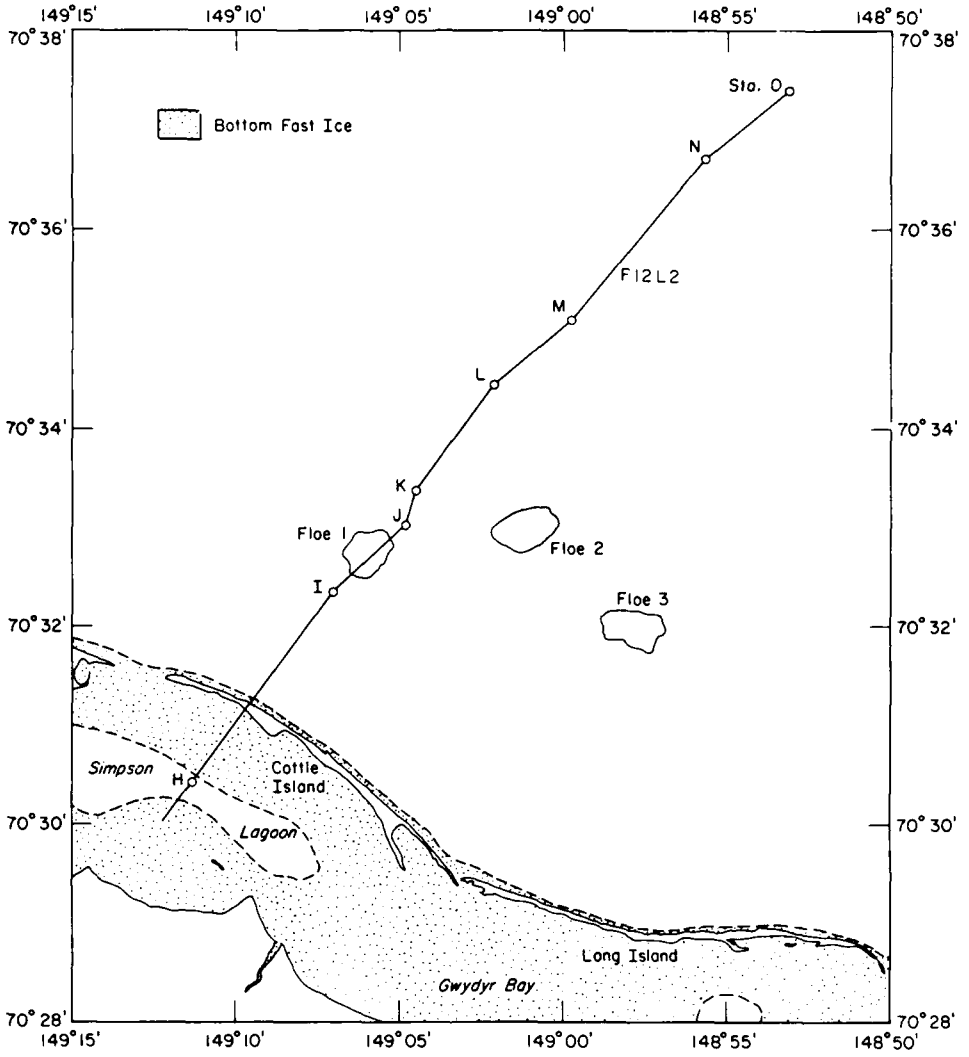

Figure 5. Location of flight line F12L2, stations H through O and the three multiyear ice floes at which AEM soundings were made.

ously discussed. The final flight consisted of a *northing*, a long flight out over the pack ice. Repeat passes were made over all sites for which ground-truth information had been obtained. Most flying was done over the four grid sites. Total line coverage was on the order of 100 km.

Every attempt was made to limit survey altitude in an effort to reduce footprint size. At the four grid sites, multiple passes were made to ensure that three or more "good runs" down the center of the grid would be obtained. Flights were made under GPS control, when three or more "visible" satellites made this possible, along the survey lines with ground truth stations, the grid sites, and the northing line and at several other locations . The satellite-positioned flight lines discussed in this report are shown in Figure 6. The bird was also taken to zeroing altitude (about 300-m elevation) before and after each sounding run. At this altitude the energy emitted by the transmitter coils is no longer capable of inducing an eddy current secondary system in the conductive seawater that is detectable at the receiver coils. Thus, no secondary electromagnetic field is sensed by the receiver coils. Measurement of baseline response of the AEM system before and after each sounding run helped to determine the amount of drift and allowed for the removal of this drift from the data. In almost all cases, this approach to baselining paid off in terms of simplified post-flight data processing and improved data quality. However, in some cases, nonlinear drift could not be compensated for, particularly on long lines.

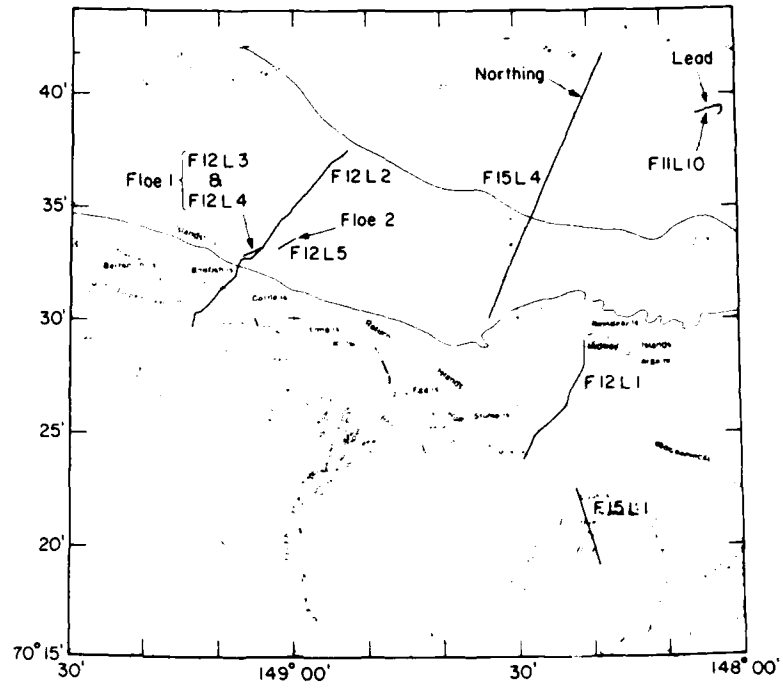

Figure 6. Location map showing flight lines determined by use of the satellite global positioning system (GPS).

Calibration

System calibration, initially performed using standard external on-ground techniques, was refined by flying over a known thickness of sea ice. The standard ground calibration procedure, undertaken after system warmup, consisted of first aligning the phase of the system ("phasing"), then setting its gain. Phasing was accomplished by rotating a ferrite bar in and out of alignment with the maximum electromagnetic field of a given coil pair. This rotation generated a purely in-phase variation in the measured secondary field. Any deflection observed in the out-of-phase or quadrature signal amplitude during this procedure is evidence of an incorrect phase adjustment and was eliminated by successive phasing adjustments at the receiver module for the particular coil and frequency being calibrated. The gain was set by placing an "external Q–coil" on a test jig (Fig. 7) at a known distance from the receiver coil in question. A contact was then opened and closed, to make and break a

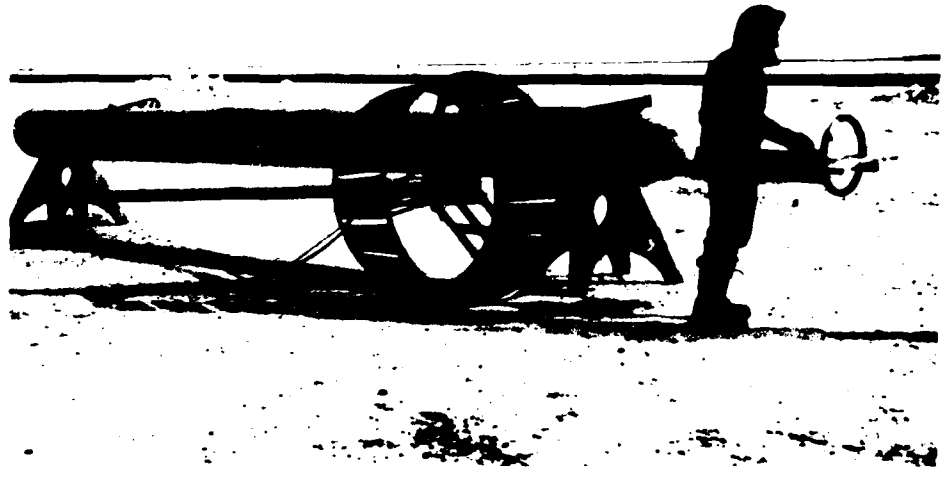

Figure 7. Ground calibration using the standard Q-coil. Black line above bird is the runway pavement.

tuned circuit consisting of the coil and a calibration resistor. This circuit generated a known anomaly, with equal in-phase and quadrature components, which was used to adjust the amplitude response of the system.

The other form of calibration used was ground-truth recalibration. This technique is far more accurate than the standard on-ground calibration technique when good, unambiguous ground-truth and altimeter data are available. However, when ice of irregular thickness is present and/or the laser altimeter is not performing properly, systematic errors can arise from this procedure that will bias the results, particularly in the ice thickness estimate. The ideal situation for ground-truth recalibration (assuming proper altimeter operation) is therefore a wide area of deep ice-free water. Since such lead conditions may not be available when required, an internal, absolute calibration system will be essential for a fully operational AEM sea ice measurement system.

AEM data processing

A field processing station was set up. It consisted of a minicomputer (MicroVAX II), two terminals, a cassette tape drive, a graphic printer and related processing software. Analysis of the AEM data followed the general theory outline in Kovacs et al. (1987a). After the first survey's data were read into the computer and an analysis attempt made, serious difficulties in processing began to be encountered. This was characterized by an inability to get even moderately reasonable ice thickness results out of the survey data while at the field station. Resolution of this problem is discussed below.

POST-SURVEY RESULTS

Processing problem

The source of the problem that prevented in-field data processing eventually turned out to be surprisingly simple: a time offset was discovered between the laser altimeter data and the rest of the survey data. The altimeter data were delayed by about 2.5 seconds from the AEM data on the storage tapes. This was a serious problem, because normal changes in laser altitude, due to flight height and bird pitch and roll, were effectively differentiated and added into the ice thickness, causing very substantial, time-varying errors in the interpreted results. Suffice it to say that this time skew was very difficult to identify, as similar data degradation effects might have been caused by a variety of sources. (Even after the error had been found to be in a time skew between the laser and the EM measurements, identification of the source of the problem proved difficult. Some possibilities considered were errors in tape writing or transcription, errors in MASCAL, and the effects of a long filter time constant in the analog receiver, as described by Becker and Cheng [1988]. Errors in MASCAL and tape transcription were eliminated as the cause after careful analysis, and since the time constant in the small bird analog receivers was 0.1 second, it could not have been the reason for the time offset either.) In the final analysis, it appears that the delay arose in the interface between the laser process and the data acquisition system. The problem can be eliminated by triggering the laser console for each sample desired.

After the time delay was accounted for, the AEM data were recalibrated using the snow plus ice (S-I) thickness measurements from the flat ice area in front of the first-year pressure ridge grid site. It should be noted that ground-truth recalibration of the AEM system was carried out at this single site, and that this calibration was then used for all other AEM flight data. Profiles of the S-I thickness obtained over all of the major ice structures were then prepared.

Some difficulties were encountered during the reduction and interpretation of the AEM data from the long survey lines. Drift in the F3 data (50-kHz frequency) was the culprit in this case. Removal of the F3 data from the interpretation solved this problem.

An example of the time-delay corrected data collected during flight 13, line 3 (F13L3) is shown in Table 2. This survey line consisted of a pass down the 200-m-long grid on multiyear floe 2. The nine reference station locations, spaced 25 m apart along the grid, are listed by fiducial number at the bottom of the table. In the analysis of this data set the conductivities of the seawater and seabed were set at 2.6 and 0.5 S/m, respectively, rather than being interpreted by analysis of the AEM data. Note that the bulk S-I conductivity is also listed. These S-I conductivity determinations were found to be inconsistent. At times the values appeared very representative of the type of ice over-flown (based on analyses of Kovacs et al. 1987b) but often they varied inconsistently and are therefore considered unreliable. This problem appeared to reside with the nonlinear drift and noise experienced with the AEM system and not with the algorithm used to estimate the bulk S-I conductivity. In the near future we hope to rectify this problem through hardware improvements and the use of higher frequencies.

Table 2. Example of processed AEM sounding results. Data are from flight line F13L3.

FID. NO.	SAT. POSITION* NORTH	WEST	BIRD PITCH DEG.	BIRD ROLL DEG.	AVG. ALT. m	S-I THICK. m	S-I COND. S/m	WATER THICK. m	WATER COND. S/m	SED. COND. S/m
3320	4194650	8832990	2.0	-1.4	23.36	2.57	0.0050	13.37	2.60	0.5000
3321	4194640	8832940	1.9	-1.6	22.62	2.49	0.0069	13.20	2.60	0.5000
3322	4194640	8832940	2.1	-1.3	22.35	2.20	0.0109	13.12	2.60	0.5000
3323	4194630	8832900	1.8	-1.3	22.18	2.10	0.0077	13.04	2.60	0.5000
3324	4194630	8832900	1.7	-1.9	22.02	2.10	0.0154	13.04	2.60	0.5000
3325	4194630	8832900	1.9	-2.1	21.66	2.10	0.0154	13.04	2.60	0.5000
3326	4194620	8832850	2.3	-0.7	21.32	1.98	0.0008	13.48	2.60	0.5000
3327	4194620	8832850	2.3	-0.2	20.02	2.60	0.0007	13.52	2.60	0.5000
3328	4194610	8832820	2.0	-0.5	19.34	2.46	0.0009	13.49	2.60	0.5000
3329	4194610	8832820	2.2	-0.6	19.05	2.10	0.0014	13.38	2.60	0.5000
3330	4194610	8832820	2.4	0.3	19.02	1.82	0.0020	13.39	2.60	0.5000
3331	4194600	8832760	2.6	-0.1	19.13	1.68	0.0010	13.53	2.60	0.5000
3332	4194600	8832760	2.6	-0.6	19.13	1.77	0.0010	13.48	2.60	0.5000
3333	4194590	8832720	2.8	-1.0	19.09	1.77	0.0021	13.48	2.60	0.5000
3334	4194590	8832720	3.0	-1.0	19.11	1.77	0.0042	13.48	2.60	0.5000
3335	4194590	8832720	3.3	-1.6	19.47	1.52	0.0022	13.24	2.60	0.5000
3336	4194570	8832660	3.2	-1.3	19.83	1.52	0.0044	13.24	2.60	0.5000
3337	4194570	8832660	3.5	-2.1	20.90	0.96	0.0009	13.55	2.60	0.5000
3338	4194560	8832620	4.0	-1.1	21.45	1.07	0.0007	13.25	2.60	0.5000
3339	4194560	8832620	4.3	-1.0	21.76	1.43	0.0007	13.23	2.60	0.5000
3340	4194560	8832620	4.2	-1.0	22.05	1.80	0.0007	13.04	2.60	0.5000
3341	4194550	8832570	3.9	-0.4	22.33	2.07	0.0011	12.85	2.60	0.5000
3342	4194550	8832570	3.3	-0.4	22.47	2.51	0.0012	12.42	2.60	0.5000
3343	4194540	8832530	2.9	-0.4	22.57	3.01	0.0019	12.17	2.60	0.5000
3344	4194540	8832530	2.7	-0.4	23.26	2.88	0.0032	11.87	2.60	0.5000
3345	4194540	8832530	2.2	-0.8	23.24	3.47	0.0067	11.71	2.60	0.5000
3346	4194530	8832500	2.0	-1.0	23.21	3.78	0.0172	11.69	2.60	0.5000
3347	4194530	8832500	2.4	-1.0	23.52	3.78	0.0172	11.69	2.60	0.5000
3348	4194520	8832440	2.2	-1.3	24.07	3.41	0.0038	11.53	2.60	0.5000
3349	4194520	8832440	1.8	-1.9	24.43	3.41	0.0076	11.53	2.60	0.5000
3350	4194520	8832440	1.7	-1.1	25.34	2.86	0.0180	11.61	2.60	0.5000
3351	4194510	8832390	1.6	-1.1	25.51	3.02	0.0238	11.62	2.60	0.5000
3352	4194510	8832390	1.3	-1.2	25.68	3.02	0.0238	11.62	2.60	0.5000
3353	4194500	8832350	1.0	-1.0	25.93	3.12	0.0052	11.54	2.60	0.5000
3354	4194500	8832350	0.8	-0.3	25.74	3.62	0.0126	11.60	2.60	0.5000
3355	4194500	8832350	0.7	-1.0	25.93	3.73	0.0172	11.60	2.60	0.5000
3356	4194490	8832300	0.4	-0.4	26.26	3.96	0.0256	11.56	2.60	0.5000
3357	4194490	8832300	-0.1	-0.8	26.37	3.96	0.0256	11.56	2.60	0.5000
3358	4194480	8832260	-0.1	-1.2	26.56	4.08	0.0069	11.30	2.60	0.5000
3359	4194480	8832260	-0.2	-0.8	26.76	4.08	0.0138	11.30	2.60	0.5000
3360	4194480	8832260	-0.6	-0.9	26.42	4.62	0.0211	10.99	2.60	0.5000
3361	4194470	8832210	-0.6	-1.8	26.61	4.62	0.0211	10.99	2.60	0.5000
3362	4194470	8832210	-0.7	-1.0	26.80	4.62	0.0042	10.99	2.60	0.5000
3363	4194460	8832170	-0.8	-1.6	27.00	4.62	0.0084	10.99	2.60	0.5000
3364	4194460	8832170	-0.9	-1.3	27.40	4.62	0.0169	10.99	2.60	0.5000
3365	4194460	8832170	-0.7	-1.1	27.40	4.62	0.0169	10.99	2.60	0.5000
3366	4194440	8832110	0.2	-0.9	27.28	5.57	0.0040	9.86	2.60	0.5000
3367	4194440	8832110	-0.3	-0.8	25.80	7.43	0.0100	9.81	2.60	0.5000
3368	4194430	8832070	-1.3	-0.8	26.18	7.43	0.0200	9.81	2.60	0.5000
3369	4194430	8832070	-1.3	-1.3	26.62	6.08	0.0269	9.88	2.60	0.5000
3370	4194430	8832070	-1.3	0.0	25.32	6.08	0.0269	9.88	2.60	0.5000
3371	4194410	8831980	-1.4	-1.2	25.94	5.48	0.0080	9.90	2.60	0.5000
3372	4194410	8831980	-1.7	-0.6	25.29	5.48	0.0160	9.90	2.60	0.5000
3373	4194410	8831980	-2.1	-2.1	24.07	5.48	0.0160	9.90	2.60	0.5000
3374	4194410	8831980	-2.3	-0.5	24.38	5.48	0.0032	9.90	2.60	0.5000
3375	4194410	8831980	-2.7	-1.4	24.04	5.48	0.0064	9.90	2.60	0.5000
3376	4194400	8831920	-2.8	-1.5	23.44	5.48	0.0128	9.90	2.60	0.5000
3377	4194400	8831920	-2.4	-1.3	23.72	4.06	0.0134	10.72	2.60	0.5000
3378	4194390	8831880	-1.8	-1.4	23.74	3.08	0.0154	11.84	2.60	0.5000
3379	4194390	8831880	-2.0	-0.4	23.74	2.60	0.0165	12.55	2.60	0.5000
3380	4194390	8831880	-2.2	-1.7	23.32	2.76	0.0182	13.19	2.60	0.5000
3381	4194380	8831830	-2.5	-0.8	22.96	2.92	0.0213	13.47	2.60	0.5000
3382	4194380	8831830	-2.7	-0.7	22.73	2.76	0.0254	13.31	2.60	0.5000
3383	4194370	8831790	-2.3	-1.1	22.57	2.64	0.0323	12.96	2.60	0.5000
3384	4194370	8831790	-2.0	-1.1	22.12	2.95	0.0346	12.71	2.60	0.5000
3385	4194370	8831790	-1.1	-0.8	22.67	2.45	0.0321	12.73	2.60	0.5000

0 !NUMBER OF SATURATED DATA SECTIONS
0 !NUMBER OF NEGATIVE VALUES IN EM
9 !NUMBER OF MANUAL TICKS (Stations)

3363	3368	3373
3364	3370	3374
3366	3372	3375

*4,194,650 ÷ 60,000 = 69.9109^{O} = 69^{O} 54' 39"

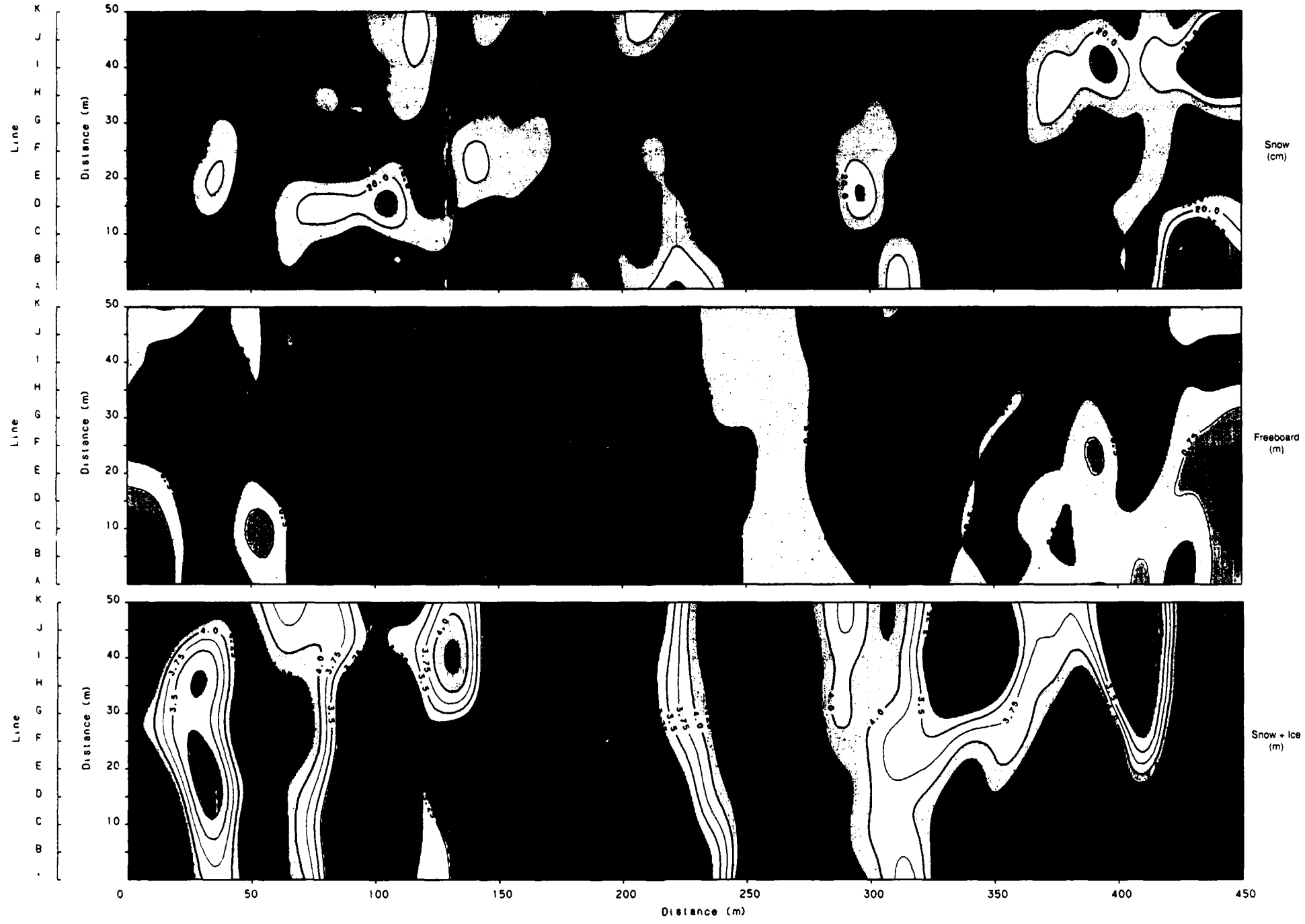

Figure 8. Snow, freeboard and snow plus ice thickness contour maps of multiyear floe 1 (courtesy Anthony Valentine).

Ground truth data

As previously stated, large grids were established at four sea ice sites. Their 50-m width was divided into 11 longitudinal lines, A through K, spaced 5 m apart. Grid length was similarly divided by lateral rows 5 m apart. At the intersections of each row and line, the snow and ice thickness and freeboard were determined by drill hole measurement. These data were used to construct an S-I thickness contour map for multiyear floe grid sites 1, 2 and 3. These maps are shown in Figures 8, 9 and 10, respectively. The relief in Figure 8 shows that the ice was thicker at each end of the grid, as well as at about the 260-m distance location, and that ice relief features tended to be perpendicular to the long axis of the grid. A melt pond is centered at about the junction of line I and the 340-m distance position.

The S-I thickness contours for grid site 2 show thick ice (a pressure ridge) extending from line A, at about the 60-m distance location, to line K, at about the 85-m distance. Another thick ice feature (a ridge) runs from about line I, at a distance of about 110 m, to about line C near the 200-m distance location.

The contour map for grid site 3 shows a major ice thickness increase (a ridge) extending across the grid beginning in the area of the 140-m-distance location.

From the drill hole measurements the average row snow and ice thickness and ice freeboard and draft were determined for grid lines A–K, C–I and E–G at each grid site. These values are listed in Tables 3 through 6 for multiyear floes 1 through 3 and the first-year pressure ridge site, respectively. Note that in Table 6 the average ice freeboard on row 45 at the first-year ridge was a negative value. Indeed, the ice in this area was depressed by snow loading and by ridge subsidence. Drilling through the ice along this line resulted in upward movement of seawater into the snow.

At the bottom of each table is listed the average value for each column of data. The deviation in the average ice thickness for lines A–K, C–I and E–G for any grid site does not exceed 4%. This suggests that ice thickness measurements needed to be obtained only along three of the lines in order to assess the average grid area ice thickness.

Table 7 lists the mean and standard deviation of the snow and the ice thickness, the ice freeboard and draft and the combined snow and ice thickness for lines A–K, C–I and E–G for each grid site. The maximum deviation of the mean values for the snow-ice thickness data, the thickness that would be measured by the AEM system, is again very low (less than 3%) for each group of lines. This again suggests that data collected along lines C–I may be used to assess the mean snow, ice, S-I thickness etc., for the entire related grid area. For the multiyear grid sites, the standard deviation of the snow thickness and the ice freeboard values is seen to be comparable to the mean thickness. This is as expected since the floes had considerable undulating relief and significant variation in snow drift accumulation. Such topographic variation is even more pronounced at the first-year pressure ridge site, as indicated by the standard deviations shown in Table 7.

While the mean S-I thickness values for lines A–K, C–I and E–G for each grid site are quite similar, there was variation between them on a row-by-row basis or with distance down the grid axis. This is graphically shown in Figures 11 through 14 for grid sites 1 through 3 and the first-year ridge site, respectively. Our assessment of the S-I thickness data indicated that line group C–I was more representative of the average S-I thickness variation along the grid and was, therefore, used to evaluate the AEM-determined measurements of S-I thickness.

To show how the S-I thickness can vary along individual grid lines, we include Figures 15 through 17 for multiyear flows 1 through 3, respectively. The difference between the lines in each figure as well as between the related average S-I thickness lines given in Figures 11 and 13 indicate that the variation can be appreciable. This is not unexpected.

Cross sections constructed from the drill hole data for combined lines A–K, C–I and E–G for multiyear grid sites 1 through 3 are shown in Figures 18 through 20, respectively. These cross sections again give a visual indication of the floes' snow thickness variation as well as the variation in their freeboard and keel relief.

To give an appreciation of the ice and snow thickness variation along each grid line at the first-year ridge, cross-section plots were made. These are presented in Figure 21 for lines A to K. In the area of the grid, the keel of the ridge was apparently in contact with the sea bed. Note the variations in ridge keel and sail geometry as well as in snow accumulation depths.

Averaging the cross section data by line groups A–K, C–I and E–G gives the cross sections shown in Figure 22. The ice sheet on the left of the ridge had a relatively uniform snow-ice thickness of about 1.45 m. The ice on the right side was about 15% thicker. Ice blocks in the ridge varied from 0.5 to 1.5 m in thickness.

It should be noted that unlike relatively solid

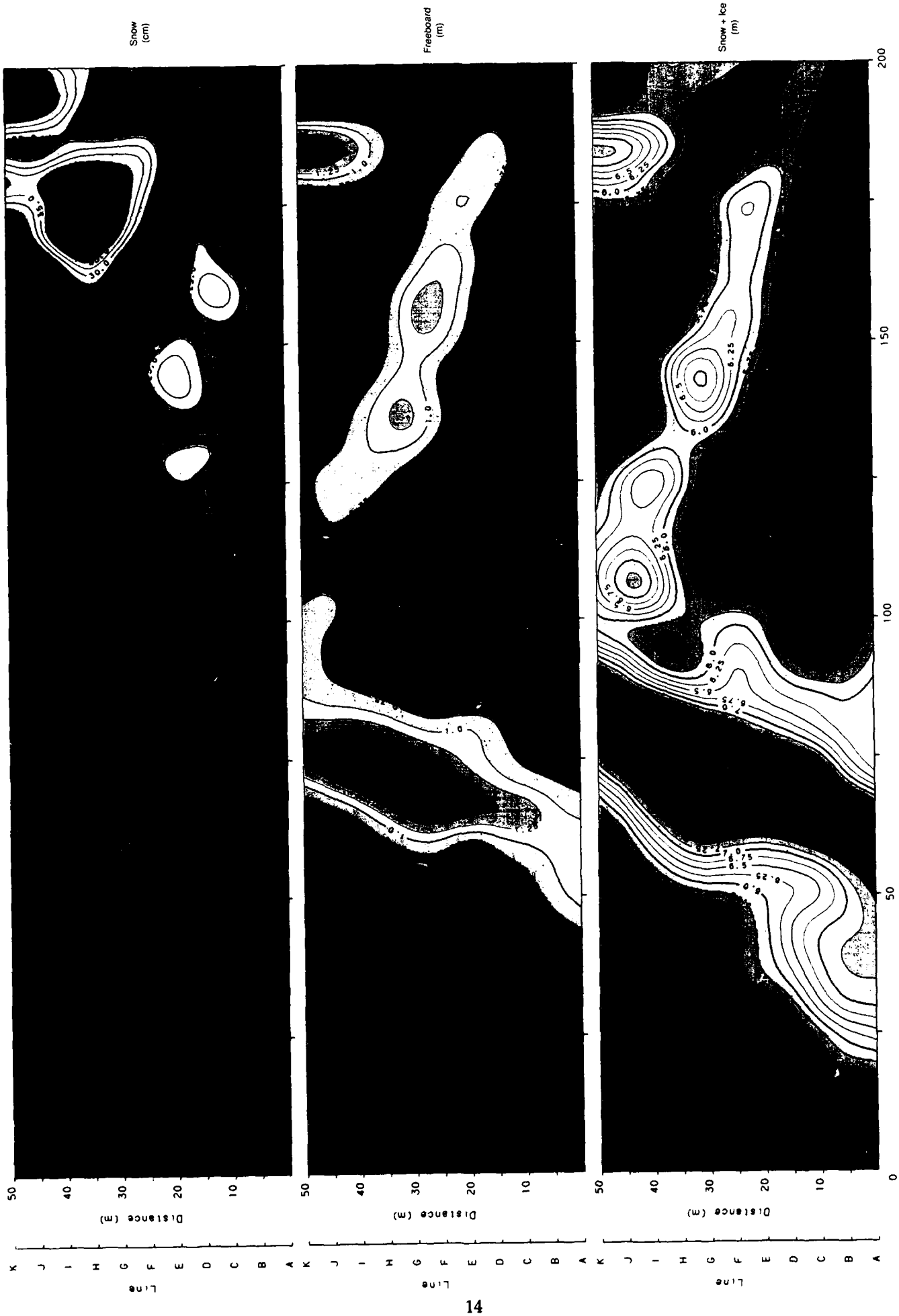

Figure 9. Snow, freeboard and snow plus ice thickness contour map of multiyear floe (courtesy Anthony Valentine).

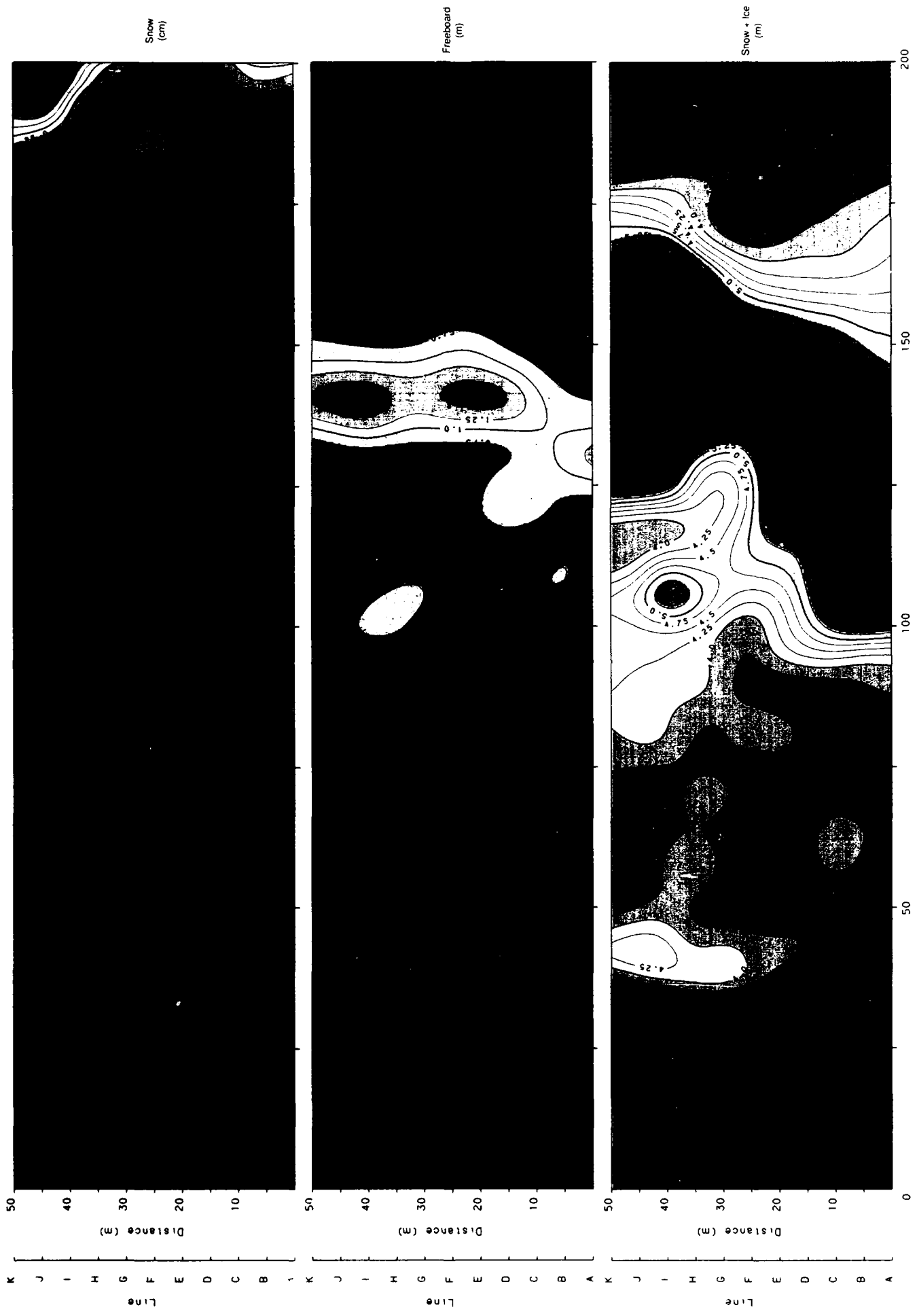

Figure 10. Snow, freeboard and snow plus ice thickness contour map of multiyear floe 3 (courtesy Anthony Valentine).

Table 3. Average row snow depth and ice thickness, freeboard and draft for lines A–K, C–I and E–G at multiyear floe grid site 1.

	Average of lines A–K				*Average of lines C–I*				*Average of Lines E–G*			
Row no. and dist. (m)	*Snow depth (m)*	*Ice thickness (m)*	*Free-board (m)*	*Keel depth (m)*	*Snow depth (m)*	*Ice thickness (m)*	*Free-board (m)*	*Keel depth (m)*	*Snow depth (m)*	*Ice thickness k (m)*	*Free-board (m)*	*Keel depth (m)*
0	0.07	5.95	0.66	5.29	0.05	6.00	0.67	5.34	0.05	5.53	0.59	4.93
5	0.06	6.21	0.82	5.39	0.06	5.59	0.70	4.88	0.09	4.63	0.42	4.21
10	0.12	5.56	0.83	4.73	0.10	4.76	0.56	4.20	0.10	4.22	0.36	3.86
15	0.07	4.85	0.62	4.23	0.05	4.17	0.43	3.75	0.06	3.81	0.42	3.39
20	0.09	4.16	0.44	3.72	0.11	3.68	0.32	3.36	0.15	3.30	0.23	3.08
25	0.10	3.70	0.36	3.34	0.10	3.23	0.32	2.91	0.07	3.05	0.36	2.69
30	0.13	3.28	0.25	3.03	0.14	2.86	0.24	2.62	0.19	2.81	0.29	2.52
35	0.13	3.30	0.26	3.04	0.16	2.92	0.18	2.74	0.17	3.08	0.24	2.84
40	0.15	3.50	0.25	3.25	0.19	3.32	0.17	3.15	0.29	3.40	0.09	3.30
45	0.12	4.33	0.46	3.87	0.13	4.39	0.48	3.91	0.14	4.62	0.51	4.11
50	0.05	4.87	0.67	4.20	0.03	5.04	0.72	4.32	0.03	5.19	0.64	4.55
55	0.11	4.67	0.61	4.06	0.10	4.81	0.62	4.19	0.11	4.73	0.34	4.39
60	0.11	4.30	0.46	3.83	0.14	4.41	0.40	4.01	0.15	4.58	0.22	4.36
65	0.13	3.98	0.36	3.63	0.11	4.19	0.38	3.81	0.11	4.55	0.34	4.20
70	0.11	3.98	0.41	3.57	0.09	4.16	0.45	3.70	0.09	4.42	0.51	3.92
75	0.15	3.93	0.37	3.56	0.20	3.94	0.36	3.59	0.07	4.18	0.51	3.67
80	0.08	3.76	0.42	3.34	0.10	3.79	0.40	3.39	0.10	3.93	0.39	3.54
85	0.17	2.85	0.24	2.61	0.17	2.86	0.23	2.63	0.04	3.49	0.45	3.05
90	0.12	2.50	0.23	2.27	0.16	2.22	0.16	2.06	0.18	1.83	0.11	1.73
95	0.09	2.22	0.17	2.05	0.10	2.11	0.18	1.92	0.06	2.00	0.14	1.87
100	0.13	2.18	0.17	2.01	0.12	2.11	0.18	1.93	0.07	1.98	0.10	1.87
105	0.15	2.21	0.16	2.05	0.16	2.02	0.15	1.87	0.09	1.96	0.08	1.88
110	0.19	2.30	0.14	2.16	0.24	2.13	0.10	2.03	0.22	2.01	0.09	1.93
115	0.15	2.89	0.27	2.62	0.15	2.83	0.24	2.59	0.12	2.85	0.30	2.55
120	0.16	3.38	0.32	3.06	0.11	3.54	0.36	3.18	0.04	3.50	0.40	3.10
125	0.13	3.35	0.33	3.02	0.16	3.27	0.29	2.98	0.10	3.03	0.26	2.78
130	0.10	3.31	0.33	2.98	0.08	3.14	0.33	2.81	0.11	2.44	0.21	2.23
135	0.12	3.24	0.30	2.94	0.16	3.00	0.26	2.74	0.14	2.66	0.26	2.40
140	0.15	2.91	0.26	2.64	0.17	2.78	0.28	2.50	0.24	2.29	0.19	2.10
145	0.13	2.87	0.25	2.62	0.13	2.82	0.27	2.54	0.26	2.24	0.02	2.22
150	0.14	2.40	0.26	2.14	0.13	2.39	0.27	2.12	0.18	2.28	0.24	2.04
155	0.16	2.01	0.16	1.85	0.14	2.11	0.19	1.93	0.14	2.37	0.34	2.02
160	0.10	2.49	0.21	2.28	0.14	2.49	0.18	2.31	0.18	3.04	0.29	2.75
165	0.14	2.55	0.20	2.36	0.14	2.53	0.19	2.34	0.19	2.47	0.12	2.36
170	0.12	2.81	0.27	2.54	0.14	2.72	0.22	2.50	0.22	2.39	0.09	2.30
175	0.08	2.98	0.33	2.65	0.08	3.10	0.33	2.77	0.08	3.03	0.33	2.70
180	0.10	2.69	0.27	2.43	0.09	2.85	0.31	2.54	0.04	3.22	0.41	2.80
185	0.14	2.06	0.10	1.96	0.13	2.00	0.12	1.88	0.11	2.01	0.17	1.84
190	0.12	2.70	0.21	2.49	0.09	2.63	0.22	2.41	0.07	2.56	0.23	2.33
195	0.07	2.95	0.31	2.64	0.08	2.78	0.30	2.48	0.09	2.79	0.29	2.50
200	0.13	2.60	0.22	2.38	0.13	2.58	0.21	2.37	0.06	2.63	0.27	2.36
205	0.15	2.67	0.21	2.46	0.07	2.75	0.25	2.50	0.08	2.83	0.28	2.55
210	0.10	2.86	0.30	2.56	0.07	2.87	0.29	2.58	0.08	2.66	0.26	2.40
215	0.16	2.68	0.21	2.47	0.13	2.83	0.26	2.58	0.26	2.54	0.09	2.45
220	0.17	2.64	0.21	2.43	0.15	2.76	0.23	2.53	0.12	3.11	0.31	2.80
225	0.19	3.01	0.26	2.76	0.17	3.17	0.29	2.88	0.08	3.49	0.45	3.04

Row no. and dist. (m)	Average of lines A–K: Snow depth (m)	Ice thickness (m)	Free-board (m)	Keel depth (m)	Average of lines C–I: Snow depth (m)	Ice thickness (m)	Free-board (m)	Keel depth (m)	Average of Lines E–G: Snow depth (m)	Ice thickness k (m)	Free-board (m)	Keel depth (m)
230	0.11	3.52	0.41	3.11	0.07	3.64	0.44	3.20	0.06	3.64	0.43	3.21
235	0.11	3.70	0.40	3.30	0.09	3.77	0.42	3.35	0.09	3.83	0.42	3.40
240	0.10	4.06	0.47	3.59	0.06	4.20	0.51	3.69	0.07	4.14	0.49	3.65
245	0.07	4.29	0.51	3.78	0.06	4.46	0.55	3.91	0.10	4.49	0.51	3.97
250	0.09	4.70	0.48	4.22	0.12	4.75	0.45	4.31	0.15	5.24	0.43	4.81
255	0.08	5.12	0.52	4.60	0.06	5.30	0.56	4.74	0.08	5.88	0.52	5.36
260	0.06	5.53	0.55	4.98	0.06	5.82	0.48	5.34	0.07	6.72	0.45	6.27
265	0.09	4.89	0.64	4.25	0.08	4.55	0.64	3.91	0.03	4.36	0.71	3.65
270	0.08	5.20	0.76	4.44	0.07	5.45	0.82	4.63	0.03	5.78	0.88	4.89
275	0.06	5.48	0.57	4.91	0.04	5.55	0.59	4.96	0.04	5.51	0.62	4.89
280	0.08	5.06	0.45	4.61	0.06	4.89	0.42	4.47	0.10	4.64	0.30	4.34
285	0.07	4.34	0.47	3.87	0.06	4.19	0.42	3.77	0.07	4.06	0.38	3.68
290	0.11	3.93	0.34	3.59	0.11	3.91	0.35	3.56	0.15	3.75	0.23	3.52
295	0.16	3.86	0.32	3.54	0.16	3.98	0.36	3.63	0.22	3.87	0.21	3.67
300	0.17	3.96	0.37	3.59	0.22	3.92	0.32	3.61	0.26	3.96	0.24	3.72
305	0.11	3.98	0.41	3.58	0.15	3.92	0.36	3.56	0.08	3.94	0.33	3.61
310	0.15	3.86	0.36	3.50	0.13	3.75	0.35	3.40	0.19	3.44	0.20	3.23
315	0.18	3.71	0.36	3.35	0.13	3.69	0.38	3.31	0.18	3.39	0.24	3.15
320	0.08	3.71	0.44	3.27	0.08	3.75	0.45	3.30	0.06	3.66	0.50	3.16
325	0.13	3.52	0.30	3.22	0.09	3.58	0.37	3.21	0.11	3.38	0.27	3.10
330	0.08	3.52	0.37	3.15	0.09	3.32	0.31	3.01	0.10	3.36	0.33	3.03
335	0.10	3.41	0.31	3.10	0.08	3.30	0.31	2.99	0.09	3.41	0.33	3.09
340	0.07	3.60	0.39	3.22	0.09	3.71	0.36	3.35	0.09	3.89	0.35	3.54
345	0.07	3.50	0.38	3.12	0.07	3.57	0.42	3.15	0.05	4.01	0.50	3.51
350	0.05	3.47	0.40	3.07	0.07	3.45	0.41	3.04	0.06	3.95	0.56	3.39
355	0.16	3.43	0.27	3.17	0.13	3.42	0.33	3.09	0.03	3.88	0.55	3.33
360	0.08	3.82	0.40	3.42	0.08	3.63	0.38	3.25	0.10	3.65	0.37	3.29
365	0.10	4.26	0.44	3.81	0.09	4.19	0.46	3.73	0.12	3.73	0.32	3.41
370	0.10	4.48	0.49	3.98	0.15	4.41	0.44	3.96	0.17	3.98	0.25	3.73
375	0.13	4.46	0.43	4.03	0.13	4.60	0.45	4.14	0.16	4.62	0.37	4.25
380	0.13	4.56	0.38	4.17	0.16	4.66	0.35	4.30	0.08	4.96	0.48	4.48
385	0.14	4.87	0.38	4.50	0.15	5.03	0.34	4.68	0.14	5.26	0.36	4.89
390	0.10	5.47	0.54	4.92	0.13	5.69	0.56	5.13	0.17	6.08	0.58	5.50
395	0.15	5.51	0.62	4.89	0.15	5.96	0.80	5.16	0.06	6.70	1.08	5.63
400	0.15	4.67	0.55	4.12	0.15	5.04	0.64	4.40	0.06	5.64	0.77	4.87
405	0.15	3.58	0.33	3.26	0.18	3.54	0.30	3.23	0.13	3.88	0.36	3.52
410	0.18	3.33	0.30	3.03	0.18	3.16	0.21	2.95	0.12	2.86	0.15	2.71
415	0.09	3.67	0.51	3.16	0.09	3.49	0.39	3.10	0.12	2.93	0.18	2.75
420	0.20	3.56	0.39	3.17	0.21	3.48	0.28	3.19	0.20	3.25	0.15	3.10
425	0.22	4.16	0.46	3.70	0.25	4.05	0.48	3.56	0.26	3.82	0.41	3.41
430	0.17	5.44	0.61	4.83	0.10	5.66	0.71	4.94	0.05	5.42	0.86	4.56
435	0.26	5.88	0.64	5.24	0.20	6.17	0.70	5.47	0.09	6.07	0.78	5.29
440	0.28	5.82	0.53	5.28	0.23	5.99	0.52	5.47	0.07	6.83	0.71	6.12
445	0.29	5.95	0.73	5.22	0.26	6.24	0.70	5.54	0.11	7.85	0.84	7.01
450	0.22	5.31	1.03	4.28	0.15	5.42	1.17	4.25	0.10	5.07	1.34	3.73
Avg.	0.13	3.83	0.4	3.44	0.12	3.81	0.39	3.42	0.12	3.83	0.38	3.45

Table 4. Average row snow depth and ice thickness, freeboard and draft for lines A–K, C–I and E–G at multiyear floe grid site 2.

	Average of lines A–K				*Average of lines C–I*				*Average of lines E–G*			
Row no. and dist. (m)	*Snow depth (m)*	*Ice thick. (m)*	*Free-board (m)*	*Keel depth (m)*	*Snow depth (m)*	*Ice thick. (m)*	*Free-board (m)*	*Keel depth (m)*	*Snow depth (m)*	*Ice thick. (m)*	*Free-board (m)*	*Keel depth (m)*
0	0.11	4.11	0.41	3.71	0.07	4.31	0.48	3.83	0.12	4.35	0.48	3.87
5	0.06	4.24	0.47	3.76	0.05	4.28	0.48	3.81	0.08	4.03	0.31	3.72
10	0.03	4.35	0.48	3.87	0.05	4.23	0.42	3.80	0.09	3.74	0.19	3.55
15	0.02	4.53	0.46	4.07	0.02	4.30	0.40	3.90	0.05	3.74	0.18	3.56
20	0.04	4.73	0.49	4.24	0.06	4.37	0.40	3.97	0.07	3.88	0.27	3.62
25	0.04	4.85	0.46	4.39	0.07	4.46	0.36	4.10	0.14	3.93	0.18	3.75
30	0.05	5.21	0.41	4.80	0.04	4.91	0.38	4.53	0.08	4.63	0.23	4.40
35	0.07	5.51	0.38	5.14	0.05	5.25	0.36	4.89	0.10	5.25	0.28	4.97
40	0.10	5.51	0.37	5.14	0.09	5.41	0.37	5.04	0.16	5.17	0.37	4.80
45	0.10	5.64	0.39	5.25	0.10	5.54	0.34	5.19	0.06	5.37	0.38	4.99
50	0.07	5.80	0.53	5.27	0.09	5.67	0.44	5.23	0.13	5.66	0.48	5.17
55	0.08	6.35	0.60	5.74	0.12	6.30	0.52	5.78	0.12	6.39	0.61	5.78
60	0.12	7.06	0.71	6.35	0.18	7.29	0.72	6.57	0.28	7.27	0.68	6.59
65	0.07	8.00	1.29	6.71	0.08	8.61	1.64	6.97	0.00	8.69	1.96	6.74
70	0.04	8.09	1.40	6.69	0.02	9.00	1.71	7.29	0.00	9.05	2.02	7.03
75	0.01	8.17	1.38	6.79	0.01	8.84	1.47	7.37	0.02	8.65	1.33	7.32
80	0.05	7.49	1.03	6.46	0.02	7.75	1.06	6.69	0.02	7.69	1.13	6.56
85	0.05	6.81	0.64	6.17	0.05	6.73	0.59	6.14	0.08	6.40	0.42	5.98
90	0.07	6.20	0.50	5.69	0.07	5.88	0.41	5.47	0.13	6.24	0.34	5.90
95	0.11	5.49	0.45	5.04	0.11	5.39	0.31	5.09	0.05	6.12	0.39	5.73
100	0.05	5.55	0.53	5.02	0.06	5.54	0.38	5.16	0.00	5.89	0.52	5.37
105	0.04	5.69	0.52	5.17	0.04	5.45	0.40	5.04	0.04	5.07	0.38	4.69
110	0.08	5.42	0.50	4.92	0.08	5.25	0.42	4.82	0.13	4.61	0.34	4.27
115	0.10	4.86	0.45	4.41	0.13	4.66	0.38	4.28	0.18	4.30	0.32	3.98
120	0.11	4.76	0.50	4.26	0.16	4.56	0.42	4.14	0.04	4.39	0.50	3.90
125	0.10	4.88	0.57	4.31	0.12	4.89	0.57	4.32	0.18	4.30	0.37	3.93
130	0.14	4.69	0.53	4.16	0.20	4.95	0.55	4.39	0.23	4.74	0.47	4.27
135	0.09	4.64	0.61	4.03	0.08	5.10	0.78	4.32	0.07	5.57	0.98	4.59
140	0.12	4.70	0.50	4.19	0.13	5.17	0.64	4.53	0.17	6.04	0.85	5.19
145	0.16	4.91	0.41	4.51	0.22	5.44	0.48	4.95	0.26	6.13	0.74	5.39
150	0.14	4.69	0.44	4.25	0.17	5.21	0.59	4.61	0.15	6.02	1.03	4.99
155	0.12	4.47	0.47	4.00	0.16	5.06	0.69	4.37	0.07	6.17	1.29	4.89
160	0.16	4.27	0.43	3.83	0.22	4.82	0.62	4.19	0.07	5.80	1.21	4.59
165	0.14	4.34	0.38	3.95	0.19	4.91	0.57	4.34	0.01	5.90	1.05	4.85
170	0.31	4.37	0.31	4.06	0.40	4.78	0.43	4.35	0.27	5.59	0.74	4.84
175	0.27	4.93	0.49	4.44	0.30	5.36	0.66	4.70	0.27	5.84	0.93	4.91
180	0.29	5.02	0.65	4.37	0.31	5.03	0.66	4.37	0.31	5.08	0.59	4.49
185	0.18	5.74	1.04	4.70	0.22	5.42	0.82	4.60	0.29	4.81	0.54	4.27
190	0.20	5.11	0.50	4.62	0.15	5.25	0.56	4.69	0.13	4.98	0.43	4.55
195	0.28	5.00	0.33	4.67	0.23	5.29	0.38	4.91	0.10	5.18	0.37	4.81
200	0.18	4.94	0.37	4.57	0.18	5.49	0.41	5.07	0.22	5.46	0.26	5.21
Avg.	0.11	5.39	0.57	4.82	0.12	5.52	0.59	4.92	0.12	5.56	0.64	4.93

Table 5. Average row snow depth and ice thickness, freeboard and draft for lines A–K, C–I and E–G at multiyear floe grid site 3.

	Average of Lines A-K				Average of Lines C-I				Average of Lines E-G			
Row no. and dist (m)	Snow depth (m)	Ice thickness (m)	Free-board (m)	Keel depth (m)	Snow depth (m)	Ice thickness (m)	Free-board (m)	Keel depth (m)	Snow depth (m)	Ice thickness (m)	Free-board (m)	Keel depth (m)
0	0.08	3.07	0.28	2.79	0.04	3.32	0.34	2.97	0.05	3.40	0.38	3.02
5	0.07	3.14	0.33	2.81	0.04	3.43	0.40	3.03	0.03	3.51	0.41	3.10
10	0.02	3.23	0.40	2.84	0.01	3.50	0.45	3.06	0.01	3.66	0.53	3.13
15	0.03	3.05	0.31	2.74	0.03	3.25	0.35	2.90	0.00	3.69	0.54	3.16
20	0.08	2.45	0.16	2.28	0.11	2.52	0.14	2.39	0.20	2.63	0.09	2.54
25	0.09	1.94	0.10	1.84	0.09	2.04	0.13	1.91	0.05	1.94	0.16	1.78
30	0.09	2.53	0.40	2.13	0.10	2.51	0.37	2.14	0.11	2.37	0.28	2.09
35	0.09	3.42	0.28	3.14	0.11	3.55	0.25	3.30	0.12	3.57	0.31	3.26
40	0.04	3.83	0.43	3.40	0.03	3.92	0.51	3.41	0.00	4.11	0.59	3.52
45	0.06	3.69	0.30	3.39	0.07	3.76	0.26	3.50	0.04	3.83	0.29	3.54
50	0.04	3.45	0.39	3.06	0.02	3.48	0.40	3.08	0.04	3.19	0.21	2.98
55	0.06	3.54	0.43	3.12	0.03	3.63	0.49	3.14	0.07	3.37	0.33	3.04
60	0.05	3.57	0.44	3.13	0.04	3.65	0.51	3.14	0.07	3.42	0.34	3.08
65	0.05	3.57	0.44	3.13	0.08	3.5[illegible]	0.41	3.13	0.14	3.29	0.21	3.07
70	0.08	3.49	0.36	3.13	0.05	3.58	0.43	3.15	0.00	3.59	0.49	3.10
75	0.05	3.42	0.32	3.10	0.03	3.42	0.34	3.08	0.04	3.38	0.40	2.99
80	0.10	3.69	0.39	3.31	0.11	3.73	0.39	3.34	0.07	4.08	0.47	3.60
85	0.13	3.63	0.34	3.29	0.11	3.57	0.29	3.28	0.15	3.57	0.31	3.27
90	0.08	3.78	0.43	3.36	0.09	3.69	0.42	3.27	0.15	3.43	0.22	3.21
95	0.05	4.10	0.56	3.55	0.04	4.10	0.53	3.57	0.00	3.93	0.59	3.34
100	0.06	4.65	0.56	4.09	0.04	4.43	0.58	3.85	0.07	3.82	0.36	3.46
105	0.01	5.31	0.63	4.68	0.02	5.20	0.70	4.50	0.01	4.41	0.58	3.83
110	0.05	5.02	0.49	4.53	0.06	5.13	0.51	4.61	0.01	4.84	0.54	4.30
115	0.11	4.67	0.34	4.33	0.16	4.70	0.29	4.41	0.16	4.85	0.32	4.53
120	0.05	5.00	0.50	4.50	0.05	5.10	0.58	4.52	0.12	4.88	0.36	4.53
125	0.05	5.88	0.57	5.31	0.05	5.62	0.55	5.08	0.05	4.99	0.42	4.57
130	0.06	6.21	0.72	5.49	0.05	6.00	0.58	5.41	0.06	5.31	0.59	4.73
135	0.08	6.82	0.98	5.83	0.06	6.89	1.02	5.87	0.14	5.82	0.87	4.95
140	0.01	8.06	1.53	6.52	0.00	8.24	1.67	6.57	0.01	8.02	1.74	6.28
145	0.03	7.26	1.06	6.21	0.02	7.50	1.15	6.35	0.03	7.67	1.28	6.39
150	0.02	6.30	0.68	5.63	0.03	6.34	0.72	5.62	0.03	6.56	0.86	5.70
155	0.04	5.83	0.48	5.35	0.04	5.80	0.45	5.35	0.02	5.67	0.56	5.12
160	0.06	5.39	0.38	5.01	0.07	5.28	0.33	4.95	0.05	4.65	0.41	4.24
165	0.08	4.72	0.32	4.40	0.09	4.59	0.26	4.33	0.12	4.01	0.25	3.76
170	0.07	4.01	0.30	3.71	0.09	3.74	0.20	3.54	0.07	3.36	0.13	3.23
175	0.07	3.88	0.40	3.49	0.07	3.66	0.33	3.33	0.03	3.42	0.19	3.22
180	0.09	3.52	0.35	3.16	0.13	3.57	0.30	3.27	0.13	3.55	0.25	3.30
185	0.15	3.06	0.36	2.71	0.17	3.03	0.41	2.61	0.23	2.75	0.40	2.35
190	0.17	2.81	0.28	2.53	0.09	2.63	0.34	2.29	0.14	2.19	0.18	2.01
195	0.23	2.32	0.21	2.10	0.15	2.33	0.25	2.09	0.13	2.31	0.25	2.06
200	0.39	2.00	0.17	1.83	0.31	2.27	0.20	2.07	0.22	2.51	0.23	2.28
Avg.	0.08	4.13	0.45	3.68	0.07	4.15	0.46	3.69	0.08	3.99	0.44	3.55

Table 6. Average row snow depth and ice thickness, freeboard and draft for lines A–K, C–I and E–G at the first-year pressure ridge grid site.

Row no. and dist. (m)	Average of Lines A–K				Average of Lines C–I				Average of Lines E–G			
	Snow depth (m)	Ice thickness (m)	Free-board (m)	Keel depth (m)	Snow depth (m)	Ice thickness (m)	Free-board (m)	Keel depth (m)	Snow depth (m)	Ice thickness (m)	Free-board (m)	Keel depth (m)
0	0.06	1.45	0.13	1.32	0.07	1.44	0.14	1.30	0.06	1.45	0.15	1.30
5	0.06	1.46	0.13	1.33	0.06	1.45	0.13	1.32	0.06	1.43	0.12	1.31
10	0.06	1.49	0.14	1.36	0.07	1.49	0.14	1.36	0.09	1.49	0.12	1.37
15	0.05	1.45	0.12	1.34	0.06	1.45	0.12	1.34	0.10	1.39	0.11	1.29
20	0.06	1.44	0.11	1.33	0.06	1.43	0.11	1.32	0.06	1.42	0.11	1.31
25	0.04	1.43	0.13	1.30	0.05	1.44	0.14	1.30	0.04	1.45	0.13	1.32
30	0.06	1.38	0.14	1.24	0.08	1.37	0.13	1.24	0.10	1.35	0.13	1.22
35	0.06	1.40	0.12	1.28	0.06	1.41	0.12	1.29	0.06	1.41	0.11	1.31
40	0.06	2.33	0.08	2.24	0.08	2.34	0.07	2.28	0.08	2.28	0.07	2.20
45	0.35	4.30	–0.05	4.35	0.39	4.08	–0.05	4.13	0.35	3.75	–0.05	3.80
50	0.27	7.66	0.35	7.31	0.42	6.94	0.28	6.67	0.60	6.62	0.08	6.54
55	0.37	9.76	0.74	9.01	0.48	9.25	0.88	8.37	0.64	7.99	0.75	7.24
60	0.13	14.24	1.88	12.36	0.15	12.76	1.55	11.21	0.17	13.13	1.32	11.82
65	0.11	17.55	3.35	14.21	0.11	17.75	3.29	14.46	0.13	16.98	2.94	14.04
70	0.12	16.72	3.63	13.09	0.14	18.18	4.57	13.61	0.12	18.94	4.11	14.83
75	0.16	12.72	1.35	11.37	0.13	13.86	1.62	12.24	0.12	13.38	1.60	11.78
80	0.16	11.38	0.75	10.63	0.19	11.14	0.71	10.43	0.19	9.85	0.64	9.20
85	0.16	8.04	0.68	7.36	0.14	7.55	0.76	6.79	0.14	7.89	0.96	6.93
90	0.15	7.05	0.47	6.58	0.20	6.79	0.52	6.27	0.29	8.11	0.62	7.48
95	0.12	2.63	0.30	2.34	0.10	2.62	0.30	2.32	0.09	2.59	0.29	2.30
100	0.18	1.89	0.10	1.80	0.17	1.78	0.08	1.70	0.11	1.90	0.13	1.77
105	0.13	2.26	0.16	2.10	0.09	2.12	0.13	1.99	0.08	2.01	0.14	1.87
110	0.13	2.09	0.16	1.93	0.14	2.06	0.14	1.91	0.14	2.28	0.16	2.11
115	0.16	2.09	0.16	1.93	0.16	2.02	0.16	1.87	0.13	2.12	0.14	1.98
120	0.10	1.91	0.15	1.76	0.10	1.89	0.15	1.75	0.12	1.91	0.16	1.75
125	0.11	1.90	0.14	1.76	0.10	1.88	0.14	1.74	0.14	1.77	0.10	1.67
130	0.09	1.95	0.17	1.78	0.09	1.92	0.17	1.75	0.06	1.85	0.14	1.71
135	0.10	1.85	0.16	1.69	0.10	1.86	0.16	1.70	0.10	1.75	0.15	1.61
140	0.08	1.81	0.15	1.66	0.09	1.82	0.15	1.67	0.09	1.74	0.14	1.61
145	0.09	1.81	0.14	1.67	0.08	1.79	0.14	1.65	0.08	1.74	0.13	1.61
150	0.07	1.92	0.18	1.74	0.08	1.84	0.17	1.67	0.11	1.79	0.16	1.64
155	0.06	1.91	0.17	1.74	0.06	1.86	0.16	1.70	0.06	1.84	0.15	1.68
160	0.07	1.88	0.18	1.70	0.07	1.90	0.20	1.70	0.08	1.90	0.24	1.66
165	0.07	1.91	0.19	1.73	0.07	1.97	0.20	1.77	0.06	1.97	0.18	1.79
170	0.07	2.02	0.19	1.83	0.08	2.04	0.19	1.85	0.05	1.96	0.18	1.78
175	0.08	1.97	0.19	1.78	0.08	2.03	0.21	1.83	0.09	1.89	0.14	1.76
180	0.09	1.93	0.15	1.78	0.11	1.96	0.15	1.81	0.10	1.84	0.15	1.69
185	0.07	2.00	0.19	1.81	0.07	2.07	0.21	1.86	0.08	2.07	0.24	1.84
190	0.06	2.01	0.20	1.81	0.06	2.09	0.20	1.89	0.08	2.16	0.17	1.99
195	0.07	2.02	0.17	1.85	0.06	2.13	0.19	1.94	0.08	2.33	0.25	2.08
200	0.07	2.01	0.20	1.81	0.08	2.10	0.22	1.88	0.09	2.35	0.31	2.04
205	0.07	1.85	0.16	1.68	0.06	1.90	0.18	1.71	0.04	2.00	0.22	1.79
210	0.07	1.76	0.16	1.60	0.08	1.75	0.16	1.60	0.08	1.74	0.15	1.59
215	0.08	1.90	0.18	1.72	0.08	1.76	0.19	1.58	0.09	1.76	0.20	1.55
220	0.10	1.76	0.14	1.62	0.08	1.70	0.13	1.57	0.00	1.71	0.13	1.58
225	0.15	3.26	0.30	2.96	0.15	3.15	0.28	2.87	0.16	3.41	0.36	3.05
230	0.20	3.11	0.37	2.74	0.21	3.17	0.39	2.78	0.17	3.93	0.42	3.51
Avg.	0.11	3.84	0.41	3.43	0.12	3.82	0.43	3.38	0.13	3.80	0.41	3.39

Table 7. Ice and snow variation in the mean drill hole measured data between line groups E–G, C–I and A–K for the grids at the three multiyear (MY) ice floes and the first-year pressure ridge (FYR) site.

		Snow thickness		S-I thickness		Ice thickness		Ice-freeboard		Ice draft	
Grid site	Grid lines	Mean (m)	Std. dev. (m)	Mean (m)	Std. dev. (m)	Mean (m)	Std. dev. (m)	Mean (m)	Std. dev. (m)	Mean (m)	Std. dev. (m)
MY 1	E-G	0.115	0.092	3.945	1.369	3.830	1.390	0.380	0.260	3.450	1.221
MY 1	C-I	0.122	0.110	3.934	1.318	3.812	1.338	0.391	0.265	3.421	1.158
MY 1	A-K	0.125	0.118	3.958	1.314	3.833	1.330	0.397	0.274	3.436	1.140
MY 2	E-G	0.121	0.144	5.685	1.341	5.564	1.378	0.637	0.515	4.927	1.025
MY 2	C-I	0.124	0.158	5.639	1.394	5.516	1.434	0.593	0.470	4.923	1.106
MY 2	A-K	0.111	0.146	5.505	1.444	5.394	1.472	0.570	0.456	4.823	1.155
MY 3	E-G	0.077	0.091	4.067	1.353	3.989	1.383	0.437	0.337	3.553	1.124
MY 3	C-I	0.073	0.094	4.225	1.506	4.152	1.536	0.460	0.341	3.693	1.299
MY 3	A-K	0.079	0.109	4.209	1.543	4.130	1.578	0.448	0.334	3.681	1.341
FYR	E-G	0.129	0.141	3.929	4.280	3.801	4.240	0.412	0.757	3.389	3.591
FYR	C-I	0.120	0.133	3.935	4.351	3.816	4.320	0.433	0.842	3.382	3.616
FYR	A-K	0.111	0.118	3.955	4.326	3.844	4.301	0.412	0.789	3.432	3.662

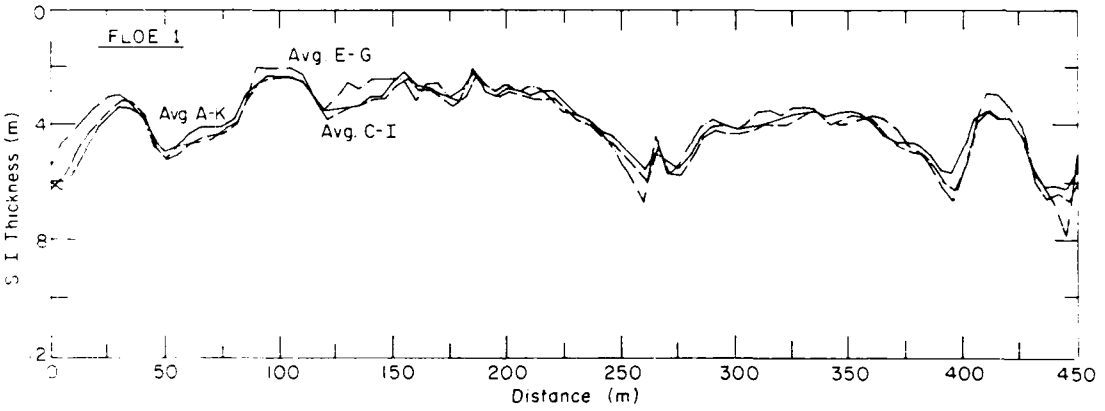

Figure 11. Average snow plus ice thickness along MY floe 1's 50- × 450-m grid. Profile A–K represents the full 50-m width of the grid, C–I the center 30-m width and E–G the center 10-m width.

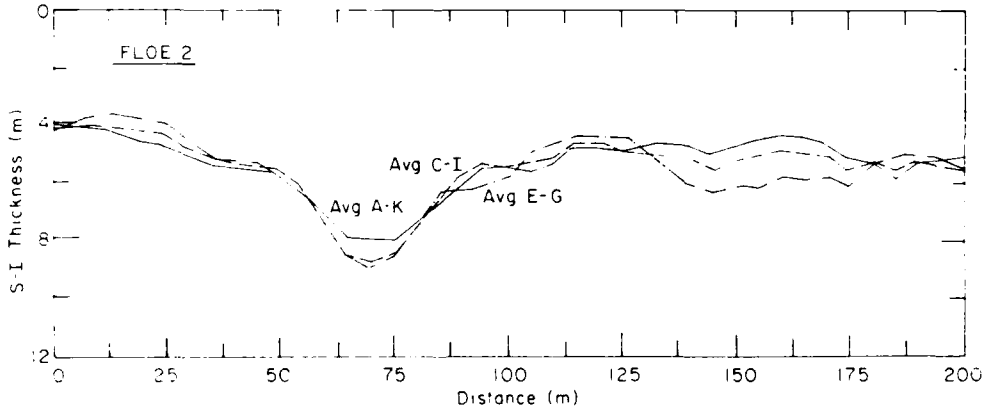

Figure 12. Average snow plus ice thickness along MY floe 2's 50- × 200-m grid for swath widths A–K, C–I and E–G.

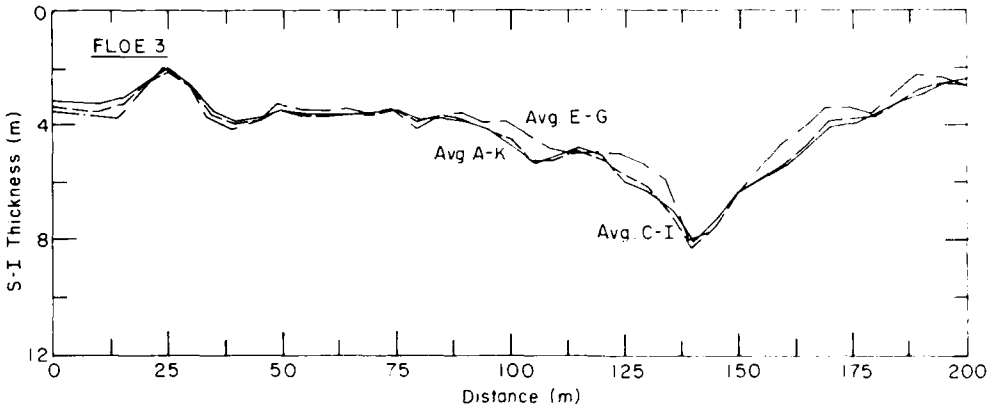

Figure 13. Average snow plus ice thickness along MY floe 3's 50- × 200-m grid for swath widths A–K, C–I and E–G.

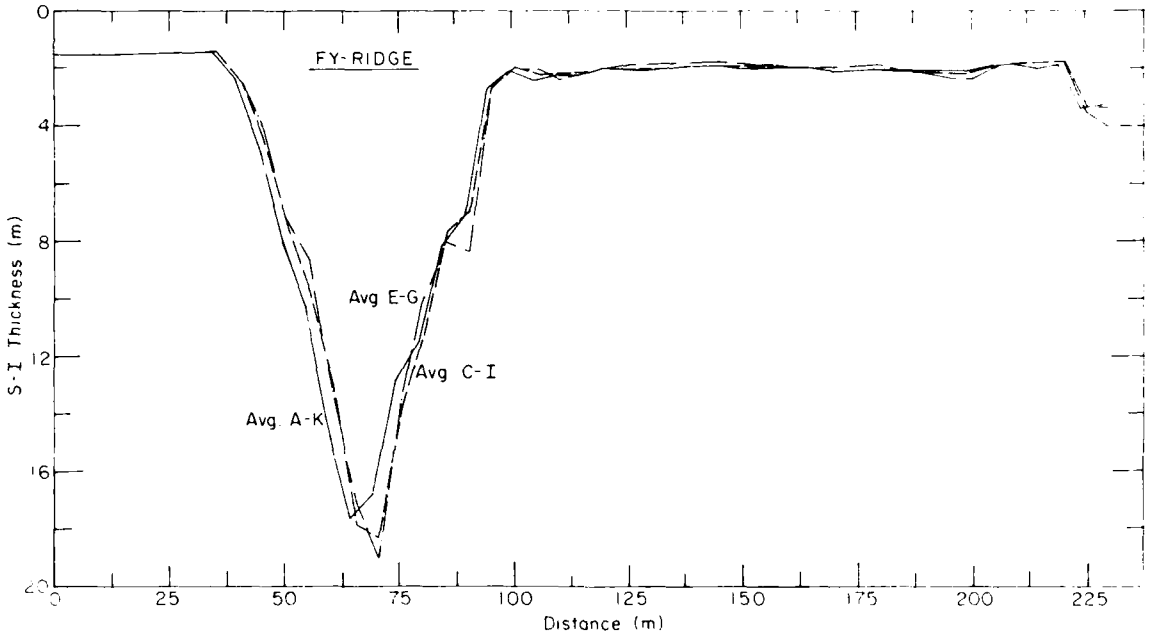

Figure 14. Average snow plus ice thickness along the FY-ridge 50- ×225-m grid for swath widths A–K, C–I and E–G.

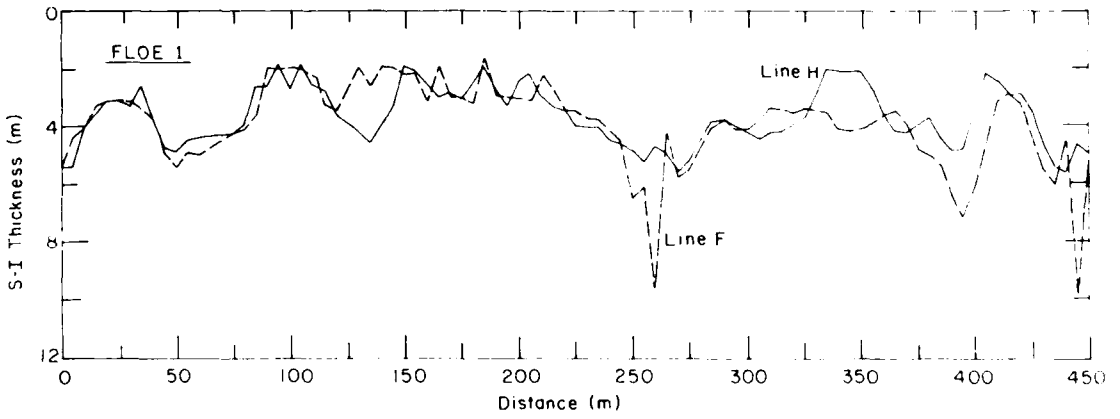

Figure 15. Example of snow plus ice thickness variations along MY floe 1's grid for lines F and H (see Fig. 6 for line location).

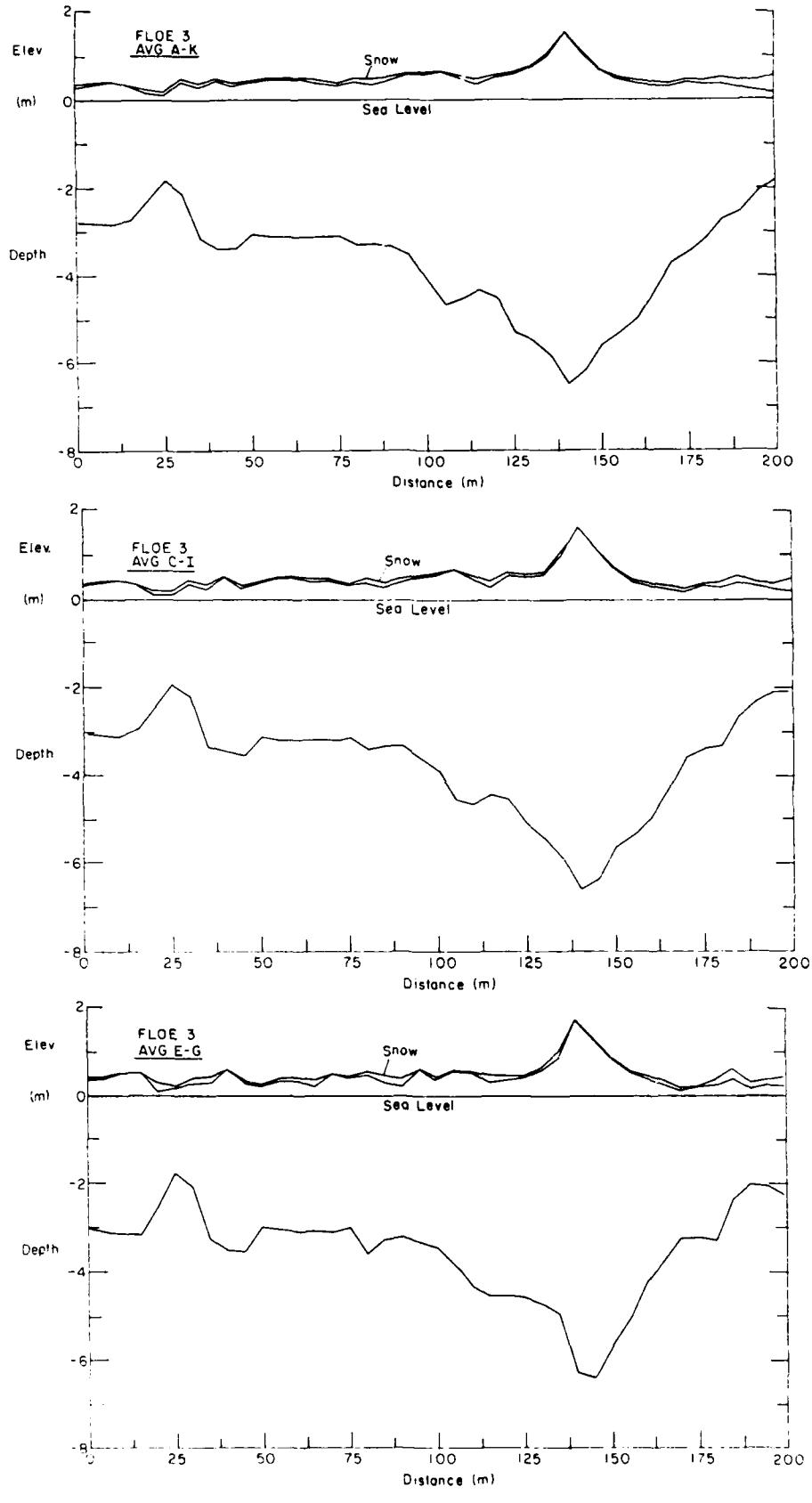

Figure 20. Cross section along MY floe 3's grid for swath widths A–K, C–I and E–G (see Fig. 8).

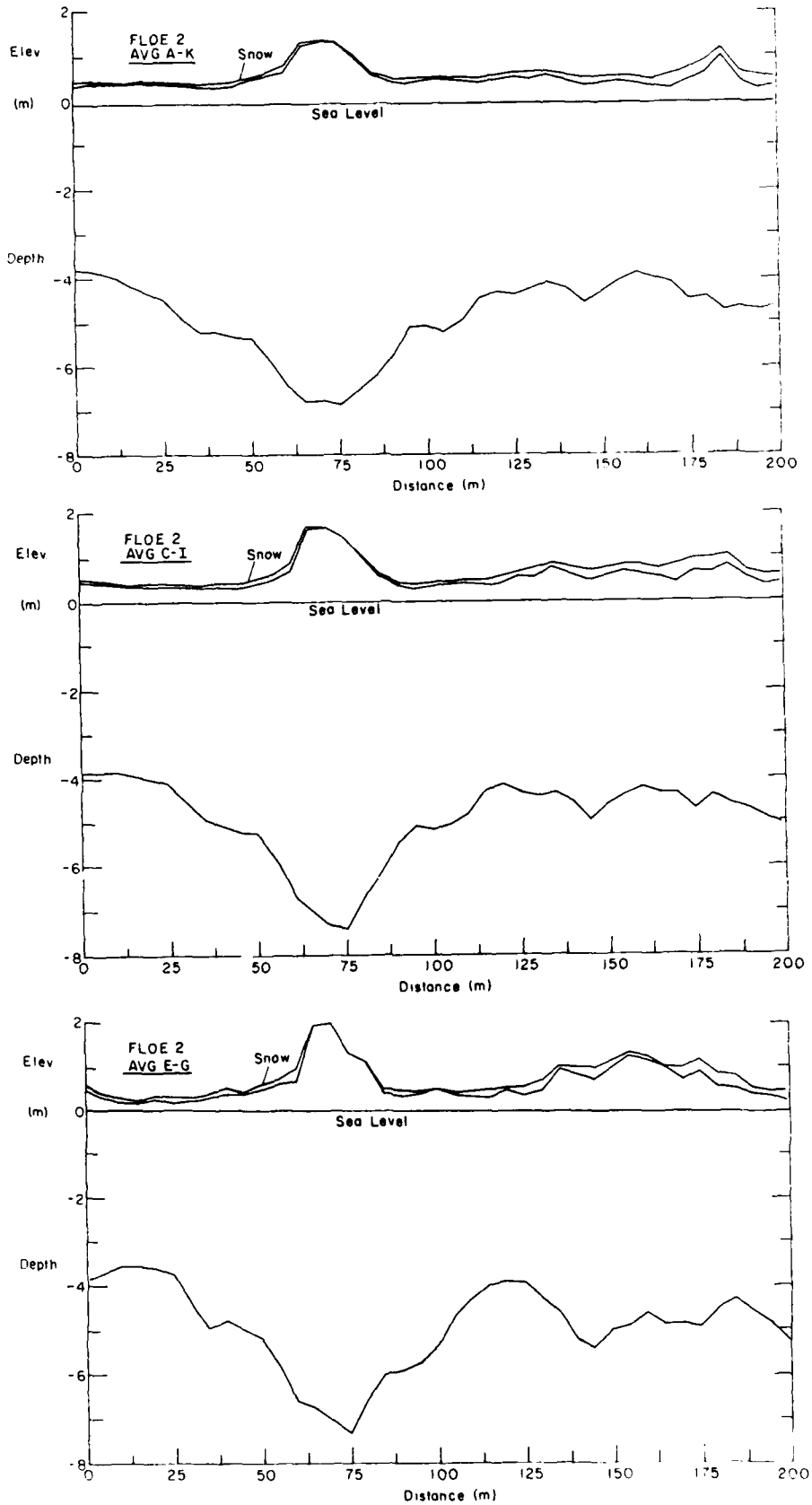

Figure 19. Cross section along MY floe 2's grid for swath widths A–K, C–I and E–G (see Fig. 7).

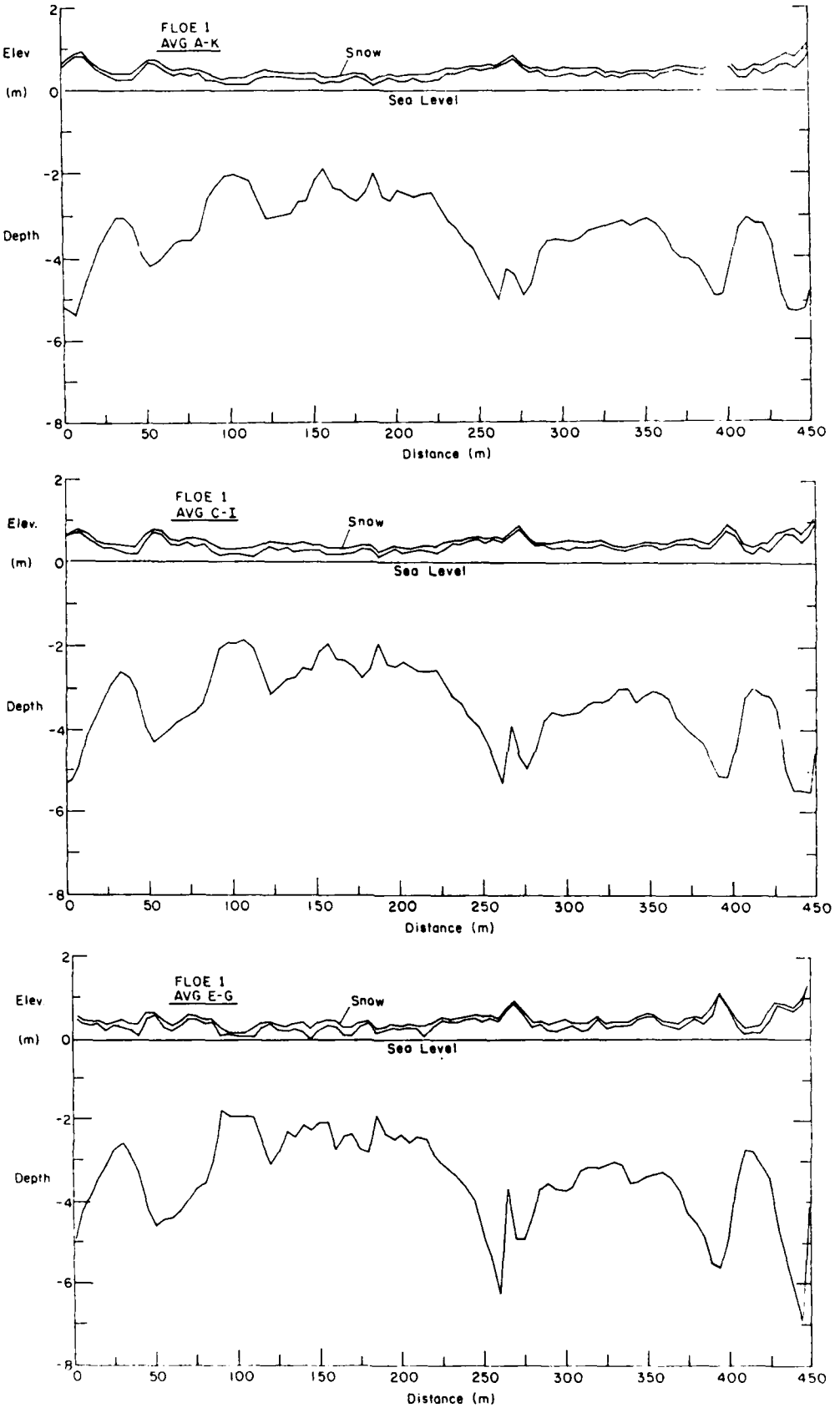

Figure 18. Cross section along MY floe 1's grid for swath widths A–K, C–I and E–G (see Fig. 6).

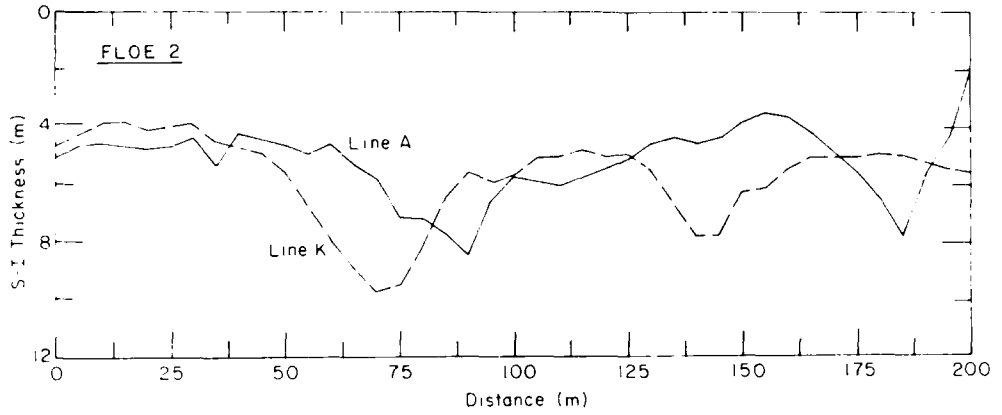

Figure 16. Example of snow plus ice thickness variation along MY floe 2's grid for lines A and K (see Fig. 7 for line location).

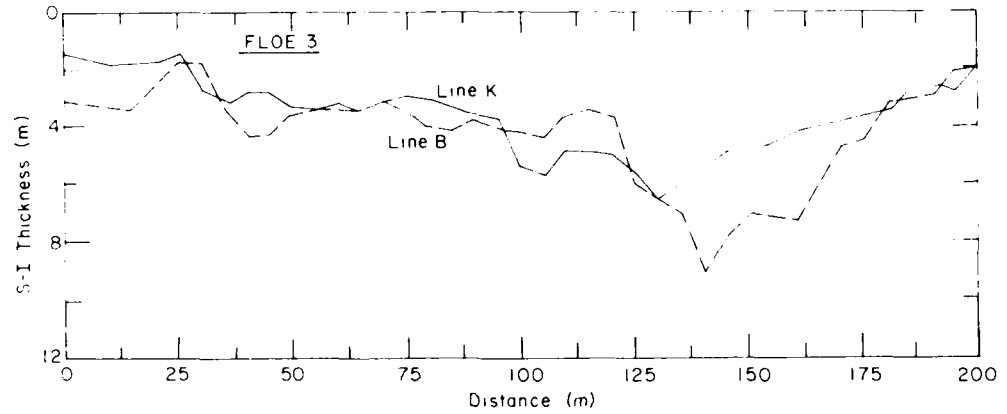

Figure 17. Example of snow plus ice thickness variation along MY floe 3's grid for lines B and K (see Fig. 8 for line location).

multiyear pressure ridges, first-year ridges are a conglomerate of ice blocks and fragments. Air fills the inter-block voids of the sail and seawater fills the voids of the keel extending below the "solidification" zone, a seawater freezeback zone extending to about the depth of the adjoining level ice. The EM secondary field associated with this high conductivity keel structure is different from that associated with the low seawater or brine content and therefore lower conductivity of a multiyear ridge keel. Analysis of the EM data taken over the first-year ridge is more ambiguous because there is no well-defined ice/water interface and is further complicated by the relatively narrow width and steep slope of the keel (= 30), its three-dimensional geometric variation and the proximity of another conductive zone, the sea bed.

Floe freeboard vs thickness analysis

The drill hole data for the multiyear floes, listed in Tables 3, 4 and 5, were used to assess the average density of the ice floes and their equivalent freeboard vs draft. The equivalent freeboard is determined by converting the snow cover depth into an equivalent ice thickness and adding this value to the measured ice freeboard. The average snow cover was of unusually low density. Indeed, almost all of it was blown away during a period of high winds at the end of our field program. The average measured snow specific gravity ρ_f for the snow was 0.318 and for the freeboard ice it was 0.880. Therefore, each unit of snow depth is equivalent to 0.364 unit of freeboard ice. For all lines (A–K) on multiyear floe 1, the average snow depth was 0.125 m, which is equivalent to 0.046 m of freeboard ice. The average measured ice freeboard was 0.397 m and the equivalent freeboard F_e now becomes 0.443 m. The average ice draft D was 3.436 m, which gives for F_e/D a value of 0.129 or a ratio of 1 to 7.756. Buoyancy considerations dictate that

$$\frac{F_e}{D} + 1 = \frac{\rho_w}{\rho_i} \qquad (1)$$

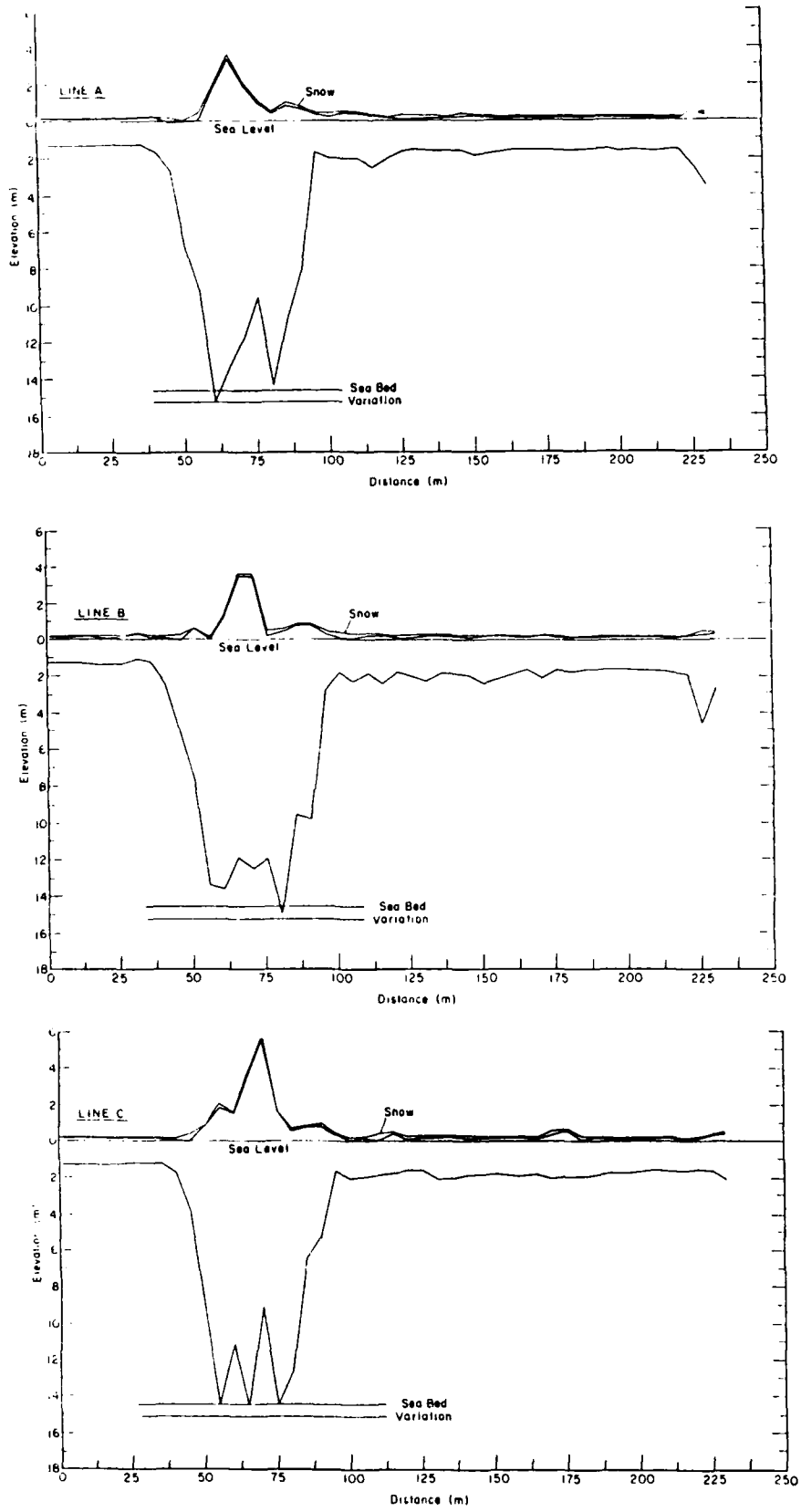

Figure 21. Cross section along FY ridge grid for lines A–K. Note the variations in the ridge keel from line to line (5-m spacing).

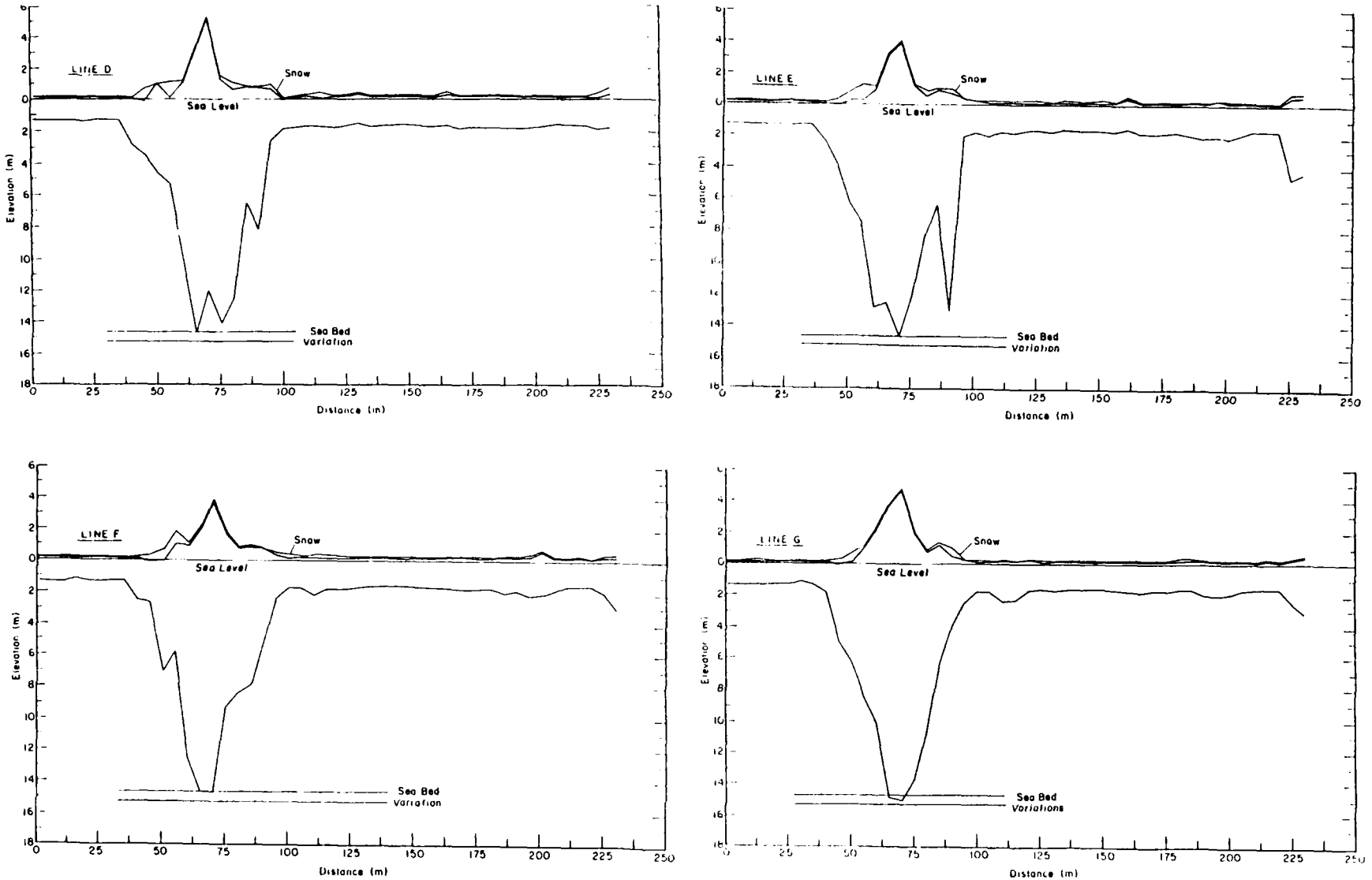

Figure 21 (cont'd). Cross section along FY ridge grid for lines A through K. Note the variations in the ridge keel from line to line (5-m spacing).

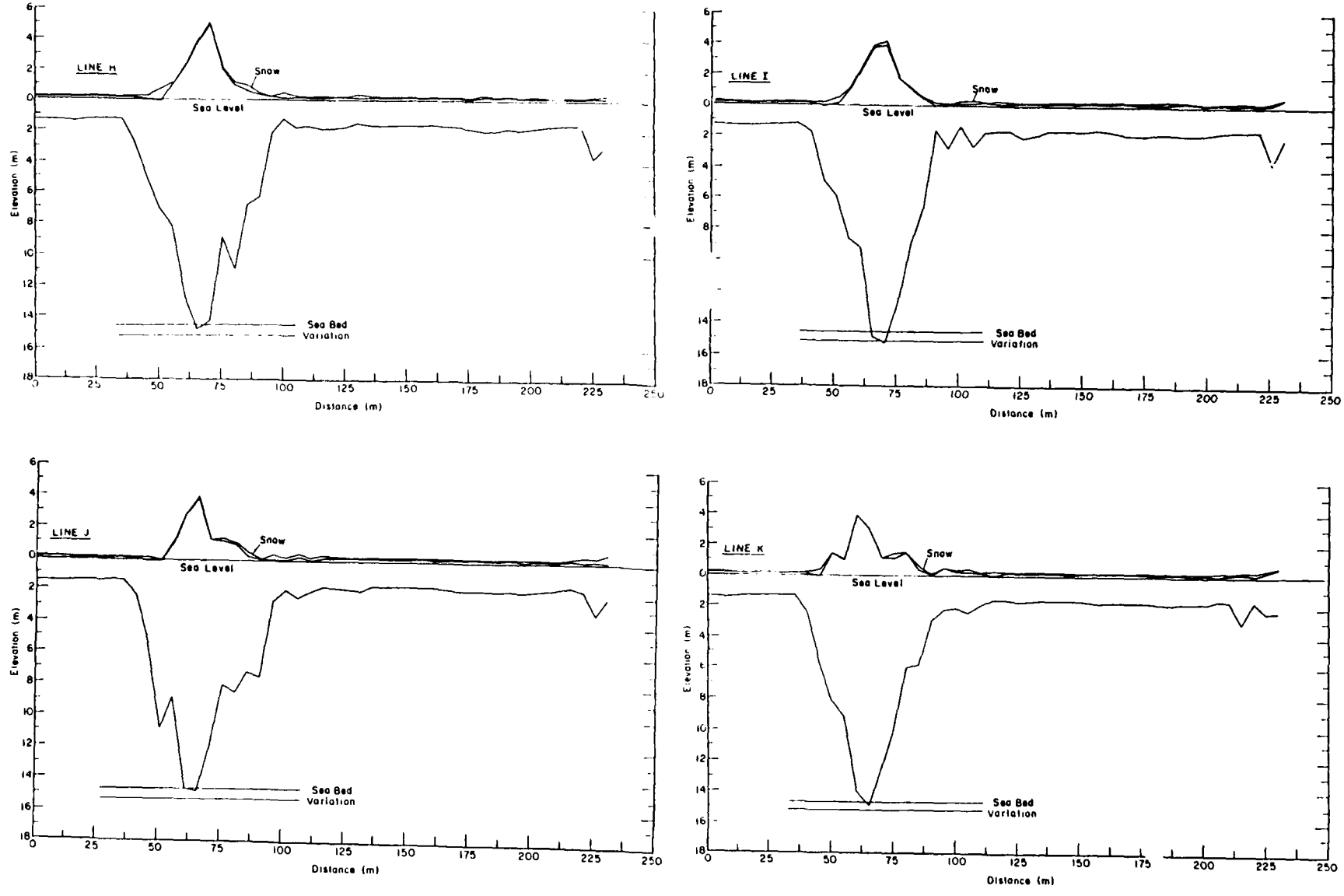

Figure 21 (cont'd).

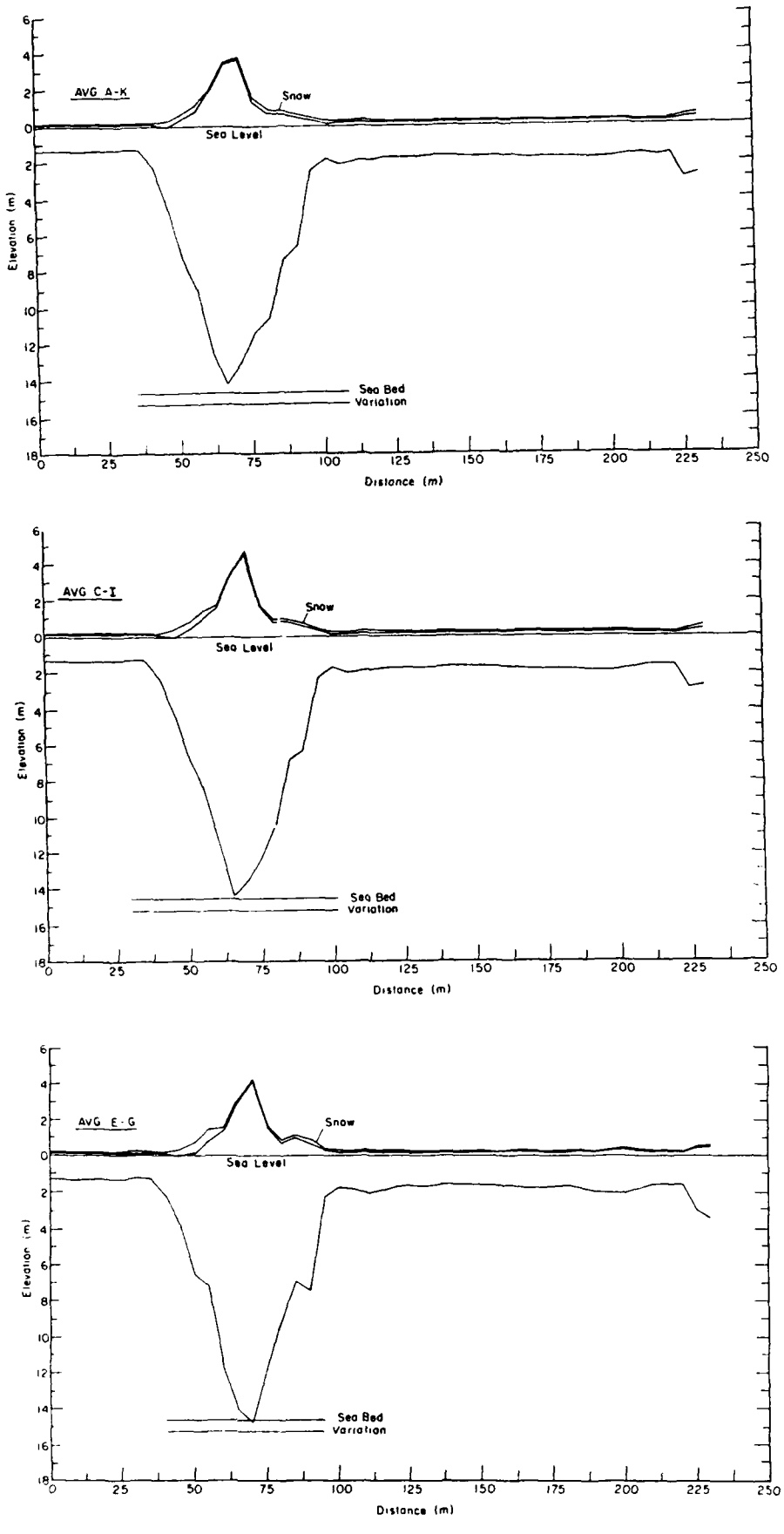

Figure 22. Cross section along the FY ridge grid for swath widths A–K, C–I and E–G.

where ρ_w is the specific gravity of seawater and ρ_i is the equivalent specific gravity of the ice floe. The seawater salinity Sw (in parts per thousand) was measured as 31.5‰. Since $\rho_w = 1 + 0.0008$ Sw, the specific gravity of the seawater was 1.025 and, and, from 1, ρ_i is found to be 0.908. The apparent specific gravity of the submerged ice ρ_s may be found from

$$\rho_s = \rho_w - \rho_i (F_e/D). \quad (2)$$

Substituting 0.880 for ρ_f, 1.025 for ρ_w and 0.129 for F_e/D in eq 2, a value of 0.912 for ρ_s is obtained.

Making similar calculations for the lines A–K on multiyear floe 2 gives 0.126 for $F_e/D = 0.910$ for ρ_i and 0.914 for ρ_s. For the lines on multiyear floe 3 the values are 0.130 for F_e/D, 0.907 for ρ_i and 0.911 for ρ_s. The variation in the above values is due in part to ice and snow property variations between the ice floes, to spatial relief variations along each grid and to abrupt F_e/D variations at the transition area between a ridge sail and the surrounding ice floe, as may be inferred from the Kovacs first-year and multiyear pressure ridge models (Wright et al. 1981) shown in Figure 23. Large pressure ridges are known to have proportionally less dense ice in the ridge sails and increasing ice density with depth in the keel. Such density variation can upset the average ratio of ice freeboard to equivalent draft of ~1:7.8 which can be determined from the F_e vs D values. It is known, for example, that the mean freeboard/draft ratio, obtained from sail height and keel draft measurements, of multiyear pressure ridges is ~1:3.2 as shown in Figure 24. Ridges in the floes studied may have biased the equivalent freeboard/ice draft results in favor of the lower elevation portion of the ice floes. This is indicated in a plot of the average grid row F_e vs D values which are listed in Table 8 and plotted in Figure 23. The data in Figure 25 indicate that for ice drafts over about 6.5 m there is a marked increase in F_e/D. The deep draft data, as presented in this figure, are simply too limited to support this view. The analysis for the line passing through the data in Figure 25 did not include the four data points for ice drafts over 6.5 m. Because of this, the slope of the line shown (0.125) is lower than the average of 0.128 for the three F_e/D. values previously presented. Using a value of 0.125 for F_e/D. and ρ_w of 1.025 in eq 1 gives a value of 0.911 for ρ_i.

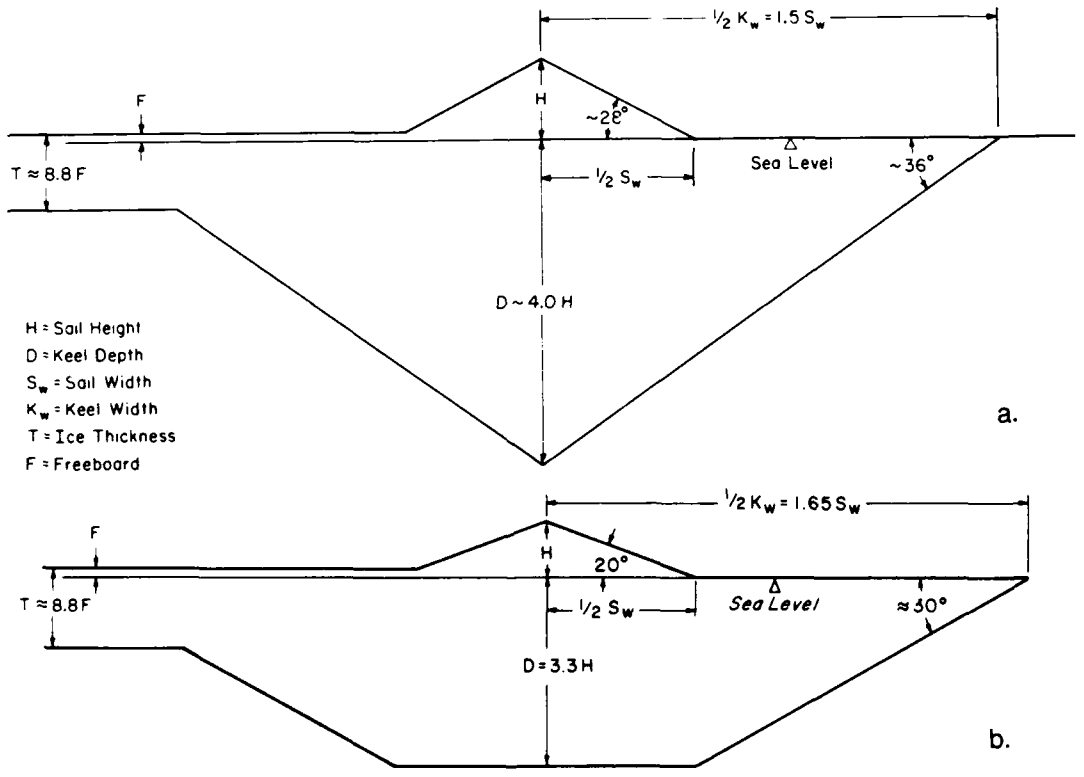

Figure 23. Kovacs first-year (a) and multiyear (b) pressure ridge models. These idealized models are in hydrostatic equilibrium for the conditions when $\rho_i = 0.92$ and $\rho_w = 1.025$ for seawater of salinity = 31.5‰

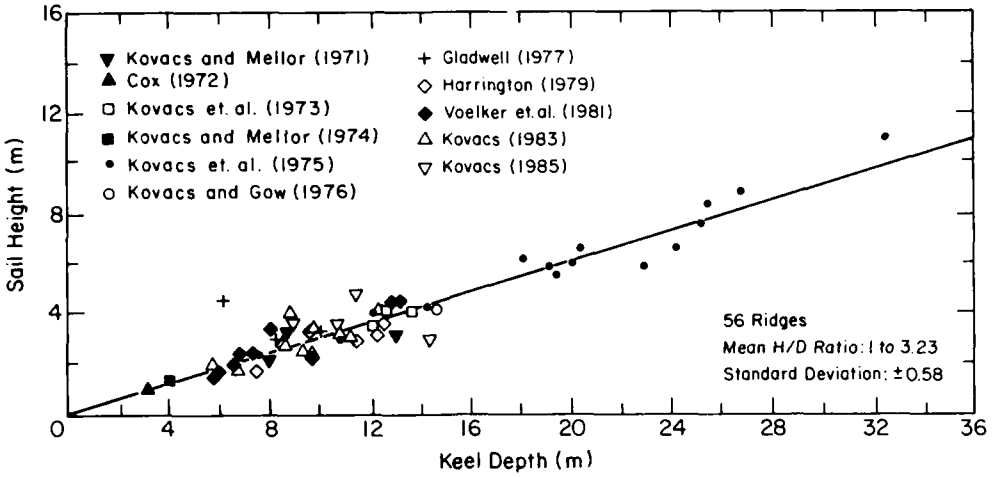

Figure 24. Multiyear pressure ridge sail height vs keel depth (revised from Kovacs 1975 and 1983).

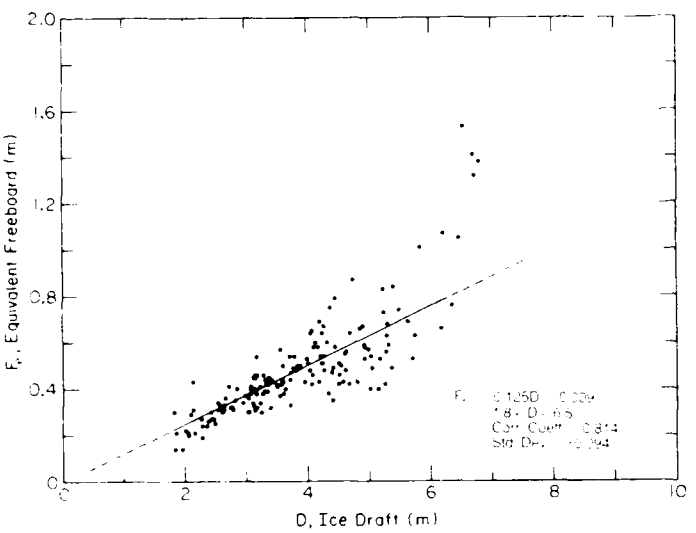

Figure 25. Multiyear sea ice equivalent freeboard vs draft.

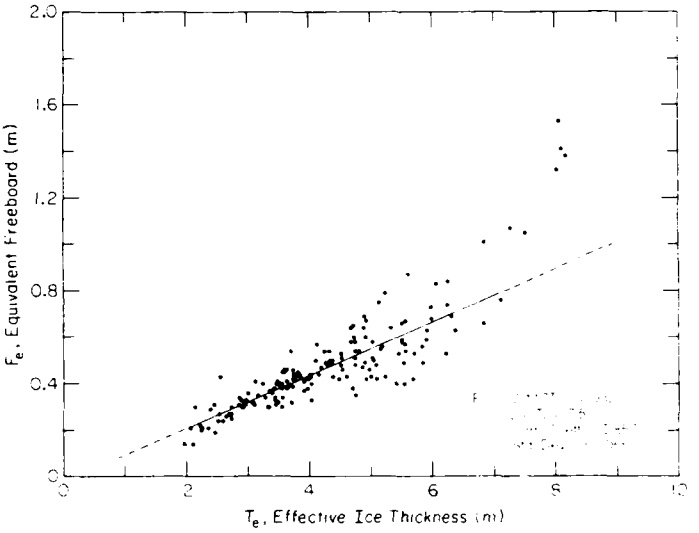

Figure 26. Multiyear sea ice equivalent freeboard vs effective ice thickness.

A more appropriate presentation of the data is given in Figure 26. Here F_e is plotted vs the effective ice thickness T_e. T_e was determined by adding the equivalent freeboard ice thickness of the snow to the drill-hole-measured ice thickness from Tables 3, 4 and 5 (lines A–K) to obtain an effective total ice thickness. Therefore, the plot in Figure 26 should be representative of snow-free ice floes. The linear regression for the line passing through the data did not include the four data points for T_e values over 8 m (for reasons previously mentioned).

The slope of the line in Figure 26 is in good agreement with a regression line put through similar F_e vs T_e data by Kovacs (1977). His analysis included T_e data up to about 4 m, as shown in Figure 27. Beyond this thickness the limited data suggested an abrupt increase in the F_e/T_e ratio. The data presented in Figure 26 indicate that the abrupt change shown in Figure 27 is not realistic. It may be noted that the data in Figure 27 fall very nicely within the data presented in Figure 26.

For a snow-free multiyear ice floe, the analysis given in Figure 26 may allow for a reconstruction of the floe's apparent cross section from the AEM sounding data. Since analysis of the AEM sounding data gives ice thickness, it would be a simple matter to use the equation in Figure 26 to determine an approximate ice freeboard.

For the snow-covered multiyear sea ice, a more representative plot of the measured data is shown in Figure 28. This plot shows the measured surface elevation E (snow plus freeboard) vs the S–I thick-

Table 8. Average row effective freeboard vs ice draft for multiyear floe grid sites 1, 2 and 3.

Effective freeboard (m)	*Ice draft (m)*	*Effective freeboard (m)*	*Ice draft (m)*	*Effective freeboard (m)*	*Ice draft (m)*
0.30	1.83	0.32	3.17	0.67	4.26
0.14	1.84	0.46	3.17	0.48	4.26
0.21	1.86	0.41	3.22	0.54	4.26
0.14	1.96	0.34	3.22	0.60	4.31
0.22	2.01	0.30	3.25	0.38	4.33
0.21	2.05	0.38	3.26	0.75	4.37
0.20	2.06	0.46	3.27	0.47	4.39
0.29	2.10	0.39	3.29	0.35	4.40
0.43	2.13	0.44	3.30	0.49	4.41
0.31	2.14	0.42	3.31	0.79	4.44
0.21	2.16	0.39	3.34	0.58	4.44
0.27	2.27	0.44	3.34	0.42	4.50
0.24	2.28	0.42	3.35	0.51	4.50
0.19	2.28	0.45	3.36	0.46	4.51
0.24	2.36	0.32	3.39	0.50	4.54
0.26	2.38	0.44	3.40	0.43	4.57
0.30	2.43	0.43	3.42	0.55	4.60
0.27	2.43	0.42	3.49	0.48	4.61
0.27	2.46	0.41	3.50	0.56	4.62
0.27	2.47	0.37	3.54	0.42	4.67
0.25	2.49	0.57	3.55	0.64	4.68
0.34	2.53	0.42	3.57	0.87	4.73
0.31	2.54	0.44	3.57	0.43	4.80
0.33	2.56	0.44	3.58	0.66	4.84
0.30	2.61	0.43	3.59	0.67	4.89
0.30	2.62	0.50	3.59	0.59	4.91
0.32	2.62	0.38	3.60	0.58	4.92
0.33	2.64	0.40	3.63	0.53	4.92
0.31	2.64	0.54	3.70	0.57	4.98
0.36	2.65	0.44	3.71	0.40	5.01
0.41	2.71	0.33	3.71	0.54	5.02
0.32	2.74	0.47	3.72	0.49	5.04
0.32	2.76	0.49	3.76	0.40	5.14
0.31	2.79	0.54	3.78	0.40	5.14
0.35	2.81	0.48	3.81	0.53	5.17
0.40	2.84	0.50	3.83	0.83	5.22
0.34	2.94	0.49	3.83	0.73	5.24
0.37	2.98	0.49	3.87	0.42	5.25
0.37	3.02	0.49	3.87	0.56	5.27
0.36	3.03	0.50	3.87	0.63	5.28
0.30	3.03	0.43	3.95	0.68	5.29
0.30	3.05	0.53	3.98	0.59	5.31
0.38	3.06	0.51	4.00	0.49	5.36
0.40	3.06	0.48	4.03	0.84	5.39
0.41	3.07	0.64	4.04	0.74	5.49
0.34	3.10	0.65	4.06	0.69	5.63
0.14	1.97	0.46	3.59	0.35	4.75
0.21	2.07	0.45	3.59	0.54	4.80
0.14	2.11	0.41	3.63	0.47	4.86
0.30	2.14	0.46	3.63	0.64	4.88
0.22	2.23	0.38	3.63	0.69	4.89
0.20	2.25	0.39	3.67	0.49	4.90
0.21	2.26	0.54	3.70	0.60	4.91
0.21	2.36	0.32	3.71	0.67	4.92
0.29	2.39	0.42	3.73	0.42	4.92
0.31	2.45	0.39	3.73	0.46	4.97
0.19	2.47	0.46	3.73	0.43	5.00
0.24	2.52	0.44	3.74	0.51	5.02
0.27	2.54	0.42	3.77	0.58	5.02
0.43	2.55	0.44	3.79	0.50	5.04
0.24	2.60	0.45	3.81	0.48	5.08
0.26	2.65	0.44	3.84	0.42	5.09
0.27	2.70	0.43	3.85	0.75	5.12
0.27	2.72	0.42	3.91	0.55	5.15
0.30	2.73	0.41	3.91	0.56	5.18
0.27	2.74	0.37	3.91	0.79	5.22
0.25	2.74	0.38	3.97	0.43	5.23
0.31	2.85	0.42	3.98	0.64	5.32
0.34	2.86	0.44	4.01	0.40	5.41
0.33	2.89	0.43	4.02	0.53	5.45
0.30	2.90	0.44	4.02	0.66	5.50
0.30	2.92	0.40	4.03	0.58	5.50
0.32	2.94	0.33	4.03	0.59	5.50
0.31	2.96	0.50	4.10	0.49	5.53
0.33	2.97	0.57	4.12	0.40	5.54
0.36	3.00	0.44	4.15	0.40	5.54
0.32	3.06	0.47	4.19	0.57	5.55
0.32	3.08	0.54	4.24	0.67	5.56
0.31	3.10	0.49	4.26	0.54	5.56
0.41	3.12	0.48	4.29	0.87	5.60
0.35	3.16	0.54	4.32	0.42	5.68
0.40	3.24	0.49	4.32	0.53	5.70
0.34	3.28	0.50	4.33	0.56	5.83
0.30	3.32	0.49	4.36	0.49	5.84
0.30	3.34	0.49	4.36	0.59	5.9[illegible]
0.37	3.35	0.50	4.37	0.63	5.91
0.36	3.39	0.43	4.38	0.73	5.97
0.37	3.39	0.42	4.48	0.68	5.98
0.38	3.43	0.48	4.51	0.83	6.05
0.33	3.44	0.53	4.51	0.53	6.22
0.34	3.44	0.51	4.52	0.74	6.23
0.31	3.45	0.46	4.53	0.84	6.24
0.40	3.46	0.43	4.60	0.69	6.31
0.41	3.48	0.58	4.67	0.63	6.37
0.39	3.52	0.38	4.70	1.01	6.84
0.40	3.52	0.65	4.71	0.76	7.10
0.40	3.55	0.60	4.72	1.07	7.27
0.38	3.55	0.51	4.73	1.05	7.51
0.30	3.55	0.48	4.74	1.32	8.02
0.45	3.56	0.54	4.74	1.53	8.06
0.34	3.56	0.58	4.74	1.41	8.10
0.45	3.56	0.51	4.74	1.38	8.17
0.33	3.11	0.42	4.06	0.53	5.70
0.45	3.11	0.46	4.07	0.63	5.74
0.45	3.12	0.58	4.09	1.01	5.83
0.40	3.12	0.60	4.12	0.66	6.17
0.39	3.13	0.58	4.16	1.07	6.21
0.46	3.13	0.43	4.18	0.76	6.35
0.45	3.14	0.69	4.20	1.05	6.46
0.31	3.14	0.54	4.20	1.53	6.53
0.40	3.15	0.51	4.22	1.41	6.69
0.54	3.16	0.64	4.23	1.32	6.71
0.38	3.16	0.51	4.24	1.38	6.79

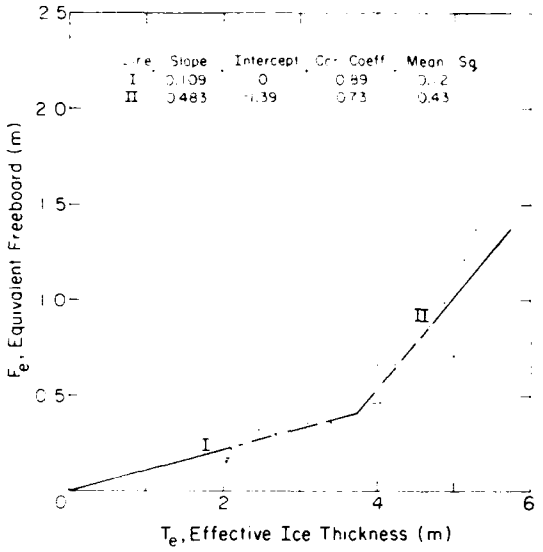

Figure 27. Multiyear sea ice equivalent freeboard vs effective ice thickness (after Kovacs 1977).

ness obtained at 1896 drill hole sites on floes 1, 2 and 3. This presentation clearly reveals the wide scatter in the *E* vs S-I data due to the snow and ice variations previously mentioned.

The linear regressive curve shown in Figure 28 was determined by first adding increasing *E* vs S-I data until a linear regression curve through the data intercepted zero, as would occur in nature. This occurred when S-I thickness values up to 5.85 m were included. At this point there were 1593 data points and the slope of the line was 0.124, with a correlation coefficient of 0.622 and standard deviation of ±0.159. Similar results were obtained when a linear regression curve was forced through zero but included 1679 data points up to a S-I thickness of 6.25 m. This linear regression curve is presented in Figure 28 and represents an *E*/S-I thickness ratio of 1 to 8.06, which from eq 1 gives a value of 0.912 for ρ_i.

The third-degree regression curve also shown in Figure 28 is a fit to the entire data set. An apparent cross section of a snow-covered multiyear ice floe may be reconstructed from the AEM-determined S-I thicknesses by using the more representative linear curve from zero up to a S-I thickness of 5.6 m and then using the polynomial equation for higher values of S-I thickness. However, the resulting cross section may be of limited value because of the low correlation coefficient for the curves and the wide scatter of the data shown in Figure 28. In short, the resulting cross section would not reveal the highly variable hummocky relief characteristic of multiyear sea ice floes.

AEM sounding results

Station K (Fig. 5) had a measured S–I thickness of 1.79 to 1.86 but averaged 1.84 m. This site's S–I thickness was sounded on six different flights with the AEM system. The bird height at each sounding was between 19 and 23 m above the surface. On average the soundings were made at 21.5 m. The AEM determined S-I thicknesses were 1.68, 1.84, 1.90, 1.96, 2.45 and 2.50 m which gives an average of 2.06 m. This average is 12% higher than the average measured value. On an individual basis the AEM S-I thickness values varied from 9% below to 36% above the average drill-hole-measured S–I thicknesses. This wide spread is not acceptable and must be improved in the next-generation AEM sea ice sounding system. The spread is believed to be associated with nonlinear system drift.

Nonlinear drift effects may be seen in the AEM S-I thickness results (Table 9) obtained from flight

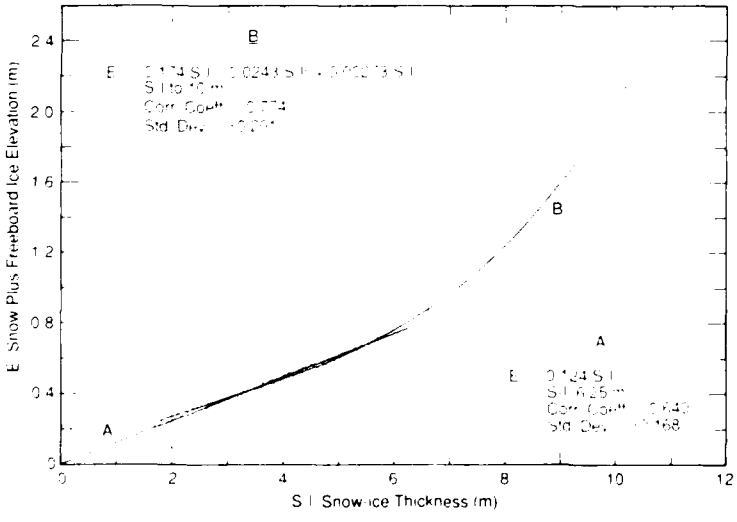

Figure 28. Snow thickness plus ice freeboard vs total snow plus ice thickness for multiyear sea ice. (See Appendix A for blowup of this figure.)

Table 9. Drill-hole-measured vs AEM-determined snow-ice thickness for stations H–O.

Station	Snow-ice thickness (m)	
	Drill hole	AEM sounding
H	1.90	1.15
I	1.91	1.75
J	1.88	2.37
K	1.84	2.50
L	1.93	2.24
M	1.95	2.45
N	1.03	0.79
0	0.94	0.83

line F12L2 for stations H and O (Fig. 5). Table 9 lists the average drill-hole-measured S-I thickness vs the AEM value for each station along the flight line.

As seen in Table 9 the AEM S-I thickness values at the beginning of the flight were lower than the measured values. As the 18-minute flight progressed the AEM values gradually increased to where they exceeded the measured ones and then decreased again. Time between zero readings was about 25 minutes. Again this variation is unacceptable and must be eliminated before AEM sounding of sea ice can be considered a viable measurement technology.

Due to the short flight lines and therefore the elapsed time between the zero calibrations made before and after each run, drift was not as severe a problem in the AEM data collected over the four grid sites. AEM sounding flights typically towed the bird at an elevation of 23 ±3 m above the surface.

The AEM sounding results for four flights over floe site 1 are shown in Figure 29. The average measured S–I thickness of lines C through I (C–I), a swath width of 30 m, is also shown. It is apparent that the AEM thickness profiles follow the measured long-period S-I thickness trends but not the short-period undulations. As previously discussed, this is due to the averaging associated with the footprint area over which the ice thickness is being integrated as well as the use of a one-dimensional model to characterize three-dimensional relief. At present, short-period thickness variations, which occur over distances of less than two or three times the bird height above the surface, are not well defined, if at all, in the AEM sounding profiles.

Sea ice thickness requirements vary depending on the user's need. A very local site-specific ice thickness is preferred by someone wanting thin ice for instrument deployment or a thick ice site to support a heavy object. An average of the relative sea ice thickness variation over a very large area would be extremely useful to someone interested in modeling ice pack movement dynamics or in assessing heat transfer from an ice-covered ocean to the atmosphere. AEM sounding would appear to provide S–I thickness information well suited to the latter user needs.

All AEM profiles appear to track the measured S-I thickness relief along the entire grid length, except for those of flight F12L3. This profile indicates greater thicknesses beyond a grid distance of about 310 m. System drift was again the problem.

Similar presentations of the flight profile data taken over floe sites 2 and 3 are presented in Figures 30 and 31. Again, note the smoothing of the ice relief in the AEM sounding results. Drift also appears to have affected the profile results over floe 3. In Figure 31, flight line F13L5's ice thickness profile is seen to be higher than the average measured

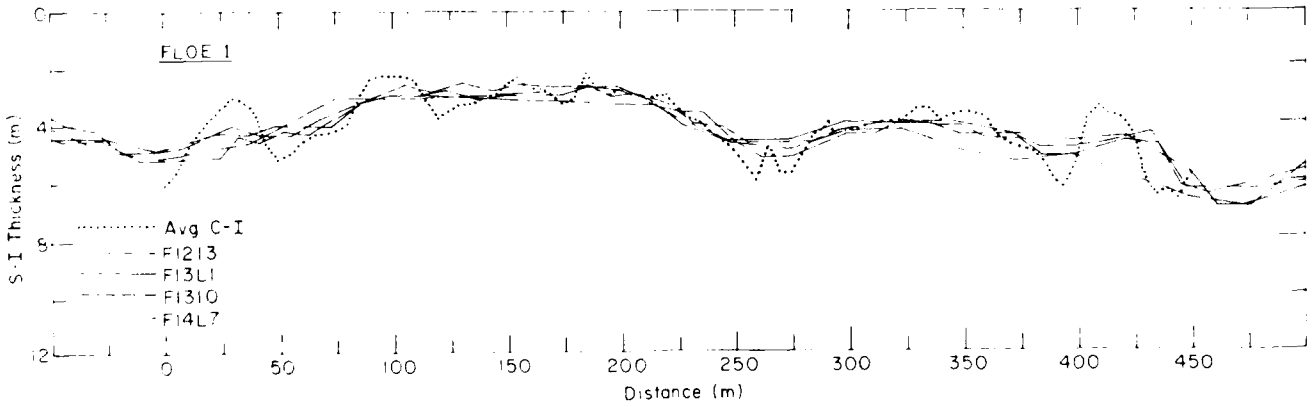

Figure 29. Average snow plus ice thickness for 30-m-wide swath C–I down center of grid on MY floe 1 vs AEM-determined snow plus ice thickness for four sounding flights (F...).

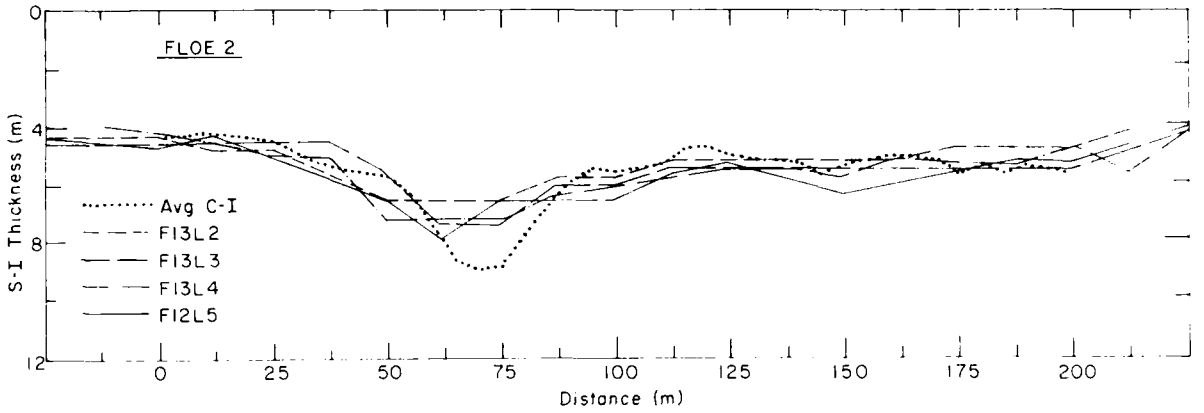

Figure 30. Average snow plus ice thickness for 30-m-wide swath C–I down center of grid on MY floe 2 vs AEM-determined snow plus ice thickness for four sounding flights (F...).

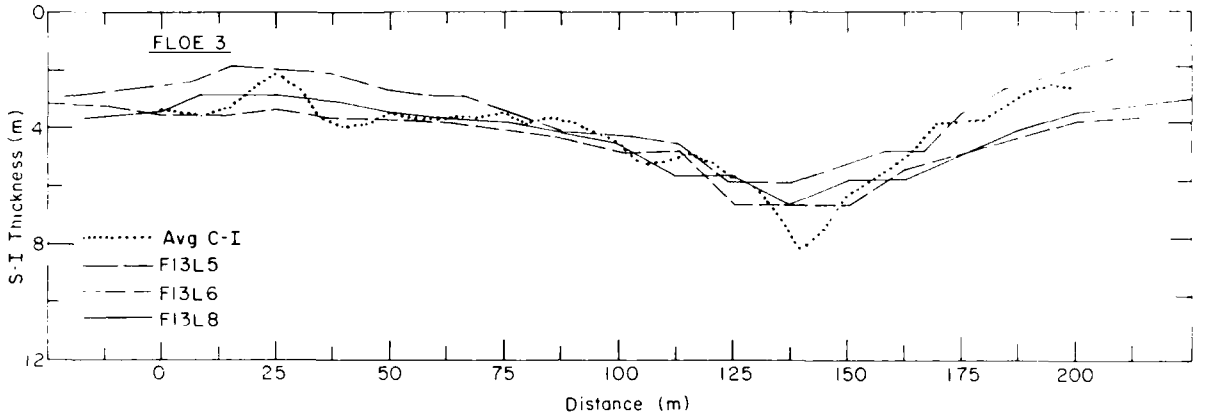

Figure 31. Average snow plus ice thickness for 30-m-wide swath C–I down center of grid on MY floe 3 vs AEM-determined snow plus ice thickness for three sounding flights (F...).

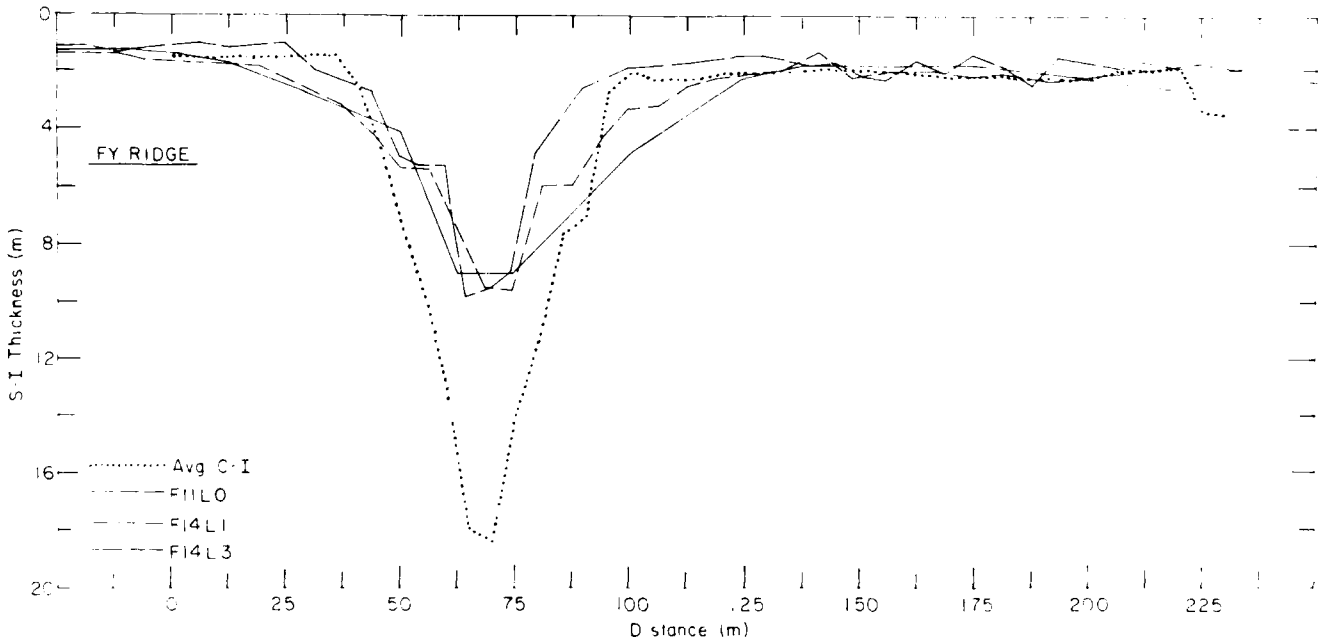

Figure 32. Average snow plus ice thickness for 30-m-wide swath C–I down center of grid at the FY ridge vs AEM-determined snow plus ice thickness for three sounding flights (F...).

values (the C–I profile line) at the beginning of the grid, while those for flight line F13L6 and F13L8 are higher than the C–I profile line at the end of the grid.

The AEM profiles taken at the first-year pressure ridge site are shown in Figure 32. The most striking aspect of the AEM profiles is that they do not adequately define the thick ice of the ridge. Here too, because of footprint size and model constraints, as well as the effect of the seawater-filled submerged ice block structure and the relatively steep-sided blocky relief of the ridge keel, it is currently not possible to properly define such short-period relief that occurs over a distance of two to three times the bird height above the surface. Since the thick ridge ice area is less than 60 m wide and the bird was flown at about 23 m above the undeformed surface relief, the results shown in Figure 32 are not unexpected. The AEM profiles do agree with the measured thickness of the thinner ice on each side of the ridge and do indicate the location of the thicker ridge ice. Smoothing of the relief in the area of the ridge is again associated with footprint size, ridge geometry, seawater between the ice blocks of the keel and 1-D model constraints.

Several methods were used to evaluate how well the AEM S-I thickness determinations agreed with the drill hole measurements. Information related to each AEM sounding flight at each grid site is listed in Table 10, and a comparison between the average drill-hole-measured S-I thickness and the average AEM-determined S-I thickness for each sounding flight is listed in Table 11.

The results in Tables 10 and 11 for floes 1, 2, and 3 do not provide a clear indication of the effect of flight speed, and therefore the number of soundings, on the variation between the average AEM-determined S–I thickness and the measured value. One would expect that better agreement would have occurred as more AEM soundings were obtained along a grid. Indeed, just the opposite is apparent for the flights down floe 3 and at the FY ridge site. However, these may have been the result of one or more inconsistencies. For example, one flight line did not exactly follow the track of another, the flight elevations and therefore footprint size varied, and because electronic drift was not necessarily linear for each sounding run, the S-I thickness determinations may be slightly different. The effect of flight speed on the sounding results therefore needs further study.

The data in Table 11 do indicate that for ice floes with low to moderate relief, AEM sounding is capable of providing a good assessment of an ice floe's average S-I thickness. Indeed, it seems that once drift and calibration problems are resolved it should be possible to determine the average S-I thickness of ice floes, with "moderate" relief, to within 5%.

Table 10. Average AEM S-I thickness and related standard error for each sounding flight down grids on multiyear floes 1, 2, and 3 and at the first-year ridge site.

Grid site	Grid length (miles)	Flight		No. of soundings	Mean AEM S-I thickness (m)	Std. dev. (m)
		Flight no.	Speed (km/hr)			
Floe 1	450	F12L3	77	22	4.27	1.09
		F13L0	52	32	4.29	0.86
		F13L1	54	31	4.09	0.92
		F14L7	43	37	4.11	0.88
Floe 2	200	F12L5	60	13	5.84	0.99
		F13L2	51	15	5.64	0.75
		F13L3	60	13	5.68	0.91
		F13L4	42	17	5.76	0.87
Floe 3	200	F13L5	36	21	3.65	1.33
		F13L6	42	18	4.30	1.23
		F13L8	45	17	4.51	1.14
FY ridge	230	F11L0	67	13	3.61	2.69
		F14L1	25	33	3.25	2.16
		F14L3	21	40	2.74	2.31

Table 11. Percent difference between average measured S-I thickness for lines C–I vs average S-I thickness determined by AEM sounding for each flight down the grids on multiyear floes 1, 2, and 3 and at the first-year ridge sites.

Grid site	Flight no.	Measured S-I thickness (m)	AEM S-I thickness (m)	Difference Meas vs AEM (%)
Floe 1	F12L3	3.93	4.27	+9
	F13L0		4.29	+9
	F13L1		4.09	+4
	F14L7		4.11	+5
Floe 2	F12L5	5.64	5.84	+4
	F13L2		5.64	=
	F13L3		5.68	~
	F13L4		5.76	+2
Floe 3	F13L5	4.22	3.65	−14
	F13L6		4.30	+2
	F13L8		4.50	+7
FY ridge	F11L0	3.94	3.61	−8
	F14L1		3.25	−18
	F14L3		2.74	−30

Another assessment between the measured and AEM determined S-I thickness was made by comparing the measured vs AEM thickness values at stations spaced 25 m apart along the center grid line on floes 1 and 2. Floe 1 was chosen because of its relatively low-lying relief and floe 2 because of its thicker, more complex relief. The S-I thickness at each station was determined by averaging the drill hole measurements along lines C through I (a 30-m-wide spacing) and for the row on which the station occurred as well as on the three rows before and after the station (a 30-m-wide spacing). Thus, the S-I thickness used for each station was the average of the drill hole measurements made on a 5-m grid within a 30-m-square area centered at the station. This average or measured S–I thickness for each station was used because it is a reasonable approximation to the integrated thickness sounded within the AEM footprint. Since there was no ice thickness information taken before the first or after the last station on each grid, these two stations were not included in the assessment.

The measured and AEM-determined station S-I thickness for each flight over the grid on floes 1 and 2 are listed in Tables 12 and 13, respectively. Also listed is ΔT, the difference of the AEM-determined S-I thickness from the measured value. The most significant difference occurred at the 25-m station on flight F13L0 over floe 1. Here the AEM-determined thickness value was 37% above the measured one. However, at most stations the difference is less than 15%. The standard deviation of the ΔT values for each flight is also listed. These statistical values are an indication of the relative dispersion that occurred between the measured and the AEM-determined S-I thicknesses. The dispersion is numerically larger for the flights over the rougher relief of floe 2, but in relation to individual station S-I thickness the deviations are quite similar, again about 15%. In short, the AEM S-I thickness determination for each grid station was generally within 15% of the measured value.

Flight line F15L1 ran from near Gull Island to the southeast shore of Prudhoe Bay (Fig. 1 and 6). A portion of this line included ice that had grown down and became frozen to the shallow seabed. The ice cover along the line was not deformed with pressure ridges. The AEM-determined S–I thickness and sub-ice water depth along the flight line are shown in Figure 33. Large variations are clearly

Table 12. Measured and AEM determined S-I thickness for the 25–m stations along the center line of the grid on multiyear floe 1.

		AEM flight							
Measured		F12L3		F13L0		F13L1		F14L7	
Dist. (m)	S-I thickness (m)	S-I thickness (m)	ΔT* (m)	S-I thickness (m)	ΔT (m)	S-I thickness (m)	ΔT (m)	S-I thickness (m)	ΔT (m)
0	—	—	—	—	—	—	—	—	—
25	3.68	4.80	+1.12	5.04	+1.36	4.39	+0.71	4.54	+0.86
50	4.27	3.94	–0.33	4.36	+0.09	4.13	–0.14	4.55	+0.28
75	3.79	3.11	–0.68	3.88	+0.09	4.13	+0.34	4.04	+0.25
100	2.49	3.06	+0.57	2.96	+0.47	3.02	+0.53	3.22	+0.73
125	3.11	3.06	–0.05	3.24	+0.13	2.86	–0.25	3.09	–0.02
150	2.73	2.91	+0.18	3.31	+0.58	3.02	+0.29	3.06	+0.33
175	2.72	2.79	+0.07	3.24	+0.52	3.02	+0.30	2.93	+0.21
200	2.73	2.68	–0.04	3.28	+0.55	2.89	+0.16	3.24	+0.51
225	3.43	3.98	+0.55	3.71	+0.28	3.89	+0.46	3.48	+0.05
250	4.77	4.75	–0.02	4.77	0.00	4.66	–0.11	4.32	–0.45
275	4.98	4.98	0.00	5.31	+0.33	4.66	–0.32	4.87	–0.1
300	4.05	4.25	+0.20	4.48	+0.43	4.00	–0.05	4.45	+0.40
325	3.69	4.25	+0.56	4.10	+0.41	4.00	+0.31	4.18	+0.49
350	3.70	4.89	+1.19	4.25	+0.55	4.42	+0.72	4.18	+0.48
375	4.73	5.29	+0.56	4.72	–0.01	4.42	–0.31	4.61	–0.12
400	4.71	5.15	+0.44	5.34	+0.63	4.60	+0.63	5.07	+0.36
425	4.69	5.85	+1.16	4.81	+0.12	5.09	+0.40	4.77	+0.08
450	—	—	—	—	—	—	—	—	—
Mean	3.78	4.10	+0.32	4.16	+0.38	3.94	+0.17	4.04	+0.25
Std. dev.	0.83	1.01	0.52	0.78	0.33	0.72	0.34	0.71	0.33

* ΔT is difference between measured and AEM determined S–I thickness for related flight (F.....).

Table 13. Measured and AEM determined S-I thickness for the 25-m stations along the center line of the grid on multiyear floe 2.

		AEM flight							
Measured		F12L5		F13L2		F13L3		F13L4	
Dist. (m)	S-I thickness (m)	S-I thickness (m)	ΔT* (m)	S-I thickness (m)	ΔT (m)	S-I thickness (m)	ΔT (m)	S-I thickness (m)	ΔT (m)
0	—	—	—	—	—	—	—	—	—
25	4.75	5.11	+0.36	4.62	–0.13	5.11	+0.36	5.05	+0.30
50	6.39	6.88	+0.29	5.57	–0.82	7.31	_0.92	6.53	+0.14
75	7.79	6.88	–0.91	7.43	_0.36	6.44	–1.35	6.67	–1.12
100	5.64	6.08	+0.44	6.08	+0.44	5.80	+0.16	6.67	+1.03
125	5.07	5.49	_0.42	5.48	_0.41	5.53	+0.46	5.38	+0.31
150	5.27	5.49	+0.22	5.48	_0.21	5.14	–0.13	6.39	+1.12
175	5.34	5.01	–0.33	5.48	+0.14	5.30	–0.04	5.83	+0.49
200	—	—	—	—	—	—	—	—	—
Mean	5.75	5.85	+0.07	5.73	–0.02	5.80	–0.21	6.07	+0.32
Std. dev.	1.04	0.78	0.51	0.86	0.45	0.81	0.68	0.66	0.74

* ΔT is difference between measured and AEM determined S-I thickness for related flight (F.....).

seen in the S–I thickness profile which cannot be explained by snow drift features or seabed topography. The former were short-period surface relief features of less than 0.5-m-height and the latter is a mild relief feature sloping into deeper water. The variations shown are an example of AEM system noise and instability effects, which occurred unexpectedly or were not adequately attended to prior to the flight. While the average AEM-determined S-I thickness may be representative of that along the flight line, it is clear that improvements in system performance are in order.

Flight line F12L1 was a flight over the fast ice, which began south of Reindeer Island and ended near the Prudhoe Bay West Dock (Fig. 4). The AEM sounding data for the southern half of this flight line were processed to provide both S–I thickness and sub-ice water depth as shown in Figure 34. In the analysis of the AEM data the conductivity of the seawater was set at 2.6 S/m. As seen in Figure 34, stations D, E and F were over-flown. Also shown is that the AEM-determined S-I thickness is in good agreement with the measured value at stations E and F and that the AEM-determined sub-

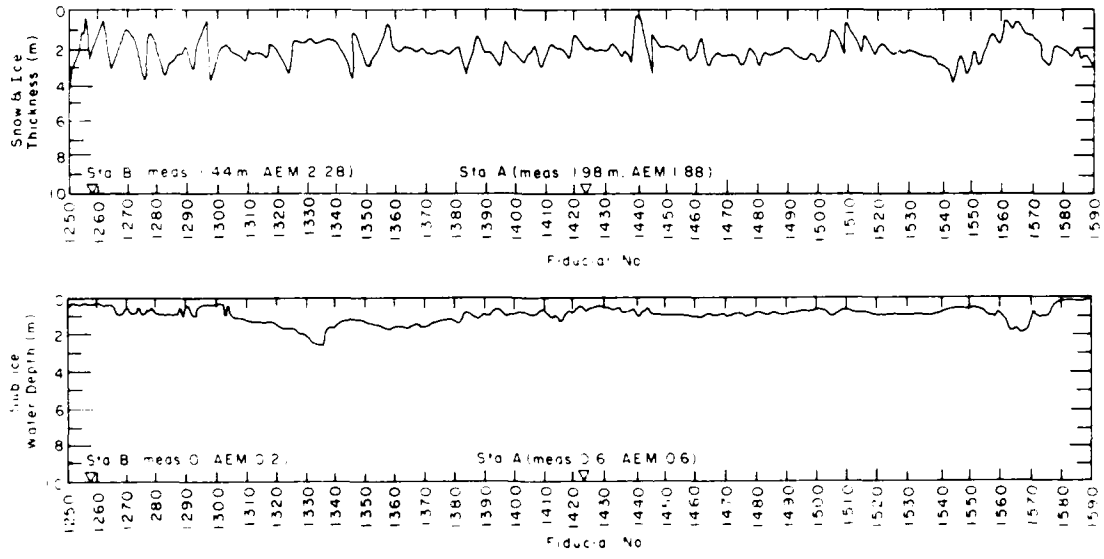

Figure 33. AEM-determined snow plus ice thickness and sub-ice water depth for flight line F15L4. See Figures 1 and 4 for line location.

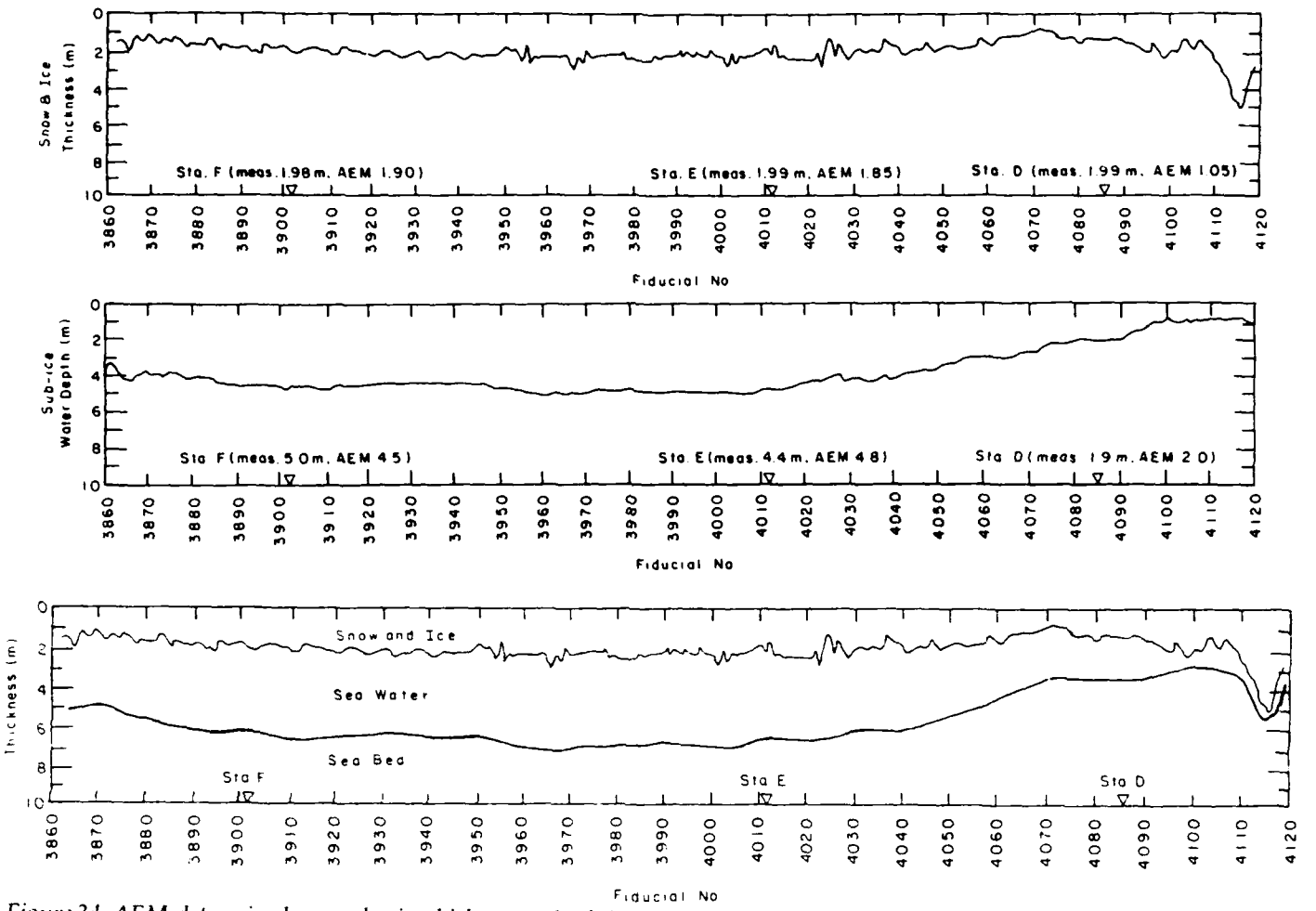

Figure 34. AEM-determined snow plus ice thickness and sub-ice water depth and a composite cross section of these measurements for flight line F12L1. See Figure 2 for line location.

ice water depths at each station are within 10% of the measured ones. There is a significant difference in the AEM vs measured S-I thickness at station D. This could be the result of system drift, which may have affected the data after about fiducial number 4025 and could bethe reason for the anomalous S-I thickness area between fiducial numbers 4110 and 4120.

Flight line F11L10 (Fig. 6) was flown over a first-year sea ice rubble area and then down an approximately 700-m-long section of 20 cm ± 2 cm thick snow-free lead ice. The AEM S-I thickness profile along this flight line is shown in Figure 35. The lead began at about fiducial number 4850. The average AEM-determined lead ice thickness was 23 cm, which is in good agreement with the measured value given above.

Flight line F15L4, as located in Figure 6, was an approximately 20–km-long sounding run made over the near-shore sea ice. This run was intended to represent the type of AEM sounding flight that would occur during a pack ice sounding mission. The S-I thickness profile along this flight line is shown in Figure 36. At about fiducial numbers 4670 and 5150 there were no S-I thickness data available due to saturation of the receivers as a result of flying the bird too low (close to the sea water). The flight line was limited in length by an offshore cloud bank that prevented VFR flying farther north.

The relative distribution of the S-I ice thicknesses sounded along the flight line is shown in Figure 37. A thin lead ice component is revealed in the data, as is the smaller amount of thick pressure ridge ice. The average S-I thickness was 3.7 m. There are no ground truth data to validate the S-I thickness distribution shown. In addition, the flight line probably did not cross ice representative of that located in other Arctic Ocean areas. However, it may be of interest to note that Wittmann and

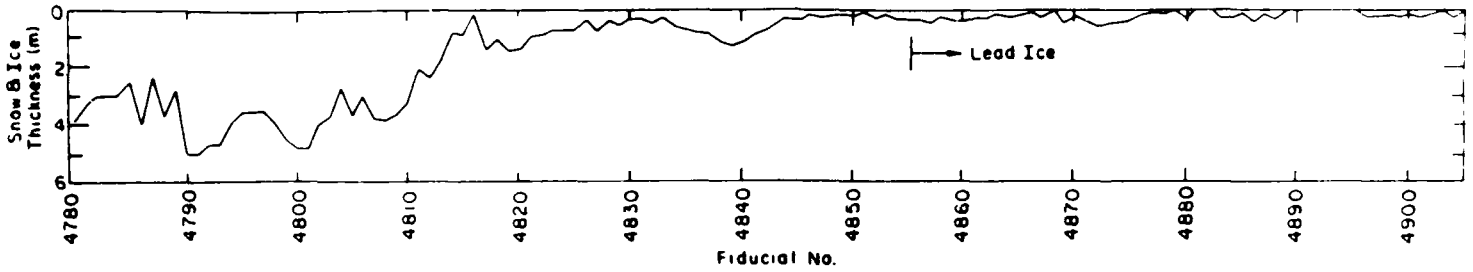

Figure 35. AEM-determined snow plus ice thickness down an approximately 700-m-long section of thin lead ice. Note variation in lead ice thickness due to extraneous noise etc.

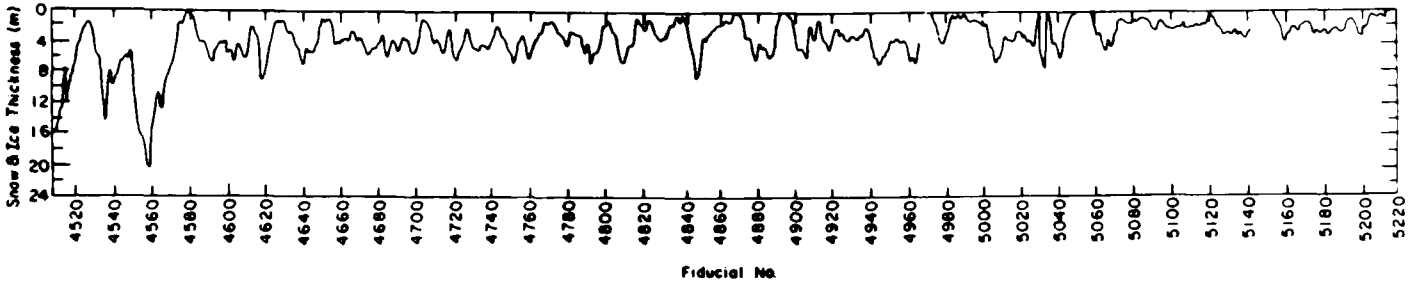

Figure 36. AEM-determined snow plus ice thickness along flight line F15L4. See Figure 4 for line location.

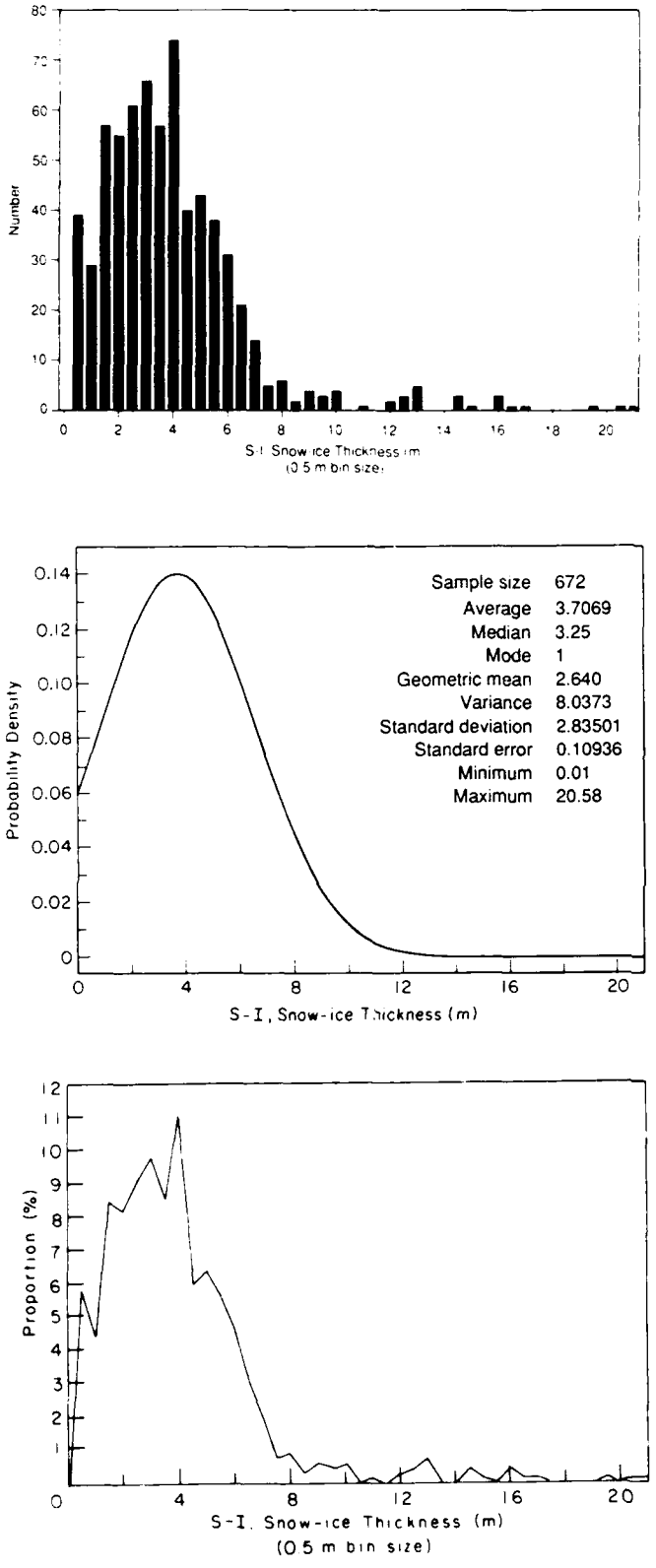

Figure 37. Histogram, probability and proportion distribution of snow plus ice thickness along flight line F15L4.

Schule (1966) estimated, from sonar profiles of under-ice relief obtained during submarine cruises, that the average arctic pack ice thickness is about 3.9 m, which is in agreement with the more recent finding of Colony (1988) of 3.8 m obtained from submarine ice bottom profile data collected in the Beaufort Sea. Both of these averages are in agreement with the average 3.7-m AEM value given above. In any event the trend of the distribution in Figure 37 is as expected and is in good agreement with the many reports that give the distribution of ice drafts obtained during submarine transects under the Arctic pack ice in the (e.g., Blidberg et al. 1979 and McLaren 1988).

CONCLUDING REMARKS

The most serious EM system problem encountered during the 1987 field work was drift, particularly in the high-frequency channels. This drift was mainly caused by temperature-related changes in the analog receiver console, particularly in the band-pass filter assemblies. Our solution to this problem will be to use a digital receiver specifically designed to minimize temperature drift-related problems.

A secondary source of drift, and one which is harder to pin down, was temperature-related drift in the bird's transmitter and receiver assemblies. As transmitter coils warm up and expand, there is a slight shift in transmitter coil frequency and moment. Frequency drift is the more important of these two changes. The receiver coils have a relatively sharp resonance, with a Q factor of 10. Therefore, a small frequency shift in transmitter frequency will result in a significant amplitude and phase change in the received signal, which in turn leads to systematic errors in the ice thickness and conductivity estimates as well as in the bathymetric results. Moment drift results in smaller absolute secondary field pickup at the receiver, which in turn causes small changes in both phase components. Both of these problems must be resolved in the development of a new transmitter module.

An annoying but less important problem was the presence of a significant amount of noise in the high frequency channel. This noise was correlated with motion of the tow cable with respect to the bird, and was reduced by immobilizing the cables as much as possible near the bird and by tying spoiler flags to the tow cable to reduce the amplitude of wind-driven oscillation. However, the key source of noise was discovered after the field survey. A few inches of unshielded wiring was found

in the bird. This wiring acted as an electrostatic antenna that picked up EM radiation noise. Such shielding errors should have been detected and corrected by the manufacturer, had proper testing occurred prior to shipping the AEM system to Alaska.

A most important problem involved the behavior of the laser altimeter's control console. As mentioned earlier, the console or the interface between it and the data recording system delayed logging of laser altitude data by 2.5 seconds. A combination of effects in the laser console and the data acquisition system's control program is probably responsible and will be resolved in the future.

The problems encountered in field- and post-processing of the AEM data derived almost entirely from a single source: the altimeter time delay. During the field processing effort, the systematic inconsistencies in the data set caused by the altimeter delay led to many fruitless hours of searching through the entire software system and the AEM data looking for pathological nonlinearities in drift. These efforts continued until the altimeter delay was discovered. Once this problem was dealt with, it was straightforward to obtain an acceptable system calibration based on ground truth (a known snow-ice thickness and water depth).

The radar altimeter used to determine helicopter elevation would frequently stop displaying altitude during a flight. The result could have been a refusal by the pilot to fly at the optimal (bird) survey height of 20 m. However, he was willing to fly using the bird altitude as determined by the laser altimeter. It seems most likely that the radar problem was produced by a combination of effects, particularly weak or diffuse reflections from the snow surface and the lack of a good ground plane around the backing plate of the radar antenna (the ASTAR helicopter used had a composite shell with a low electrical conductivity).

The failure of the RMS data recording system has already been mentioned, as were the steps used to correct it.

The main thrust of this airborne sea ice measurement program was to design, construct and test a prototype bird having a 3-m nominal coil separation and frequencies ranging from 800 Hz to 50 kHz. The prototype AEM bird was very stable in flight but the electronics did not perform as expected during arctic testing. With the corrections made after the field trials and modifications proposed, the AEM system should work very satisfactorily.

One aspect of this work was to implement and test a practical, robust and fast field-processing system for analysis of the airborne ice measurement data. Turnaround times of less than one day were demonstrated in the field, and have been further shortened by subsequent software innovations. The quality of the in-field interpretations did not meet expectations, but this was the result of an interfacing problem with the laser altimeter, not of inadequacy in the processing software. Certainly, the final interpretation conforms well with the ground-truth measurements wherever system drift was not an undue problem.

Real-time processing was one of the ultimate objectives of this program. Designing software to perform this task is now a fairly straightforward task, which mainly requires a substantial input of time and effort. However, the system will need to have sufficient "intelligence" to cope with changes in the character of the surface below, noise due to radio transmissions from the aircraft and occasional saturations of the AEM system if the bird is flown too low, all in real time. If drift cannot be effectively eliminated from the AEM system, then the software will need to predict and remove drift effects based on previous drift behavior. This may well prove rather difficult.

A number of other objectives were also achieved. For example, this work produced estimates of sea ice conductivity using an airborne measurement system. While these results were erratic, due to system drift and noise problems, they certainly constitute an exciting step toward airborne sea ice characterization.

More detailed measurement of ice conductivity over a wide range of ice types will require some additional instrument development effort, because frequencies of 200 kHz–300 kHz or higher may be necessary (Becker et al. 1987). A 100-kHz subsystem has now been installed in the small bird but has not been test-flown.

One approach toward development of an internal precision calibration system was investigated and found to be inadequate. Further development in this area is considered a requirement that must be satisfactorily implemented in an AEM system before the technology can be considered for routine sea ice thickness sounding surveys. Such equipment is essential for a production system, since ground-truth calibrations after bird modification or maintenance may not always be possible.

It is clear that one-dimensional interpretation of sea ice thickness works well for relatively flat ice, but when major changes in ice thickness occur over lateral distances of less than about two bird

elevations, errors will be introduced by the 1-D approximation due to footprint area effects. Thus, the measurement of sea ice thickness using AEM techniques may no longer be limited by instrumentation problems, but rather by inadequate interpretational capability in the vicinity of complicated 2-D or 3-D ice structures.

Becker et al. (1987) and Becker and Liu (1988) have studied the ice measurement problem and identified a method that might be suitable for 2-D or 3-D ice thickness determination, although it does not appear to address the interpretation of ice conductivity in such situations. Implementing this method in a real-time processing system may be difficult, since it requires analysis of multiple measurement points simultaneously and is currently too processing-time-intensive, requiring tens of seconds per data point on a mainframe computer.

Even if a fully developed, real-time AEM processing algorithm for sea ice thickness were available for estimating the cross-sectional variation of three-dimensional sea ice structures, it would not be possible to fully characterize all ice morphology. This would be especially true for first-year pressure ridges and rubble formations with a width of about one bird elevation and for ice formations with complex geometry. As shown in Figure 38, first-year pressure ridges can have a multitude of cross-sectional and internal geometries. These structure variations give rise to complex secondary electromagnetic field responses that would be difficult to interpret. While this structure variation certainly becomes less severe after one or more melt seasons, it is not realistic to expect that the keel relief depicted in Figure 38b, 38c or 39 could be well-defined. Smoothing of the complex ice relief will occur, with the deepest structure in an ice formation being poorly determined. Nevertheless, the results of this program indicate that it should be possible to determine the mean thickness of arctic pack ice to within 10%. Such AEM sounding capability should be of considerable interest to those studying the thermal and motion dynamics of the arctic pack ice and to those interested in locating thick or thin sea ice.

This study and our previous one (Kovacs et al. 1987a) revealed that an AEM sounding system is capable of measuring undeformed sea ice thickness from a few centimeters to 5 or more meters thick to within 10% of the drill hole measured value. Accuracies within 5% can be expected when system generated noise is eliminated and drift is properly controlled. However, conventional AEM systems use analog receivers which tend to drift with time

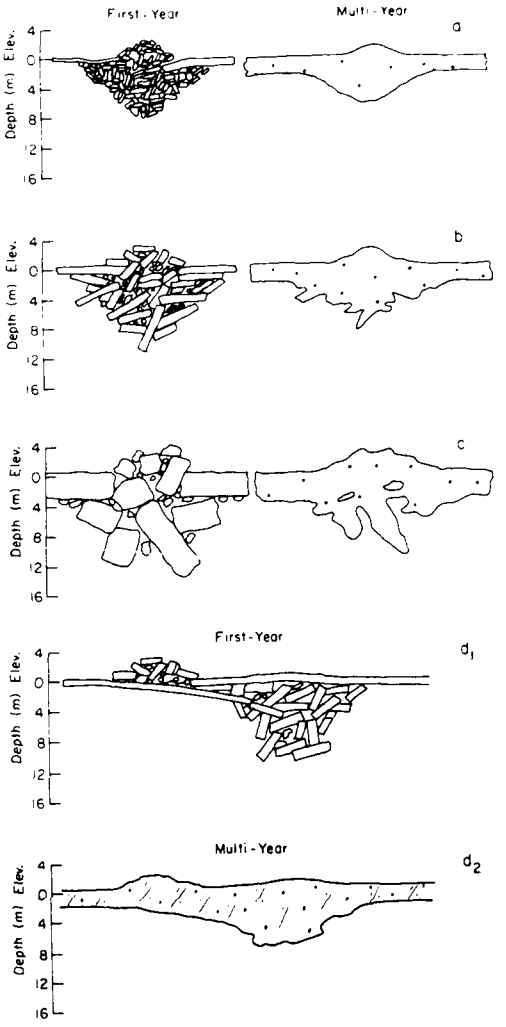

Figure 38. Examples of idealized first-year pressure ridge cross sections and their transformation into multiyear features. Cross sections a, b and c are modified from Grishchenko (1988).

and temperature variations. The result is that precise estimates of the secondary magnetic field response from the seawater become less reliable as the time of the ice sounding survey increases. In addition, the number of frequencies (transmitter-receiver coil pairs) that can be installed in a small bird is limited. This limitation prevents selection of another frequency during a survey flight should one of the built–in frequencies become affected by some interference noise.

To overcome these problems, we are developing a system with a single transmitter coil that will radiate a broad spectrum of electromagnetic energy and a receiver coil that will be used to measure the secondary magnetic field over a wide frequency

Figure 39. Inclined sea ice structure under a multiyear pressure ridge.

range. The use of a single transmitter should eliminate the cross-frequency noise that occurs in conventional multicoil pair AEM systems. In addition, digital signal processing will be used in the new system to minimize and possibly eliminate console drift. The console will have built-in computer hardware, capable of extremely rapid calculations, which will allow inflight data processing and display of S–I thickness.

LITERATURE CITED

Becker, A., G. Liu and H.F. Morrison (1987) Airborne electromagnetic sensing of sea ice thickness. University of California–Berkeley, final contract report to USA Cold Regions Research and Engineering Laboratory.

Becker, A. and G. Chang (1988) Detection of repetitive electromagnetic signals. In *Electromagnetic Methods in Applied Geophysics–Theory* (M.N. Nabighirn and J.C. Corbett, Ed.). Society of Exploration Geophysicists, vol. 1, p. 443–446.

Becker, A. and G. Liu (1988) Airborne electromagnetic sensing of sea ice thickness. University of California–Berkeley, final contract report to Naval Ocean Research and Development Activity.

Blidberg, D.R., R.W. Corell and A.S. Westneat (1979) Probable ice thickness of the Arctic Ocean. In *Proceedings of the 5th International Conference on Port and Ocean Engineering under Arctic Conditions, POAC '79, University of Trondheim, Norway*, vol. 1, p. 253–167.

Colony, R. (1988) A new look at sea ice thickness. In *Proceedings, Port and Ocean Engineering Under Arctic Conditions, Fairbanks, Alaska* (W.M. Sackinger and M.O. Jeffries, Eds.). Geophysical Institute, University of Alaska–Fairbanks, vol. 1, p 85–93.

Cox, G.F.N. (1972) Variation of salinity in the multiyear sea ice at the AIDJEX 1972 camp. M.S. thesis, Dartmouth College, Hanover, New Hampshire (unpublished).

Gladwell, R.W. (1977) Field studies of the strength and physical properties of a multiyear pressure ridge in the southern Beaufort Sea. Imperial Oil

Limited, Calgary, Alberta, Report IPRT-3ME-77, Canadian Arctic Petroleum Operators' Association, Calgary, Alberta, Canada, APOA Project 97 report.

Grishchenko, V.D. (1988) Morphometricheskie kharakteristiki griad torsov na l'dakh Arkticheskogo basseina. (Morphometric characteristics of ice pressure ridges in the Arctic Basin.) *Arctic and Antarctic Institute, Trudy*, **401**: 46–55.

Harrington, A.G. (1979) Geometry and strength of multiyear pressure ridges in the Alaskan Beaufort Sea. Gulf Research and Development Company, Houston Technical Services Center, Houston, Texas.

Kovacs, A. (1975) A study of multiyear pressure ridges and shore ice pile-up. Canadian Arctic Petroleum Operators' Association, Calgary, Alberta, Canada, APOA Project 89 report.

Kovacs, A. (1977) Sea ice thickness profiling and under-ice oil entrapment. In *Proceedings, 1977 Offshore Technology Conference, Houston, Texas*, vol. III, p. 547–554.

Kovacs, A. (1983) Characteristics of multiyear pressure ridges. In *Proceedings of the 7th International Conference on Port and Ocean Engineering Under Arctic Conditions (POAC '83), Helsinki, Finland*, vol. 3, p 173-182.

Kovacs, A. and A.J. Gow (1976) Some characteristics of grounded floebergs near Prudhoe Bay, Alaska. *Arctic*, **29** (3): 169–172.

Kovacs, A. and M. Mellor (1971) Sea ice pressure ridges and ice islands. Creare Incorporated, Hanover, New Hampshire, Creare Technical Note TN-122. (Available at the Canadian Arctic Petroleum Operators' Association, Calgary, Alberta, Canada, APOA Project No. 17 report.)

Kovacs, A. and M. Mellor (1974) Sea ice morphology and ice as a geological agent in the southern Beaufort Sea. In *The Coast and Shelf of the Beaufort Sea* (J.C. Reed and J.E. Sater, Ed.). Arctic Institute of North America, p. 113–161.

Kovacs, A. and R.M. Morey (1985) Investigation of the electromagnetic properties of multiyear sea ice. In *Proceedings of the 8th International Conference on Port and Ocean Engineering under Arctic Conditions (POAC '85), Narssarssuaq, Greenland*, vol. 1, p. 151-167.

Kovacs, A., N.C. Valleau and J.S. Holladay (1987a) Airborne electromagnetic sounding of sea ice thickness and subice bathymetry. *Cold Regions Science and Technology*, **14**: 289–311.

Kovacs, A., R.M. Morey and G.F.N. Cox (1987b) Modeling the electromagnetic property trends in sea ice, Part I. *Cold Regions Science and Technology*, **14**: 207–235.

Kovacs, A., W.F. Weeks, S. Ackley and W.D. Hibler III (1973) Structure of a multiyear pressure ridge. *Arctic*, **26**(1): 22–31.

McLaren, A.S. (1988) The under-ice thickness distribution of the Arctic Basin as recorded in 1950 and 1970: A comparison. In *Proceedings, International Conference on Port and Ocean Engineering Under Arctic Conditions, Fairbanks, Alaska* (W.M. Sackinger and M.O. Jeffries, Ed.). Geophysical Institute, University of Alaska–Fairbanks, vol. III p. 133–149.

Voelker, R.P., F.W. DeBord, F.A. Geisel, J.L. Cobrun and K.E. Dane (1981) Winter 1981 trafficability tests of the USCGC *Polar Sea*: Volume II—Environmental data. U.S. Department of Transportation, Maritime Administration.

Wittmann, W. and J.J. Schule (1966) Comments on the mass budget of arctic pack ice. In *Proceedings of the Symposium on the Arctic Heat Budget and Atmospheric Circulation*. The RAND Corporation (RM-5233-NSF), p. 215–246.

Wright, B., J. Hnatiuk and A. Kovacs (1981) Multiyear pressure ridges in the Canadian Beaufort Sea. *Coastal Engineering*, **5**: 125–145.

APPENDIX A: BLOWUP OF FIGURE 28

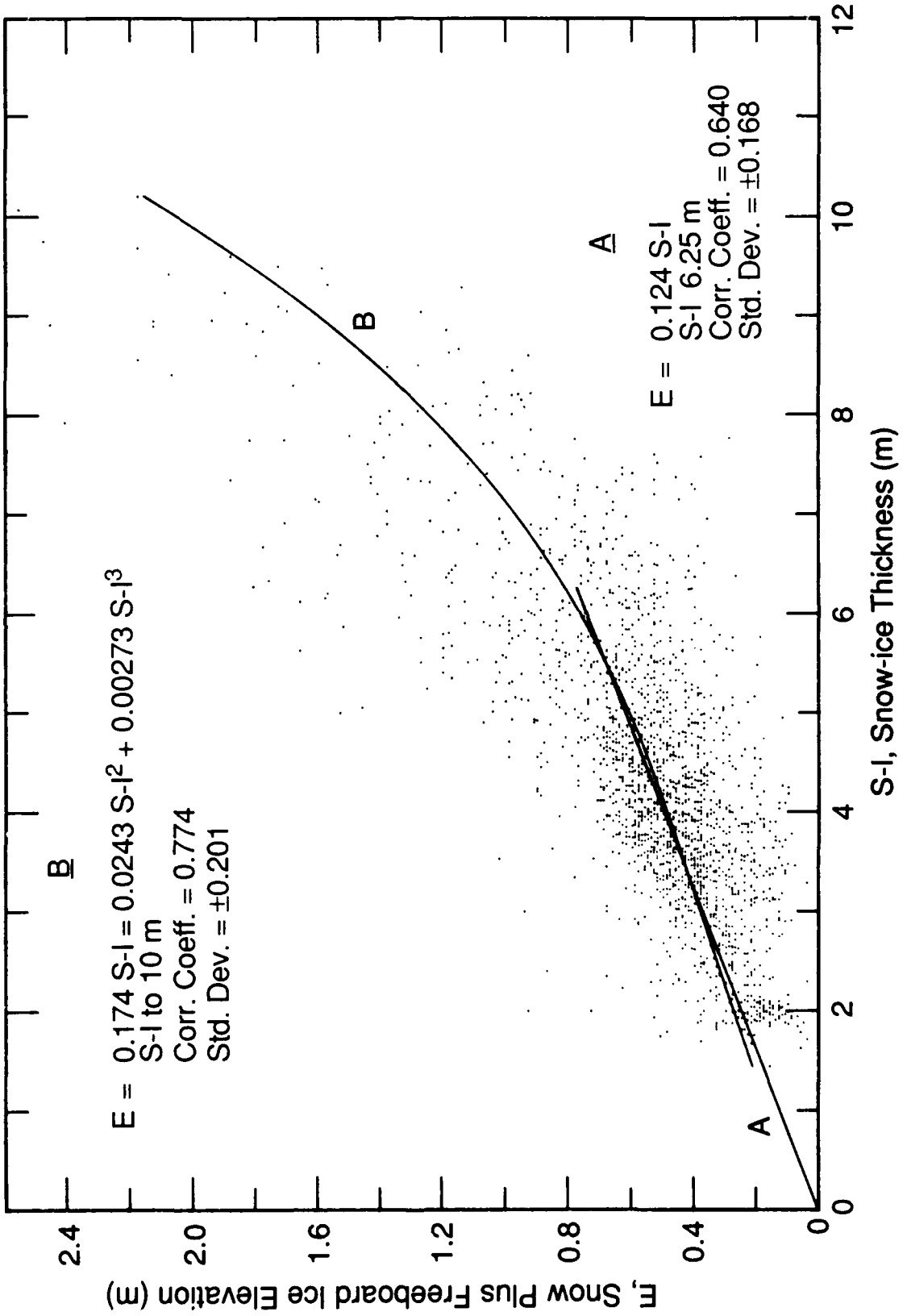

A facsimile catalog card in Library of Congress MARC format is reproduced below.

Kovacs, Austin
Development of an airborne sea ice thickness measurement system and field test results / by Austin Kovacs and J. Scott Holladay. Hanover, N.H.: U.S. Army Cold Regions Research and Engineering Laboratory; Springfield, Va.: available from National Technical Information Service, 1989.
v, 54 p., illus., 28 cm. (CRREL Report 89-19.)
Bibliography: p. 45.
1. Airborne profiling. 2. Electromagnetic induction–measurement technology. 3. Sea ice thickness. I. Holladay, J. Scott. II. United States Army. III. Corps of Engineers. IV. Cold Regions Research and Engineering Laboratory. V. Series: CRREL Report 89-19.